

# CAPILLARY MICROFLUIDIC SYSTEMS FOR BIO/CHEMISTRY

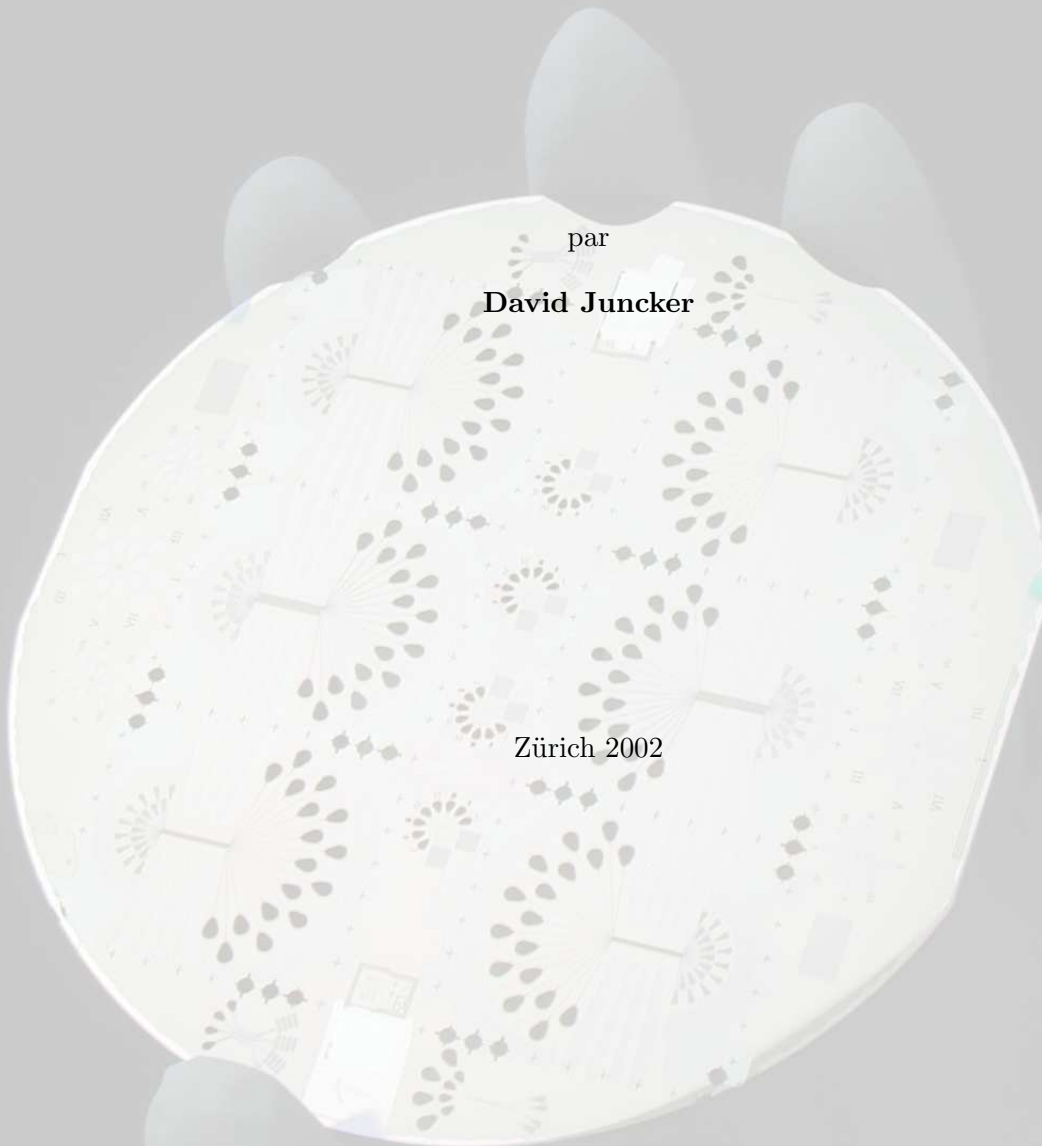
**Thèse**

présentée à la Faculté des Sciences  
**Université de Neuchâtel**  
pour l'obtention du grade de *Docteur ès Sciences*

par

**David Juncker**

Zürich 2002





“When an old and distinguished person speaks to you, listen to him carefully and with respect - but do not believe him. Never put your trust into anything but your own intellect. Your elder, no matter whether he has gray hair or has lost his hair, no matter whether he is a Nobel laureate - may be wrong. The world progresses, year by year, century by century, as the members of the younger generation find out what was wrong among the things that their elders said. So you must always be skeptical - always think for yourself.”

**Linus Pauling** in *Scientist and Peacemaker*, Clifford Mead and Thomas Hager, eds.



# IMPRIMATUR POUR LA THESE

**Capillary microfluidic systems for bio/chemistry**

de M. David Juncker

---

UNIVERSITE DE NEUCHATEL

FACULTE DES SCIENCES

La Faculté des sciences de l'Université de  
Neuchâtel sur le rapport des membres du jury,

MM. N. de Rooij (directeur de thèse), R. Tabacchi,  
E. Delamarche (Zürich) et  
M. Despont (Zürich)

autorise l'impression de la présente thèse.

Neuchâtel, le 8 mai 2002

Le doyen:



F. Zwahlen



# Contents

<b>Résumé</b>	<b>9</b>
<b>Summary</b>	<b>11</b>
<b>1 Introduction</b>	<b>13</b>
1.1 Miniaturization and bio/chemistry, and scope of the thesis . . . . .	13
1.2 Microfluidics: the transport of minute amounts of liquids . . . . .	15
1.2.1 The development of microfluidics . . . . .	15
1.2.2 External mechanical actuation . . . . .	16
1.2.3 Integrated mechanical pumps . . . . .	16
1.2.4 Electro-osmotic pumping . . . . .	17
1.2.5 Alternate pumping schemes . . . . .	17
1.2.6 Microfluidics utilizing capillary phenomena . . . . .	18
1.3 Capillary phenomena . . . . .	19
1.3.1 Wetting and interfacial free energy . . . . .	20
1.4 Dynamics of capillary flow . . . . .	21
1.4.1 Capillary pressure . . . . .	23
1.4.2 The viscosity of fluids . . . . .	27
1.4.3 Principles of liquid flow under applied force . . . . .	27
1.4.4 Flow of liquid in a conduit . . . . .	28
1.4.5 Flow-rate resistance of a conduit . . . . .	28
1.4.6 Dynamics of capillary flow in a microchannel . . . . .	29
1.5 Diffusion & depletion of reactants in a microchannel . . . . .	30
1.5.1 Diffusion in a microchannel . . . . .	32
1.5.2 The diffusion barrier . . . . .	33
1.5.3 Depletion of reagents in a microchannel . . . . .	34
1.6 Design of capillary microfluidic systems . . . . .	35
1.6.1 Advanced capillary systems . . . . .	36
<b>2 Fabrication and use of capillary microfluidic systems</b>	<b>45</b>
<b>3 Engineering of the surface chemistry of capillary systems</b>	<b>57</b>

4	Patterning of density-gradients of adsorbed proteins	65
5	Fabrication of “smart”-stamps for microarraying proteins <i>en masse</i>	73
6	The autonomous transport of liquids	79
	Conclusion	91
	Acknowledgments	93
	List of Publications	95
	Curriculum Vitae	97



# Résumé

La microfluidique – le transport de quantités infimes de liquide – est la clé de voûte à la miniaturisation, l’intégration et la parallélisation de processus chimiques, biochimiques et biologiques. Ce travail explore la possibilité d’utiliser simplement des phénomènes capillaires (= capillarité) pour effectuer toutes les opérations requises pour le transport de nanolitres de solutions dans des microcanaux et des microchambres de réaction, et illustre le potentiel de cette stratégie avec plusieurs exemples d’application.

La première partie de cette thèse décrit la fabrication de systèmes capillaires microfluidiques dans des matériaux rigides tels que le silicium avec des techniques de microusi-nage chimique conventionnelles et dans des matériaux élastomériques avec des techniques de réplication non-conventionnelles. Les systèmes fabriqués peuvent être opérés manuellement car ils contiennent de larges zones de remplissage sur la face arrière qui sont reliés à des micro-chambres de réaction dans la face avant. Ces systèmes sont construits pour délivrer dans la chambre de réaction de multiples fois son volume propre en liquide grâce à des “pompes capillaires” sous forme de structures arborescentes. Ce re-remplissage devient d’autant plus crucial que les dimensions diminuent et que le rapport surface/volume augmente. Différentes stratégies sont présentées pour localement modifier la chimie des surfaces, afin de rendre les surfaces externes aux microcanaux hydrophobes (*c. à. d.*, qui repoussent le liquide) et l’intérieur des canaux à la fois hydrophile (*c. à. d.*, qui aime le liquide) et biocompatibles pour prévenir l’adsorption incontrôlée des biomolécules en solution. Nous avons également fabriqués des microsystèmes fluidiques qui peuvent confiner et guider le flux d’une solution sur une surface par des effets capillaires uniquement, sans besoin de paroi ni de “joint étanche”.

La deuxième partie de ce travail décrit la déposition de multiples molécules différentes sur des surfaces de taille millimétrique à l’aide de systèmes capillaires microfluidiques. Par exemple, des surfaces sont structurées avec des polymères colorés en rouge, vert, et bleu, correspondant aux colorants-filtres utilisés pour la fabrication des écrans plats d’ordinateurs. Le centre de nos efforts est cependant la déposition de biomolécules et l’utilisation de substrats ainsi décorés dans des tests biologiques selon des procédures similaires à celles des diagnostics médicaux; ces tests illustrent le potentiel de notre approche dans ce domaine. De plus, notre technique offre la possibilité d’ajuster la densité des protéines adsorbées sur une surface, et surtout, de créer des gradients de densité de protéines adsorbées et d’en contrôler précisément la “pente” et la longueur à des régimes sub-millimétriques. De tels gradients sont d’un intérêt particulier pour l’étude de l’effet de la densité locale de protéines immobilisées sur leur aptitude à se conjuguer avec leur parte-

naire. La seconde application proposée dans cette thèse est la structuration de tampons élastomériques de lithographie douce avec des matrices de protéines, qui ici sont attachées de manière covalente à la surface. Ces tampons décorés de biomolécules sont utilisés dans un processus original de “réplication complémentaire” à quatre pas: (i) encrage – purification, extraction à partir d’une solution impure et auto-assemblage sur le tampon des immunopartenaires par reconnaissance de la molécule préimmobilisée, (ii) rinçage et séchage, (iii) impression – transfert des immunopartenaires qui se dissocient des molécules préimmobilisées au moment de la séparation du tampon doux avec le substrat, et (iv) répétition du processus. Cette méthode permet grâce à la “réplication complémentaire” de fabriquer des “biochips” avec des ensembles de protéines de dimension et de nombre arbitraire (à créer une unique fois sur le tampon) en trois pas élémentaires.

La dernière partie de cette thèse démontre le potentiel qu’offre l’intégration dans la structure de systèmes microfluidiques de fonctions capillaires, qui remplacent avantageusement pompe, valves, senseurs et systèmes de synchronisation, et qui permettent le transport autonome de liquides. De tels systèmes capillaires offrent la possibilité de (i) remplir et rincer une microchambre de réaction avec une variété de solutions, librement, et autant de fois que désiré, (ii) de créer des ensembles de systèmes capillaires autonomes par simple clonage d’une unité fonctionnelle, (iii) de contrôler le transport des solutions, si désiré, ce qui n’est pas plus difficile pour un ensemble de systèmes que pour un seul, et (iv) d’interconnecter des systèmes capillaires et former des réseaux fonctionnels grâce à la synchronisation par “encodage structural” des pressions capillaires.

Les systèmes capillaires microfluidiques sont *a priori* attractifs pour un grand nombre de procédés chimiques, biochimiques et biologiques grâce à leur capacité de transport autonome de multiples solutions, à leur simplicité d’utilisation qui rend superflu tout équipement périphérique coûteux et encombrant, et à la possibilité d’utiliser des procédés de réplication pour une fabrication en masse économique.

# Summary

Microfluidics – the transport of minute amounts of liquid – is the key to miniaturization, integration and parallelization of chemical, biochemical, and biological processes. In this thesis, we explore the possibilities of simply using capillary phenomena to effect all the operations required for the transport of nanoliters of liquids in small channels, and we illustrate the possibilities of this strategy with different examples.

The first part of this thesis describes the manufacture of microfluidic systems in hard materials such as silicon by conventional microfabrication techniques and in soft elastomers by replication from a “master” using unconventional techniques. Systems structured on multiple levels with vias and high aspect ratios were fabricated in both materials. These systems were convenient to use because they had large openings on the back-side for the manual delivery of reagents and micrometer-scale reaction chambers on the front side. The systems were specially designed to generate supplementary flow that could efficiently replenish the reaction chambers with solution and prevent the adverse depletion of the reagents, which becomes crucial as the size is reduced and the surface/volume ratio increases. The surface of the conduits in our systems were engineered to be hydrophilic (*i.e.*, attract the liquid) to ensure rapid filling of the channels with liquid, as well as made protein repellent to prevent adventitious adsorption of the biomolecules on the walls. The other surfaces on the other hand were made hydrophobic (*i.e.*, repel the liquid) by microcontact printing, which helped prevent spilling of liquids out of the service ports, and which could even be used to guide the flow of liquid on the surface by capillary effects, without the need of walls or “tight joints.”

These microfluidic systems were used to pattern surfaces. For example with red, green, and blue polymers such as the ones used in color-filters of the flat screens of computers. The focus of our patterning efforts were however biomolecules, and the use of the patterned substrates in the recognition of binding partners in procedures such as the ones used for medical diagnostics; it illustrates the potential of our approach in this field. In more advanced processes, the depletion of molecules was purposely pursued because it allows surface patterns of continuous density-gradients of adsorbed proteins to be generated. These protein-gradients were used in a second step to assess the influence of density on the binding of their partner, which could be performed here in a continuous line at sub-millimeter scales. Further, this patterning technique was used to create arrays of proteins that were covalently attached to a soft, elastomeric stamp. This stamp was used as a “master” in an “affinity replication” process according to the following procedure: (i) inking – self-assembly, binding and purification of the binding partner from a crude

solution onto the respective spots of the stamp containing the pre-immobilized conjugate, (ii) rinse and dry, (iii) print – transfer of the binding partner by mechanical dissociation when the stamp is separated from the substrate, and (iv) repeat. The “affinity replication” procedure allows the fabrication of “biochips” having protein arrays of arbitrary size and number (to be created once only on the master stamp) in three elementary steps.

The last part of this thesis sheds light on the vast possibilities that capillary microfluidic systems provide. The autonomous transport of multiple reagents through the reaction chamber is a striking example. Here, the capillary effects replace pump, valves, sensors and synchronization mechanisms without even a moving part. A major advantage of such a self-contained system is that arrays can be made by simply cloning a working system because it contains precisely all the functionality. Capillary systems can operate without peripherals in a standalone modus, but if desired the flow can be interactively controlled, and importantly, this control can be achieved in arrays of systems without additional effort. It is gained by locally tuning the evaporation of the liquid or by adding a secondary capillary structure that sucks liquid out of all the systems in parallel. The key is the synchronization of the meniscus pressure in the different elements.

Microfluidic capillary systems are *a priori* attractive for a great number of chemical, biochemical, and biological processes because they are self-contained and can autonomously transport many solutions, they offer a great ease of usage, which renders any peripheral, costly, and cumbersome equipment superfluous, and they are amenable to fabrication using replication processes that allow low-cost mass production.

# Chapter 1

## Introduction

### 1.1 Miniaturization and bio/chemistry, and scope of the thesis

The miniaturization and integration of electronic circuits that started about 50 years ago was the foundation stone of the computer technology, and has revolutionized the way of life of many people. The very large-scale integration of multiple functionalities has permitted it to increase in complexity, calculation power, and opened new avenues, which most notably led to computer networks, wireless communications, and the Internet. From a physicist's view, this mind-startling feat can be tracked down to the exquisite control on electrons, holes and photons ( $\equiv$  electromagnetic waves) that enables us to store, transport, and process their assigned information-contents: “0s” and “1s”.

Chemical, biochemical and biological (= bio/chemical) processes on the other hand are commonly performed on a large scale as a succession of time-consuming reactions in voluminous vessels. As pointed out by the microelectronic paradigm, miniaturization along with integration and automatization could pro-

vide parallelism, enhanced speed, portability and in this case greatly reduced consumption of bio/chemical samples. Processes that could profit from miniaturization encompass the detection of a disease in the human blood, the analysis of DNA at a crime scene, the sampling of water from a well in Africa, or of the air in a big city, to assess their purity, the synthesis of a precious antidote against snake poison, or the combinatorial search by a pharmaceutical company for a new active substance as a potential drug against a disease. The idea of miniaturizing, localizing and integrating of bio/chemical processes in a race to improve effectiveness has begun, but the achievements are still very primitive when compared to those of microelectronics. For this micro-processes, electrons are conceptually replaced by the myriad of chemical species, and electrical wires by miniaturized pipes. The transport of the chemicals at the micrometer-scale is the key to miniaturization of bio/chemistry and is most simply done in the fluid phase: this is the realm of **microfluidics**. The first envisioned goal for miniaturized bio/chemistry is to “shrink” a laboratory and virtually place it onto a chip such as to perform all tasks required for a given process – similarly to a microprocessor that can per-

form a series of operations – and reduce sample consumption by orders of magnitude. The vision of a functional system for chemical analysis housed on a single chip was described by Andreas Manz and coworkers [1] and coined as a *micro-total analysis system* ( $\mu$ TAS). The other novel acronym that renders exactly the idea of lab miniaturization is *lab-on-a-chip*; both terms are common language in the field now [2, 3, 4]. Nowadays, most systems nonetheless still rely on external, macroscopic peripherals for liquid transport and bio/chemical processing on the chip, and the prospect of a “micro-bio/chemical processor” that would be an autonomous, standalone, “smart” microsystem capable of performing multiple tasks and of responding to various “inputs” is not yet imaginable.

Nature can serve as a model because chemical processes are at the root of life. For example in a human body, a myriad of chemicals are reacting locally and simultaneously, yet the reactions are interdependent and form a complex hierarchical self-regulating “system” [5]. Nature has also developed chemical pathways for information exchange and storage, a notorious example being our DNA which is coded in the four constituting bases, but also has much more intricate “codes” expressed as the chemical and three-dimensional structure of innumerable proteins. A cell is an exquisite type of an autonomous microchemical processor that can among other things extract its fuel from the environment, regulate the intake, handle its own waste, respond to signals, send out signals, adapt to changing environments, clone itself by division, and finally initiate its self-destruction (*i.e.* apoptosis) when it becomes defective.

Whereas we already can control and alter some processes in the cell by genetic manipulation, a man made microchemical processor that could mimic but the most basic functions found in Nature’s examples is not yet doable. Yet such microchemical processors may even be connected and form networks; a thrilling idea for our imagination, but as the history of the miniaturization of electronics teaches us, such far fetched ideas may eventually prove startlingly useful, and on the path to their completion, one most certainly would open up not yet imaginable avenues...

## Scope of the thesis

This work explores the possibilities of utilizing capillary phenomena as a substitute to liquid guides, valves, pumps, and synchronization mechanisms in view of autonomously transporting minute amounts of solutions for fuelling miniaturized bio/chemical processes.

- In the following part of **Chapter 1**, the different strategies and techniques hitherto exploited to effect and control the movement of liquid at the micrometer scale are resumed. There follows an in-depth description of the different parameters essential to the design of a microfluidic capillary system (**CS**), starting from capillary phenomena, the physico-chemical principles governing wettability, the power of the geometry as a bridle for harnessing capillary effects, the dynamics of liquid flow in conduits, and the mass transport by diffusion, as well as the

depletion of reactants in a micro-channel.

- In **Chapter 2**, a set of chemical micromachining techniques that were developed for the fabrication of micro-electromechanical systems (MEMS) [2, 6, 7] are illustrated and utilized for structuring microfluidic systems into Si wafers and radiation-sensitive polymers, and for replicating them into self-sealing elastomers. The use of capillary phenomena for both propelling liquids and guiding them in open channels and the ability of microfluidic CSs for patterning (i) polymers and (ii) the adsorption of biomolecules from the solution on a solid substrate are illustrated.
- In **Chapter 3** various possibilities that can be used to tailor the surface chemistry of CSs made of different materials are explored. First, strategies to pattern wettability and non-wettability onto the channel structure are addressed, and second the issue of fouling of the channel surfaces with biomolecules is solved by attaching protein-repellent molecules to the channel walls.
- In **Chapter 4**, we examine how miniaturization affects the density of biomolecules that can adsorb to a surface from a solution. The interplay of flow, diffusion-driven mass transport and depletion of reagents reveals itself by the formation of continuous density-gradients of adsorbed proteins. This effect is tuned to the sub-millimeter scale, allowing to easily image (using fluorescent microscopy) and quantify the binding of a partner to the primarily immobilized molecules as a function of the local density of these adsorbed molecules.
- In **Chapter 5**, we illustrate how such microfluidic CSs can leverage advanced protein microarraying techniques by patterning and covalently attaching multiple biomolecules in parallel onto a stamp. The so-formed stamp can be repeatedly used for printing arrays of proteins by first capturing a binding partner from solution, which is mechanically dissociated when the stamp is contacted and separated from a substrate.
- In **Chapter 6**, we go beyond the initial capillary microfluidic systems with an original concept for the autonomous transport of multiple liquids. The mechanisms of flow generation and control are explained and illustrated, and the effectiveness of this concept in carrying out multi-step bio/chemical processes is demonstrated.

## 1.2 Microfluidics: the transport of minute amounts of liquids

### 1.2.1 The development of microfluidics

Microfluidics is the enabling and indispensable technique of the miniaturization of bio/chemical processes, and a variety

of microfluidic approaches have been explored. The life science industries have developed microfluidic devices exploiting capillary effects since more than 20 years. Porous substrates (see Ref. [8] and references therein) can generate strong capillary action while circumventing the technical difficulties associated with miniaturization, and they are therefore widely used in the commercial diagnostic devices under the form of immunochromatographic strip tests [9]. The miniaturization of one dimension by sandwiching a structured layer between a top and lower carriers also allows addressing scales that generate strong capillary effects, and such strategies have also been explored within the life science companies [10, 12, 11] since the mid-1970s.

About at the same time the initial ground-breaking demonstrations of *micro-fabricated* microfluidic systems were published by IBM workers who developed inkjet nozzles [13] and by a group of Stanford University who moreover addressed integration and conceived an on-chip gas chromatograph [14]. The interest of the academic research community in micro-fabricated microfluidic systems has really started in the middle of the eighties only, but has steadily been growing since that time. The encounter of the life science with microfabrication techniques has already led to formidable progress. Genomic analysis not yet imaginable a few years ago can now be performed using microarrays of molecules immobilized on a solid carrier. This carrier is either a chip, and the patterned chip is called a biochip, or it is an array of beads. One can use the chip or the beads to probe in a single run up to hundreds of thousands of analytes, with as little as a few micro-

liters of sample [16, 17, 18]. The refinement of the transport of small amounts of biomolecules and the scaling have had a formidable impact and allow genome-wide analyses not imaginable ten years ago to be performed routinely. This technologies have already started spreading to large scale protein (proteomics) and carbohydrates analyses [19]. Different microfluidic strategies [3, 4, 20] that are presently used in bio/chemical processes, and their merits and shortcomings, are briefly discussed below.

### 1.2.2 External mechanical actuation

The simplest microfluidic systems are made up of a capillary network that is engraved into a chip and connected to external macroscopic actuators, such as syringe pumps [21], peristaltic pumps, air pressure pumps [15] multiport valves [22], pressure, temperature, UV absorption and fluorescence sensors, and usually a computer [3, 4, 23, 24]. The computer gives the advantage of interactive control and the possibility of varying several parameters, but at the expense of complexity, portability, integration, scaling, and cost. Such setups are however very important to a variety of applications such as research, high throughput analyses and cell sorting.

### 1.2.3 Integrated mechanical pumps

Integrated microfluidic systems have been explored since the late 1980s by scientists primarily focused on the engineering aspects of the miniaturization of fluidic systems. The first electro-mechanical



systems constructed mimicked the mechanisms used for flow generation and control in macroscopic fluidic systems, but were cleverly re-engineered and miniaturized [25, 26]. Such microfluidic systems usually contain moving parts, different materials, and require on-chip flow control elements, all of which render fabrication difficult, costly, and the devices delicate. Nonetheless, such systems can directly be interfaced with microelectronic chips and the so-formed set should be amenable for mass-manufactured “smart” microsystems, should the demand arise.

#### 1.2.4 Electro-osmotic pumping

The chemists approached microfluidics from the “analysis” angle. Among the different separation techniques, capillary electrophoresis – the separation of species by their *electrophoretic* mobility in liquid under an applied electrical field – has played a major role in the miniaturization of chemical analysis systems. This technique could be directly transferred from capillaries made of glass to capillary networks engraved into chips (also made of glass) [27]. The capillary networks filled with liquid thus forming an electrically conductive circuit. The high electrical fields necessary for separation also have the ability of generating electrokinetic flow in capillaries by the electrical transport of the ions of positive (or negative) charge that preferably accumulate at the channel walls, a phenomena called electro-osmotic flow (EOF), which was already discovered in the 19th century. The liquid in the bulk of the conduit is dragged along due to the viscosity of the liquid, but this strategy is lim-

ited to sizes where the inertia is negligible, that is to say below a millimeter. The flow profile within the channel is remarkable in that it is plug-like (whereas pressure driven flow exhibits different flow speeds depending on the position within the cross-section of the conduit) and prevents adverse convective mixing of consecutive plugs of liquids flown through the channel. The direct analogy to electrical circuits, the implicit potential to create complex networks, and the inherent capacity to both transport and separate analytes spurred research and commercial development in this field of microfluidics [3, 4]. EOF has its own weaknesses however: sensitivity to impurities that adsorb on the wall of the channel, to changes in composition of the buffer, ohmic generation of heat in the fluid, and the need for high voltages (on the order of kilovolts). Such systems therefore still rely on macroscopic power supplies that are computer-controlled. Novel strategies that can separate the pumping section from the sections where the reagents are transported and analyzed ensure stable operation of the chip [28, 29], and additionally, the use of multiple pumping sections can reduce the required voltage [30], which should allow using chips made out of Si instead of glass and, more importantly, paves the way to making self-contained systems.

#### 1.2.5 Alternate pumping schemes

A variety of alternate pumping schemes have been reported in the scientific literature. For instance, the simplest of all is using hydrostatic pressure [31, 32] to drive several liquids in parallel along a microchannel, where they can react at their

liquid-liquid interfaces. Magneto-hydrodynamic pumping can be achieved by utilizing the Lorentz force created by synchronously applying an AC electrical field and an AC Magnetic field [33], or as result of an electrochemical reaction performed in the vicinity of a magnet which can generate “self-powered” flow [34]. Plugs of ferro-fluids (paramagnetic fluids) can be used to drive flow using a magnetic actuator [35]. The nucleation of a bubble can generate pressure and flow, which can be done by either heating or by an electrochemical reaction that evolves gas [36]. Travelling surface acoustic waves are also capable of creating flow in a closed conduit [37], as are arrays of asymmetrically shaped electrodes [38]. Novel, elegant approaches exploit chemically sensitive hydrogels [39, 40] for autonomous valving of liquids is a very elegant approach.

### 1.2.6 Microfluidics utilizing capillary phenomena

The physical laws describing, for example, the forces produced by inertia and interfacial tensions are valid at any scale, but the relative magnitude of these forces reverses as the volume of the liquid decreases and the surface/volume ratio increases. The passage from a bulk-dominated flow to a surface-dominated flow gradually occurs when approaching and going below the millimeter scale. If unaccounted for, interfacial effects can affect the performance of the above cited microfluidic systems, as for instance in electrophoretic separations where they can be source to adverse flow. Conversely, solid-liquid-air interfacial phenomena can be exploited and harnessed for controlling, guiding, and effecting the transport of liquids. For exam-

ple, capillary forces allow the patterned transfer of arrays of solutions (containing biomolecules) by the contact of pins with a biochip carrier [16, 19] or microfluidic service ports structured in a surface [42]; surface tension governs the operation of drop-on-demand dispensers, which by applying a pressure pulse can form and shoot picoliter-drops out of a nozzle, and are widely used to make biochips [43]; a self-sealing structured elastomer can be placed on a surface to form a network of microchannels which can be used to deliver different solutions by capillary action along the surface and thus pattern it with organic and inorganic materials [44, 45, 46] or with biomolecules [47, 48, 49] solved in the solution; hydrophobic patches can act as a valve to stop the flow [50, 51] and more advanced wettability patterns can also guide aqueous solutions in wall-less microchannels [52, 53]; hydrophobic microfluidic networks with tailored geometry can control the sequence in which different branches are filled under an applied filling force (pressure), generated with *e.g.* centrifugal motion [54, 55] or with a syringe pump [56]. Recent demonstrations based on interactive tuning of the interfacial forces are the filling of arrays of capillaries by electro-capillary adjustment of the meniscus pressure [57] and by electro-chemical concentration or dilution of a surfactant via its localized oxidation-reduction [58], the light beam controlled wettability change of a surface [59], the temperature gradient controlled flow [60] which can be combined with non-wettable patterns that confine the liquid on microscopic stripes [61, 62]. An elegant system uses evaporation to produce capillary forces that generate the flow required to perform a capillary chromatog-

raphy [63]. The latest advances demonstrate the transport and mixing of drops on non-wettable surfaces controlled by arrays of actuators, either via the electrocapillary effect [64, 65], or via surface acoustic waves [66]. A sublime example of the possibilities of capillary effects is the coating of small droplets with amphiphilic powdery material, which forms a soft outer shell around the drop and render it ultrahydrophobic for many different surfaces, and allows displacing the liquid by rolling it on a substrate like a marble [41].

Microfluidic MEMS utilizing capillary effects are recently gaining in popularity, as these examples and novel, yet large and fast growing body of literature related to this subject attest it. But these phenomena have already been exploited in technology since long time ago.

### 1.3 Capillary phenomena

Capillary phenomena are ubiquitous and, although significant at micrometer scales only, they can be observed and experienced in our everyday-life. One may think, among other things, of liquid being wiped off a table with a cloth or rolling in a teflon coated pan, of water dripping from a tap in a regular rhythm, of coffee wicking into a cookie that is dipped into one's cup, of the accurate prints that can be produced with an office stamp, and of the sharp line of ink a fountain pen leaves on a paper by writing, Fig. 1.1.

These phenomena are fundamental in many technical applications, in particular to the printing industry [67, 68], in the displacement of a liquid by another

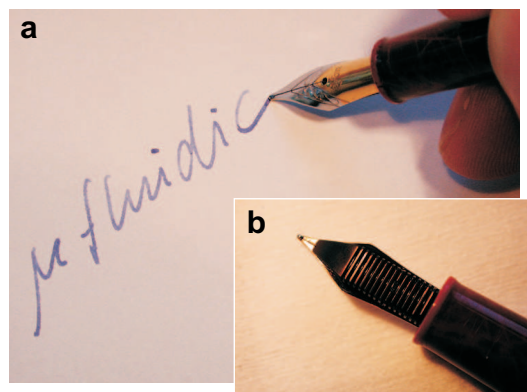


Figure 1.1: Photograph of the (a) front-side and (b) back-side of the tip of a fountain pen. Capillary effects are dominant in writing, because they draw and guide the ink along the thin slit to the rounded tip, fill the ink-reservoirs structured into the head (b) and thus prevent the ink from drying when the pen is not in use, and spread the ink between the round tip of the pen and the paper (a, the written line is wider than the slit) and thus ensure the smooth gliding of the pen on the surface.

in a porous media [69, 70], such as in petrol drilling, and, as mentioned, to the common pregnancy test [9] found in any pharmacy. Nature shows other possibilities of exploiting capillary phenomena, for example to support an aquatic insect (*i.e.* the water strider) walking across a pond, to help beetles collect water that has condensated from the humid air on their body [71], to protect the leaves of the sacred lotus from contamination [72], and to store water in the soil, transport it to the roots of plants, and from there to propel it up to the leaves at formidable height in tall trees [73, 74, 75, 76].

Capillary phenomena, as discussed previously, originate at the interfaces of liquid, solid, and vapor phases. In the

bulk of a liquid, the sum of forces exerted on a molecule by its neighbors is distributed symmetrically around it [78]. This is not the case at an interface, and therefore energy is required to bring a molecule to this interface. This energy is stored as interfacial tension [ $\text{N m}^{-1}$ ] or interfacial free energy [ $\text{J m}^{-2}$ ], both being the same. The former is commonly used for describing liquid interfaces, and the second for solid interfaces. In the case of a liquid-vapor or solid-vapor interface, this energy is called surface tension and surface free energy, respectively. Capillary phenomena designate both (i) the forces produced by these interfacial tensions and (ii) the spontaneous transformation (and dissipation) of the interfacial energy (via the force) into motion of a liquid. These effects become predominant when the forces exerted by the molecules at the interface surpass the forces arising from the molecules in the bulk and, in other words, they are inherent to miniaturization when the surface/volume ratio increases.

### 1.3.1 Wetting and interfacial free energy

When a small drop of liquid is put onto a flat solid surface, two distinct equilibrium regimes can be observed [79, 80]: partial wetting, in which case the liquid drop has a finite contact angle  $\theta$  with the surface, and total wetting where the liquid spreads out as a thin molecular film, Fig. 1.2.

In the case of partial wetting, a contact line (which is a circle for a droplet) delimits the wetted area and forms the contact between the solid, liquid, and vapor phases. Each interface (Solid, Liquid, and Vapor) has a free energy per unit area  $\gamma_{SL}$ ,  $\gamma_{SV}$ , and  $\gamma_{LV}$  (which we call  $\gamma$  for

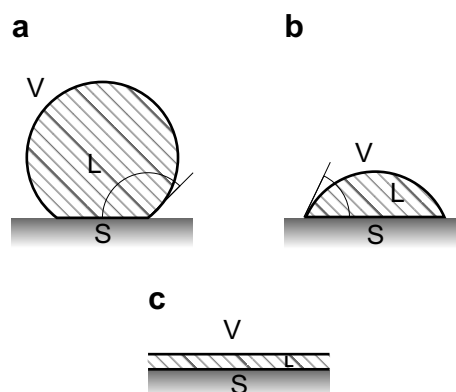


Figure 1.2: Equilibrium shape of a liquid (L) drop deposited on a solid surface (S), surrounded by vapor (V). The surface is conventionally called (a) non-wettable and (b), (c) wettable. In (a) and (b) the surface is partially wetted, in (c) it is totally wetted,  $\theta = 0^\circ$ .

simplicity). Young's equation relates the relative magnitude of the different interfacial energies via the contact angle  $\theta$  of the liquid to the surface

$$\gamma \cos \theta = \gamma_{SV} - \gamma_{SL} \quad (1.1)$$

The contact angle  $\theta$  is only a relative measure of the interfacial energy of the liquid because it depends on both the solid and the vapor phase, but the value of this angle is sufficient to describe the liquid, if (i) either the interfacial energy of the liquid with the solid surface is known, (ii) or if it is the relative difference in surface tension of a solution versus a reference solution that is of interest, and (iii) because it is only the difference  $\gamma_{SV} - \gamma_{SL}$  which is relevant for experiments involving liquids. The common definition is to call a surface wettable to a particular liquid if the the drop has a contact angle  $\theta < 90^\circ$  with the substrate, and non-wettable if the contact angle  $\theta > 90^\circ$ . In the particular case of

water, a surface is either hydrophilic or hydrophobic. Total wetting of the substrate corresponds to the contact angle  $\theta = 0$ , which occurs when the gain in free energy at the solid-liquid interface is greater than the surface free energy of the liquid, and is expressed as  $\gamma_{SV} - \gamma_{SL} \geq \gamma$ .

In the dynamic case of a droplet moving on the surface, the contact angles of the *advancing* front  $\theta_a$  (wetting) and the *receding* front  $\theta_r$  (dewetting) at the back of the droplet are different. This hysteresis is the result of physico-chemical processes at the interface, which dissipate energy upon a wetting-dewetting cycle, and oppose the displacement of the liquid. The static wettability is, strictly speaking, irrelevant in the dynamic behavior of a drop moving on a surface [81]. The length of the contact line (which depends on both volume and contact angles), the hysteresis of the advancing and receding contact angles, and the microtopography are the determining parameters, and can be used to calculate the interfacial energy balance associated with the displacement of minute amounts of liquids on solid surfaces. The particular case of strongly hydrophobic surfaces is interesting, because by microstructuring the surface topography, the contact area can be reduced to the top of the microstructures only and has the effect of further increasing both the apparent hydrophobicity and contact angle [81].

## 1.4 Dynamics of capillary flow

The geometry can largely determine the equilibrium shape or distribution of a liquid on a surface, and interfacial free energy minima can be designed to capture

a solution in wells, for example. Interestingly, the walls of these wells need not be wettable [82, 83, 84, 85] for capturing the liquid, because it is the sum of the three interfacial energies, which are each weighted by the respective change in area, that needs to be minimal [86]. A liquid deposited at the inlet of a well or a conduit with wettable walls will spontaneously fill it, and the confinement ( $\equiv$  smaller dimensions) can act as an amplifier of the capillary phenomena. The equation of the surface free energy  $\Delta G$  of a liquid is

$$\Delta G = \gamma \Delta A_{LV} + \gamma_{SV} \Delta A_{SV} + \gamma_{SL} \Delta A_{SL}, \quad (1.2)$$

where the  $\Delta A_{ij}$  are the respective changes in interfacial area. If it is possible to redistribute the liquid so that  $\Delta G < 0$ , spontaneous motion should arise (the hysteresis of contact angles can preclude such motion if the free energy gain is small). In Fig. 1.3a, a two-dimensional (or a circular) channel of constant height  $2d$  is supplied with liquid from an infinite reservoir (without pressure; a small drop of a few millimeters can already play the role of such a reservoir, because as we will see, the capillary effects non-linearly increase with smaller dimensions) and filled up to a point **A**. For the liquid to further fill this channel spontaneously, the energy balance needs to be favorable. The local environment at the liquid-air interface is not altered when the liquid front moves from **A** to **B** if the channel surface is homogeneous. The liquid-air interface “costs” energy, and its area will therefore be minimal, and because of the identical conditions, this surface minima is conserved independently of the position of the liquid

in the microchannel. Thus, when the surface in the channel exposed to vapor is reduced by a distance  $L$  (the liquid advances from **A** to **B**), the wetted surface is augmented by a length  $L$  exactly. Hence, only two interfacial areas change and exactly compensate each other, and the condition for free energy gain and spontaneous wetting simply reduces to the equation  $\gamma_{SL} - \gamma_{SV} < 0$ . If we compare this result with Eq. 1.1, we immediately see that this condition is satisfied for  $\theta < 90^\circ$ , or in other words for what we call a wettable surface.

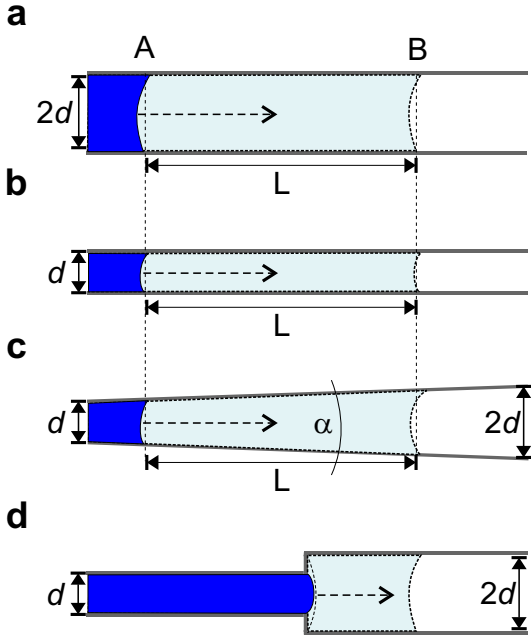


Figure 1.3: Liquid filling microchannels of different cross-sections. For explanations see text.

In Fig. 1.3b, a similar conduit to the previous one is shown and although with half depth only, it will obey to the same condition for spontaneous filling. However, for the same volume of liquid, the channel will be filled on a distance  $L$  two

times longer than in Fig 1.3a, or in other words the surface free energy gain per unit volume is higher by a factor two. The surface free energy gain for a volume of liquid  $V = Ld$  is

$$\begin{aligned} \Delta G &= (\gamma_{SV} - \gamma_{SL}) |\Delta A_{SV}| \\ &= (\gamma_{SV} - \gamma_{SL}) 2L \frac{V}{Ld} \\ &= \frac{2(\gamma_{SV} - \gamma_{SL})}{d} V. \end{aligned} \quad (1.3)$$

This equation indicates that  $\Delta G \propto 1/d$ . This relation is the expression of the ratio surface/volume and therefore also holds for three-dimensional microchannels. This  $1/d$  factor is the “geometric handle” that can be used to enhance the capillary effects, say the free energy gain per unit length of the microchannel, or reduce it, by purposely designed cross-sectional variations along the flow path. But this handle need to be manipulated with care, because as is illustrated in Fig. 1.3c, if the cross-section of the conduit is increasing, the liquid-air area will increase along the flow path. For an infinitesimal advance of the liquid, the difference in free energy of non-wetted–wetted area needs to be subtracted by the relative increase of area of the liquid-air interface. For increasing angle  $\alpha$ , the relative liquid-air interfacial area increase can become considerable and possibly prevent spontaneous filling of a microchannel despite having a wettable surface. If for example the channel has an abrupt cross-section increase with the two channel walls being at  $180^\circ$  of each other, Fig. 1.3d, the increase of wetted surface entails an equivalent increase of the liquid-air interface. To find out if the liquid can spontaneously over-

come such a geometrical irregularity, we can examine Eq. 1.2, and eliminate all the  $\Delta A_{ij}$ , and we find a condition for filling that corresponds to Young’s Eq. 1.1 with  $\theta \leq 0^\circ$ . Thus, a channel cross-section as depicted in Fig. 1.3d will stop any liquid that does not totally wet the channel surface. Such a geometry can be detrimental to the spontaneous filling of a microfluidic network, but it can also be used to make a “flow-stop valve” at an intersection with an other conduit for example [42, 87]. This qualitative free energy considerations are very useful to gain an intuitive understanding of the filling of the microchannels by capillary phenomena. In principle, it would be possible to calculate the dissipation associated with the filling of a channel. The energies involved are the kinetic energy, which is related to the speed as  $\propto v^2$ , and the surface free energy gained by filling the microchannel; the ratio of the former energy with the latter one is a measure of the energy dissipated by friction. The speed of liquid in the microchannel depends on the position within the cross-section, as will be further discussed below, and it is not clear whether the speed at each position within the cross-section can be solved analytically for various shapes, except for the case of a circular cross-section where it is relatively simple. It is therefore not possible to compute the dynamics of liquid flow based on energy considerations at the present state of our knowledge. It is possible to solve the flow dynamics by calculating the pressures (and forces) that are generated by the liquid surface tension and the overall average flow resistance of the conduit, which can be done analytically for a variety of cross-sectional shapes [88]. The calculation of the capillary pressure

and the flow resistances for circular and rectangular microchannels is described in detail below.

### 1.4.1 Capillary pressure

The liquid-air interface at the filling front connects the two walls and because the interface area “costs” energy, it follows the shape of the minimal area, which is a meniscus (or a curve in a two-dimensional case), Fig. 1.4

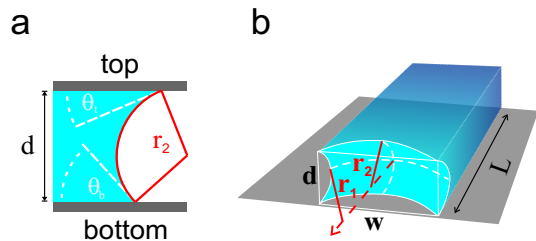


Figure 1.4: Meniscus of the filling front in (a) a two dimensional and in (b) a rectangular conduit.  $r_i$  is the radius of curvature at the filling front and the inverse of  $r_i$  multiplied by the surface tension of the liquid is directly proportional to the capillary filling force.

By virtue of the surface tension, the curved interface will produce a net force (or a negative pressure) in the direction of filling. For a conduit with a rectangular cross section, the curvature along the vertical axis of depth  $d$  and the horizontal axis of width  $w$  contribute to the meniscus pressure, Fig. 1.4b. The pressure generated by an interface curved along two perpendicular directions, as it is the case here, is described by the *Young-Laplace equation* [89], and the pressure  $P_c$  generated in the rectangular capillary can thus be written as

$$P_c = -\gamma \left( \frac{\cos \theta_b + \cos \theta_t}{d} + \frac{\cos \theta_l + \cos \theta_r}{w} \right), \quad (1.4)$$

where the indices  $b$ ,  $t$ ,  $l$ ,  $r$  of the contact angle  $\theta$  refer to *bottom*, *top*, *left*, and *right* walls, respectively. The total force exerted by the liquid meniscus at the filling front is conceptually analog to the reactive force experienced when pressing and bending the elastic membrane of a drum, for example. For a rectangular microchannel, it becomes evident that if one of the dimensions  $d$  and  $w$  is considerably larger than the other, its contribution to the overall capillary pressure becomes negligible. If we now consider such a microchannel where all the surface are identical and where  $w \gg d$ , which corresponds to a two-dimensional channel, the factor in parentheses becomes:  $\frac{2\cos\theta_b}{d} = \frac{2}{r_i}$ . First, we find again the  $1/d$  factor of Eq. 1.3 as it should be, and second here we see that the meniscus pressure is proportional the curvature of the filling front, which is the inverse of the radius  $r_i$ . From Eq. 1.4, it may appear that by increasing the surface tension, the pressure should increase, but often the opposite effect arises because the contact angles implicitly depend on the surface tension, Eq. 1.1. As a matter of fact, by reducing the surface tension the liquid is made more wettable and will more easily enter a conduit.

The surface tension can be reduced by adding surfactants to the liquid. For water, surfactants are molecules that have a polar moiety that can make water-bridges with the  $\text{H}_2\text{O}$  molecules (= hydrophilic) and a non-polar, low energy moiety formed by, *e.g.* an alkane chain (=

hydrophobic). These molecules may also preferably stay at the water-air interface, where their polar end is surrounded by water molecules and their low-energy end, which is repelled by water molecules, protrudes out of the water, and thereby minimizes the surface free energy [79]. This configuration can effectively reduce the surface tension of an aqueous solution and make it wet a surface that is hydrophobic for pure water. When a liquid containing molecules with surfactant properties is contacted with a hydrophobic surface, these surfactant molecules preferably stay at the solid-liquid interface, in a manner similar to if they were facing the vapor phase. However, if the surfactant molecules have an affinity with the surface, which because they both have hydrophobic properties is of increased probability in water (it can be evaluated or even calculated by taking into account the exact chemical composition of the surfactant and the surface), the surfactant molecules may adsorb to the surface and remain there. The free energy of the surface can be greatly altered by these “impurities”, and thus become hydrophilic for instance. The alteration of a non-wettable surface upon contact with a solution containing reactive molecules can be exploited for what is called reactive wetting. Here, the drop spreads as the molecules at its filling front adsorb to the surface. These qualitative and intuitive considerations are of relevance because bio/chemical solutions often contain surfactants and impurities, and more critical, the reagents themselves can have surfactant properties, as in the case of proteins which adsorb in fact on virtually any surface.

The contact angles of the liquid with the walls of the conduit depend on the



speed of flow, but this effect is relatively minor and interested readers can find detailed studies in the literature [90, 91]. The contact angles can however strongly vary depending on whether the liquid-solid interface is advancing,  $\theta_a$ , or receding,  $\theta_r$ . The hysteresis has the minimal value for the specific liquid-solid pair when the solid surface is chemically pure at the microscale, and generally augments when the chemical inhomogeneity of the surface increases, *e.g.* with the adsorption of impurities, for example. It may be possible to drain a microchannel, or a section of a conduit, by applying a negative pressure at an opening. Because the contact angles of a receding meniscus are lower than those of an advancing meniscus, the pressure required to empty a microchannel is higher than that was generated when filling it, and adsorbed impurities can increase this difference. The effect of hysteresis can be observed in a capillary partially filled with liquid that is slowly turned upside down: If the capillary is small enough in diameter, the liquid remains immobile and pinned at one end of the capillary, despite gravity.

The surface roughnesses of the microchannel as well as the corner formed by the intersection of the bottom (or the top) of the channel and the sidewalls also produce a meniscus pressure, Fig. 1.5

Because of the smaller dimensions of the surface roughnesses and the corner at its intersection, this pressure can be much larger and give rise to *roughness-flow* and *corner-flow*. Even on a flat surface, a molecularly thin layer of liquid often precedes the wetting front of the bulk of the liquid [79, 80], and the roughness of the surface in a microchannel can considerably enhance the thickness of the leading

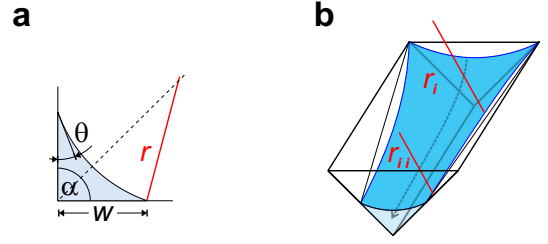


Figure 1.5: Images of liquid in a wettable corner. (a) In the two-dimensional case, the liquid interface forms a curve that connects the two walls, but the radius of curvature  $r$  of this curve continually decreases with increasing wetted width  $w$ . (b) A small groove or scratch in a surface can be approximated by a **V**-shaped corner [92]. The height of liquid in this groove is not constant, and the radius of curvature is proportional to the height which is greater in the back than at the front (see  $r_i$  and  $r_{ii}$ ), and thus the meniscus pressure is also much higher at the front. The resulting pressure difference generates the capillary flow along the groove (arrow), and this flow continues until the **V** is completely filled, or until the liquid is homogeneously distributed within this open conduit. There are four  $90^\circ$ -grooves in a rectangular channel.

film that wets the surface [70]. We could readily observe such films with an ocular as an optical change of contrast on the rough bottom of microchannels fabricated in Si using deep reactive ion etching. This corner-flow can also be observed [70] and the meniscus in the corner was analyzed with polymers that were cured while filling and thus allowed to measure the shape of the solidified liquid [45]. The meniscus pressure of liquid trapped in the corner of a rectangular microchannel ( $\alpha = 90^\circ$ ) as function of the wetted width  $w$  is:

$$P_c = -\gamma \frac{\cos \theta - \sin \theta}{w} \quad (1.5)$$

This equation defines the static pressure of the liquid front within the micro-channel, and can be used as a starting point for the hydrodynamic solution of flow in V-shaped conduits or corners [93, 94, 95]. In the case of the filling of rectangular conduits, it is interesting to compare this equation with the Laplace-Young equation derived considering the pressure generated by opposing channel walls, Eq. 1.4. For perfectly wettable walls, the case of a corner with a  $90^\circ$  angle between the two surfaces, Fig. 1.5a, leads to a two-fold pressure decrease for  $w = d$ ,  $d$  being the distance separating two parallel surfaces. Further, the sign of the equation reverses for  $\theta > 45^\circ$ , as can be deduced from Fig. 1.5. A conduit with walls displaying a  $45^\circ$  contact angle with the liquid still fills by capillary action, Eq. 1.4, but the corner-flow does not contribute to the filling pressure anymore. The comparison of the pressure between two parallel surfaces and a corner is shown in Fig. 1.6.

This ratio only compares the force, without taking into account the volume contained in the cross-section defined by the parallel plates and the corner. For the most favorable case ( $\theta = 0$ ) in a channel with a square cross-section, corner and parallel surfaces generate the same pressure for  $d = 4w$  ( $2 \times 2$  parallel surfaces), and the total volume contained in the square cross-section is  $\approx 40$  times the volume contained in the 4 corners. Moreover, the friction does increase highly non-linearly with the apparent cross-section, which indicates that the contribution of the corners is negligible in the calculation of the total flow rate. The corners can nevertheless determine the manner with which the liquid fills a network of chan-

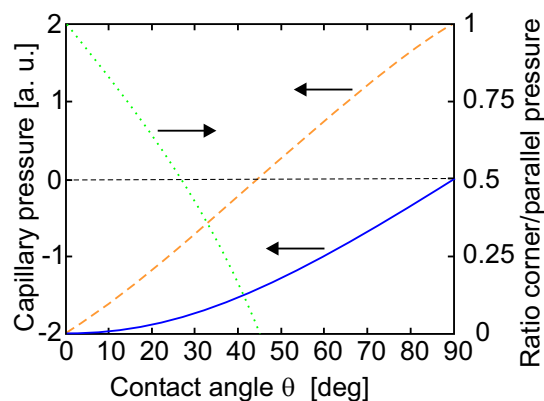


Figure 1.6: The meniscus pressure of two parallel surfaces separated by a distance  $d = 2w$  (plain line) and of the two same surfaces forming a  $90^\circ$  corner wetted on a length  $w$  (dashed line), as function of the contact angle  $\theta$  of the liquid with the surface. For  $\theta = 0$ , the pressure is equal for the corner and the parallel surface. For increasing contact angle  $\theta$ , the corner pressure reaches zero for  $\theta = 45^\circ$ , and becomes increasingly positive (liquid repellent) for  $\theta > 45^\circ$ . The ratio of corner-pressure/parallel-surface-pressure is reported on the right axis (dotted line) between  $0^\circ$  and  $45^\circ$ .

nels or a conduit with irregular cross-section [70], because they can help overcome geometrical flow-stop valves like the one drawn in Fig 1.3d. It is interesting to compare the contribution of the corner-flow to the one of the surface roughness in such a case. A comprehensive hydrodynamic description of the filling of a rectangular channel by the flow generated by the parallel surfaces, the corner-flow and the roughness-flow has never been derived to the best of our knowledge. This problem is complicated because of the mutual dependence of bulk-flow and the two secondary flows on each other, and the importance of the viscous dissipation forces not only in

the bulk of the flow, but precisely at the filling front (which can only be accounted for by lubrication theories) of *a priori* unknown shape. These effects become negligible as the length of the filled length in the channel increase, and friction due to the bulk viscosity totally predominates.

### 1.4.2 The viscosity of fluids

The empiric equation linking the local force in a liquid to the local velocity gradient is called Newton's Law of viscosity

$$T_{yx} = -\eta \frac{dv_x}{dy}, \quad (1.6)$$

where  $T_{yx}$  is the shear force in  $x$  direction on a unit area perpendicular to the  $y$  direction,  $dv_x/dy$  is the speed variation in  $x$  direction along the  $y$  axis, and  $\eta$  is an empirical constant of proportionality called the *viscosity* of the liquid and has units of [Pa·s]. It has been found that this equation adequately describes the flow behavior of both gases and liquids with a molecular weight of less than about 5000 [96]. In fluids with constant viscosity, that is independent of pressure and shear stress the rate of deformation is proportional to the applied stress. Such liquids are defined as being Newtonian, and both water and ethanol for example belong to this category.

### 1.4.3 Principles of liquid flow under applied force

In solid mechanics, a force exerted on an elementary cube can be related to compression (in  $xx$ ,  $yy$ , and  $zz$ ) and shear (in  $xy$ ,  $zx$ , and  $zy$ ) stresses. A set of 6 equations (the tensor of deformation) further relates these stresses to the 6 deformations

( $xx$ ,  $yy$ ,  $zz$ ,  $yz$ ,  $zx$ , and  $xy$ ) [97]. These equations relating force to deformation ( $\equiv$  strain) would be highly useful when describing the reaction of fluids to an applied force. The behavior of an elementary cube of fluid subjected to a force is much more difficult, because here these forces result not in a deformation, but in a rate of deformation. With the assumption that the fluid is incompressible, the stresses can be related by 6 equations (with  $\eta$  being the proportionality factor) to the deformation rate, which for compression in  $x$  takes the form  $\tau_{xx} \propto \eta \frac{\partial}{\partial x} \left( \frac{dx}{dt} \right)$ <sup>1</sup>. To the 6 linear equations in solids thus corresponds a set of 6 differential equations in incompressible fluids. These relations allow writing the general differential transport equations that describe the balance between force and momentum as three differential equations of the second order that describe all three components of the flow speed  $\frac{dx}{dt}$ ,  $\frac{dy}{dt}$ , and  $\frac{dz}{dt}$ . These equations are called the *Navier–Stokes equations* after the two scientists who helped establish them (Louis Marie Henri Navier, 1785–1836 and George Gabriel Stokes, 1819–1903) and can be found in standard fluid mechanics textbooks [98, 89]. A general solution to these equation has not been derived and they need to be solved case by case taking into account the particular flow conditions.

---

<sup>1</sup>For incompressible fluids, the conservation of mass, which is described by the equation of continuity, takes the simple form  $\text{div } \mathbf{v} = 0$ . It implies that a volume entering an elementary cube is compensated by a volume that exits it. This equation, in conjunction with the proportionality constraint  $\eta$  allows writing the equations that connect stress to deformation rate in the discussed form.

### 1.4.4 Flow of liquid in a conduit

The hydrodynamic solution describing the flow of liquid in a conduit can be derived from solving the *Navier–Stokes equations*. The boundary condition for pressure driven flow, which is necessary to solve these equations, is defined by the *no-slip* condition as  $v = 0$  at the walls. The solution for steady laminar flow (where mass and momentum can be neglected) in a circular tube that is positioned horizontally (gravity can be neglected too) is known as *Poiseuille* flow. The speed  $v = \frac{dx}{dt}$  of flow is

$$v(r) = \frac{\Delta P}{4L\eta} (R^2 - r^2), \quad (1.7)$$

where  $r$  is the position in the conduit measured from the center,  $R$  the radius of the conduit,  $L$  the length of the conduit, and  $\Delta P$  the difference in pressure between the inlet and outlet of the conduit. Characteristic of Poiseuille flow is a parabolic profile of the speed with a maxima in the center ( $r = 0$ ). For small capillaries, the effect of mass and momentum are negligible versus the viscous friction forces, and their flow profile is therefore of Poiseuille-type. This assumption will be justified in §1.4.6

The no-slip condition, albeit being a fundamental and century old tenet of fluid mechanics, has recently been found not to hold for Newtonian liquids (it was already known for high-molecular weight polymers that slip at the surface could occur) under high shear stresses [102]. This effect is nevertheless small and should not markedly alter the flow distribution in our case. It should be interesting to find out if

impurities affect the slip and, conversely, if slip has an effect on the adsorption of molecules on the walls.

### 1.4.5 Flow-rate resistance of a conduit

The flow rate in a capillary is the integral of the flow speed, expressed in Eq. 1.7, over the cross-section. For a circular conduit the flow rate  $D$  is

$$D = \frac{\Delta P}{8\eta} \frac{\pi R^4}{L} \equiv \frac{\Delta P}{8\eta} \frac{A R_H^2}{L}, \quad (1.8)$$

where  $A$  is the cross-sectional area of the channel, and  $R_h$  is the hydraulic radius defined as  $R_h = 2A/P$  with  $P$  being the perimeter of the conduit. The  $R^4$  dependency of this equation is characteristic of laminar flow in circular capillaries. The geometric and constant parameters can be grouped for convenience into a unique parameter that we call the flow-rate resistance  $R_{FR}$ ,

$$R_{FR} = \left[ \frac{1}{8} \frac{\pi R^4}{L} \right]^{-1} \equiv \left[ \frac{1}{8} \frac{A R_H^2}{L} \right]^{-1}. \quad (1.9)$$

When filling a conduit by capillary action, the parameter  $L$  corresponds to the filled length of the channel, and thus  $R_{FR}$  continuously increases with the advancement of the filling front of the liquid in the conduit.

The microchannels we fabricated for this work were rectangular in cross-section, however, and the flow-rate resistance of such microchannels is not trivial to calculate, but it can be expressed as

a Fourier series for different aspect ratios from depth  $d$  to width  $w$  [88]:

$$R_{FR} = \left[ \frac{A w^2}{12} \left\{ 1 - \frac{3w}{d} \frac{64}{\pi^5} \times \sum_{n=1}^{\infty} \frac{\tanh\left(m(n, w) \frac{w}{2}\right)}{(2n-1)^5} \right\} \right]^{-1} \quad (1.10)$$

where  $m(n, w) = \frac{\pi}{w}(2n-1)$ . This formula is impractical, and we have therefore derived a first-degree approximation which converges with the exact value for the aspect ratio  $d/w$  (or  $w/d$ ) tending towards zero, and deviating by no more than 10% for any other aspect ratio. It allows writing the friction factor as

$$R_{FR} = \left[ \frac{1}{12} \left( 1 + \frac{5a}{6b} \right) \frac{A R_h^2}{L} \right]^{-1}, \quad (1.11)$$

where  $a$  and  $b$  are either width or depth to satisfy the condition  $b \geq a$ . The difference between a circular cross-section, Eq. 1.9, and a rectangular cross-section, Eq. 1.11, becomes obvious.

#### 1.4.6 Dynamics of capillary flow in a microchannel

The dynamic filling of a capillary conduit of constant cross-section by sole capillary pressure has first been solved by Washburn in 1921 [99]. For the case of complicated geometries it is convenient to write the mass flow-rate of liquid  $D$  of the microfluidic system as function of the overall flow-rate resistance  $R_{FR}$  and the differential pressure between inlet and outlet  $\Delta P$

$$D = \frac{1}{\eta} \frac{\Delta P}{R_{FR}}. \quad (1.12)$$

The total  $R_{FR}$  of a system with varying cross-sections can be calculated as the sum of the different parts of constant cross-sections, according to Eq. 1.11. The instantaneous  $D$  during filling by capillary action can also be calculated by replacing  $\Delta P$  with the pressure generated at the liquid meniscus (which also depends on the position for channels of varying cross-sections or surface chemistry), according to Eq. 1.4, divided by  $R_{FR}$  as function of the filled channel-length.

The average flow-speed in the microchannel is calculated by dividing  $D$  by the cross-sectional area  $A$  of the channel at the position of interest. The flow-speed for a very wide conduit  $w \gg d$  (only the depth  $d$  generates considerable capillary pressure), with totally wettable surfaces (the contact angle at the walls  $\theta = 0^\circ$ ) is

$$v = \frac{\gamma}{4\eta} \frac{2R_H}{L}. \quad (1.13)$$

The flow-speed in a microchannels for constant driving forces scales  $\propto R_H^2$ , but because the meniscus pressure scales as  $\propto 1/R_H$ , overall the scaling factor is  $\propto 1/R_H$  for capillary flow. When relying on external actuation, down-scaling of the cross-section requires increasingly high pressures to maintain the flow speed, which becomes increasingly difficult to achieve because of the outside world connections and the joints which are susceptible to leakage. Capillary systems are particularly easy to scale because (i) the pumping pressure originates within the system itself and scales favorably with smaller dimensions, (ii) there are no cumbersome connections, (iii) both cross-section and length can be reduced to the same proportion and maintain the flow speed<sup>2</sup>

<sup>2</sup>The electro-osmotic flow in electro-kinetic

The Reynolds number measures the ratio between inertial forces and viscous forces

$$Re = \frac{2R_H \rho v}{\eta}, \quad (1.14)$$

where  $\rho$  is the density of the fluid and  $v$  the average speed over the cross-section. This equation is an indicator for the flow regime, which can be either turbulent or laminar (if  $Re < 2000$ ). In capillary flow systems like the ones we use, the Reynolds number is usually  $Re < 1$ , and therefore totally precludes turbulences, and *a posteriori* justifies the assumption of laminar flow in §1.4.4.

Washburn found in his original equation that the filled length of channel scales with the time  $t$  as  $\propto \sqrt{t}$ . This relation proved to be universal for the filling by capillary action of all kinds of conduits having circular, rectangular, triangular, or arbitrary shape [92, 93, 94], and both for open conduits and closed conduits, provided that the cross-section is constant. The universality of this square-root-relation can qualitatively be explained as follows: The filling pressure is different for each channel, but remains constant while the flow resistance linearly increases with the filled length irrespective of the geometry of the cross-section because the flow is laminar, and hence results in an identical scaling factor.

The scaling of the most important hydraulic parameters, which need to be considered when designing a microfluidic CS,

---

microfluidic systems originates at the surfaces, and the resistance does not depend on the cross-section. Here, the integration is rather limited by electrical and fluidic chip-to-world connections, and by the desktop size equipment required to operate them [3, 23, 24].

are resumed in Table 1.1.

The implications of the strictly laminar flow at the microscale as revealed by the small Reynolds number is important for chemical reactions because active mixing of reagents is rendered difficult. In large vessels, simple stirring is efficient for mixing because it can “fold liquid layers” by turbulent flow, and achieves mixing times in the range of minutes. At the microscale, the volumes are typically between 3 and 9 orders of magnitude lower, and for mass-throughput not to be compromised, the mixing needs to be speeded up by a few orders of magnitude. However, turbulent “folding” of “liquid layers” is not accessible at the microscale, because the viscosity of the liquid that acts as a damper, and renders mixing of chemicals an increasingly tough problem as size reduces. Therefore, “diffusion as only *mixing force*” becomes increasingly true as the scale and volume of liquid diminish.

## 1.5 Diffusion & depletion of reactants in a microchannel

At ambient temperature, thermal agitation reveals itself on small colloidal particles solved in a fluid by erratic motion, which is the result of the collisions of these particles with the molecules of the medium and with each other. This phenomena, called Brownian motion was discovered in the 18th century<sup>3</sup> and can readily be observed with a microscope on

---

<sup>3</sup>The phenomena had first been discovered by a Dutch scientist (Jan Ingenhousz) but was revealed to the scientific community by the botanist R. Brown who published the results of his observations in 1828 [100].

Table 1.1: Scaling of the hydraulic parameters for a cube and a 10-mm-long microchannel with a quadratic cross-section of side  $\mathbf{d}$ . <sup>1</sup>The meniscus pressure is calculated for pure water with a surface tension  $\gamma = 70 \text{ mN m}^{-1}$  and assuming a contact angle  $\theta = 0^\circ$  of the liquid with the walls. <sup>2</sup>The  $R_{FR}$  is calculated for pure water with a viscosity  $\rho = 1 \text{ mPa s}$ . <sup>3</sup>The mass flow rate and speed are calculated neglecting mass and inertia, hence the unrealistic values for the two widest channels.

Dimension $\mathbf{d}$	Meniscus pressure <sup>1</sup> [Pa]	Cube	Microchannel (10 mm long)			
		$R_{FR}$ <sup>2</sup> [mm <sup>-3</sup> ]	$R_{FR}$ <sup>2</sup> [mm <sup>-3</sup> ]	Mass flow rate <sup>3</sup> [ $\mu\text{l s}^{-1}$ ]	Flow speed <sup>3</sup> [mm s <sup>-1</sup> ]	Reynolds number <sup>3</sup> Re
10 mm	$2.8 \cdot 10^1$	$6.5 \cdot 10^{-3}$	$6.5 \cdot 10^{-3}$	$4.3 \cdot 10^6$	43'000	$4.3 \cdot 10^5$
1 mm	$2.8 \cdot 10^2$	6.5	$6.5 \cdot 10^1$	$4.3 \cdot 10^3$	4300	$4.3 \cdot 10^3$
0.1 mm	$2.8 \cdot 10^3$	$6.5 \cdot 10^3$	$6.5 \cdot 10^5$	4.3	430	$4.3 \cdot 10^1$
0.01 mm	$2.8 \cdot 10^4$	$6.5 \cdot 10^6$	$6.5 \cdot 10^9$	$4.3 \cdot 10^{-3}$	43	$4.3 \cdot 10^{-1}$
1 $\mu\text{m}$	$2.8 \cdot 10^5$	$6.5 \cdot 10^9$	$6.5 \cdot 10^{13}$	$4.3 \cdot 10^{-6}$	4.3	$4.3 \cdot 10^{-3}$
100 nm	$2.8 \cdot 10^6$	$6.5 \cdot 10^{12}$	$6.5 \cdot 10^{17}$	$4.3 \cdot 10^{-9}$	0.43	$4.3 \cdot 10^{-5}$
10 nm	$2.8 \cdot 10^7$	$6.5 \cdot 10^{15}$	$6.5 \cdot 10^{21}$	$4.3 \cdot 10^{-12}$	0.043	$4.3 \cdot 10^{-7}$

micrometer-sized polystyrene beads in solution. Chemical species placed as a concentrated drop in a solution will slowly move from a region of high concentration to a region of low concentration because of Brownian motion at the molecular level, until the molecules are homogeneously distributed. This process is diffusion and in thermodynamic terms, the system tends towards the state of maximal entropy. The average distance  $x$  the fictive interface drop-solution moves as function of time is given by Einstein's diffusion equation [101]:

$$x(t) = \sqrt{D_n t}, \quad (1.15)$$

where  $D_n$  is the diffusion coefficient of the element  $n$  in the medium. This equation

indicates that by reducing the distance (= scale) by a factor  $m$ , the time for a molecule to diffuse this distance is reduced by a factor  $m^2$ . If the reaction kinetics are fast enough, the speed of the reaction increases proportionally to the reduction of the distance that needs to be overcome by diffusion. This equation thus provides a practical rule of thumb to design the reaction chambers. The reactions often take place under flow conditions where the reagents are continuously resupplied and exchanged in the reaction chamber. The ratio of transport by convection due to the flow and by diffusion is expressed with the Péclet number

$$Pe = \frac{2R_H v}{D_n}. \quad (1.16)$$

For high-yield reactions under laminar flow conditions the Péclet number needs to be kept sufficiently low so that the reagents can interact before they have been flushed out of the reaction chamber.

### 1.5.1 Diffusion in a micro-channel

The distribution of reagents can be calculated precisely and is useful for a more detailed understanding of the mass transport in the microchannels. The bio/chemical processes we performed were mostly reactions taking place at one of the liquid-solid interfaces within the rectangular microchannel, such as adsorption or immunocomplexation of an immunoglobulin G (IgG) antibody with a conjugate molecule. We were therefore particularly interested to calculate the detailed kinetics of the diffusion of a chemical species from the channel to the walls, which was first done in the simpler case of a one-dimensional channel because the concentration distribution within such a channel of width  $w$ , where the two side-walls are suddenly removed can be solved analytically. The concentration  $n$  of the reactants in solution takes the form of a Gaussian function:

$$n(x, t) = \frac{n_0}{\sqrt{4\pi D_n t}} \times \int_0^w \exp\left[-\frac{(x-x_0)^2}{4D_n t}\right] dx_0, \quad (1.17)$$

where  $x$  is the position in the channel,  $t$  the time,  $n_0$  is the concentration at  $x = 0$  and  $t = 0$ , and  $x_0$  the integration parameter. The case of “sticky walls” is

more realistic of a channel where molecules adsorb. A molecule in solution reaching a sticky surface has a certain probability to adsorb to this surface, which can be modeled as the sticking coefficient. In our model, this probability is chosen to be constant without consideration of how many molecules have already adsorbed previously, and we set the sticking coefficient = 1, which consequently fixes the concentration of molecules in solution at the wall-boundary to be  $n = 0$ . The diffusion problem with such boundary conditions is more complicated, but has also been solved [103]. The distribution of antibodies in one-dimensional channels of different sizes filled with aqueous solutions can be calculated for the case where the walls are suddenly removed and for the case where the walls suddenly become sticky. The results for a diffusion and an adsorption time of 10 s, respectively, using the diffusion constant for antibodies reported in literature ( $D_n = 40 \mu\text{m}^2\text{s}^{-1}$  [48]) are shown for three different channel-sizes in Fig. 1.7.

The effect of the sticky walls is flagrant. As a first approximation, the case of a rectangular channel can be modelled as the superposition of two one-dimensional cases in the  $x$  and  $y$  directions, and the transport kinetics are qualitatively identical to the one-dimensional case. The percentage of the initial amount of molecules adsorbed on the sticky walls of a two-dimensional channel after 10 s as function of the width of the channel is reported in Fig. 1.8.

In practice the adsorbed proteins slowly cover the walls however, and make further adsorption of molecules less likely. A comprehensive solution to the surface reaction kinetics takes into account sur-



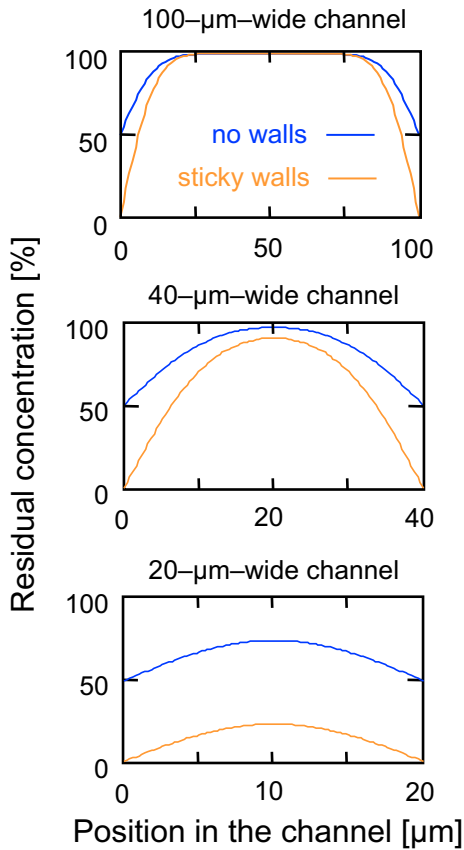


Figure 1.7: Residual concentration of molecules in a solution in a one-dimensional channel 10s after removing the sidewalls (blue line) or after sticking onto the walls (sticking coefficient = 1) has been initiated (orange line), for three different channel widths.

face coverage, Langmuir adsorption (or capture) and desorption (or release) rates, equilibrium constants, and the inhomogeneous replenishment of the conduit because of the flow profile. This imposes either simplifications to allow an analytical solution to the problem [104] or resorting to finite element models, which can only be performed with a computer [105].

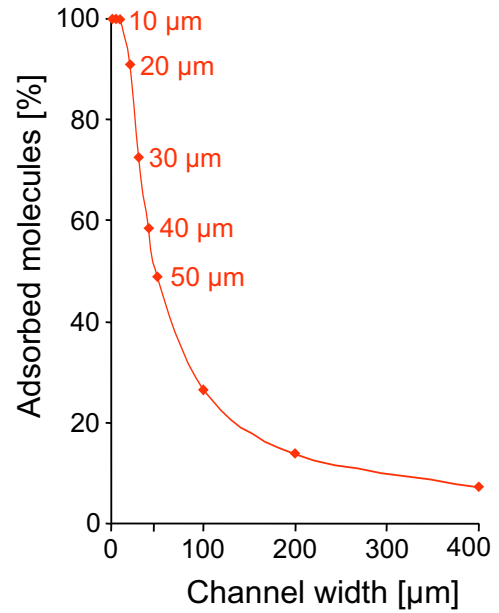


Figure 1.8: Molecules adsorbed on the sticky walls (sticking coefficient = 1) of a two-dimensional channel after 10 s as function of the width of the channel. For decreasing channel size, the amount of adsorbed molecules rapidly increases until it reaches 100%.

## 1.5.2 The diffusion barrier

As discussed previously, the last few micrometers separating two reactive species cannot be overcome by mixing but only by diffusion and we call it therefore the *diffusion barrier*. The “height” of the diffusion barrier essentially depends on the distance ( $\sim$  scale) that separates the two species, their mobility, the viscosity of the medium, and implicitly on temperature. The distance is the only parameter that we can address by design to try improving the speed of encounter of reactive molecules (viscosity and temperature cannot be widely tuned, mobility however can effectively be enhanced using ultrasonic waves [106], but is not further discussed here). Considering the typical diffusion

coefficients of biomolecules in aqueous solutions of a few tens of  $\mu\text{m}^2 \text{s}^{-1}$ , a short mixing time imposes sub-ten-micrometer length scales, considering the typical diffusion constants and Eq. 1.15. “Folding” or “fingering” of “liquid layers” can be achieved at the microscale by superposing a flow-field in a direction that is different from the direction of flow, or by generating a flow instability that gives rise to so-called chaotic mixing because a small change in the initial conditions results in widely different final states. Mixing thus can be enhanced using a cyclic pump in a lateral side channel, by superposing pressure flow and EOF at a channel-widening [107], by applying a rapidly alternating electrical field [108], by relying solely on a complicated three-dimensional geometry of the flow path [109], or on a surface structure patterned in the microchannel [110]. The most elegant solution is probably to design a serpentine channel short-cut with smaller channels of different lengths at various positions [111]. These “folding” and “fingering” strategies can efficiently reduce the diffusion barrier, but also require time to do so. The most direct approach is to simply reduce the dimensions of the mixing distance to a few tens-of-micrometers, which is the only possibility to increase the mass transport to a solid surface of a microchannel for instance. But the flow rate in the channel is  $\propto R^4$ , or  $\propto d^3$  in the case of a rectangular microchannel with  $w \gg d$ , and by reducing the channel diameters below a few tens-of-micrometers, the time to flush say 1  $\mu\text{l}$  quickly increases to impractical values. For liquid-liquid mixing, the local scale reduction can be compensated for by an arborescent architecture [28], and effective mixing of two liq-

uids can be done by merging the two flow paths at their smallest branches, or by injecting small plumes of one liquid into the another through arrays of micronozzles. Fast mixing at large flow rates can be achieved, but at the expense of surface area and of three-dimensional flow paths on multiple levels. In light of the figures of merit of the different mixing strategies mentioned above, conciliating miniaturization with high throughput (without resorting to excessive parallelization or excessive surface area) remains a perplexing challenge. Because our applications involved solid-phase reactions, the flow rate was optimized for the given reaction chamber and for either minimizing reagent consumption or maximizing reaction speed, depending on the requirements.

### 1.5.3 Depletion of reagents in a microchannel

The increase in surface/volume ratio at the microscale becomes a barrier for achieving dense coverage of the solid surface with molecules from the solution. For increasingly small channels, the own-volume of the channel is insufficient, and replenishment with fresh solution and reagents becomes necessary to achieve, for example, high and homogeneous surface coverage of adsorbed molecules. The diffusion and depletion issues associated with scaling are resumed in Table 1.2.

The simplest way to resupply a reaction chamber is to extend the flow path further, which will ensure continuous flow until this channel extension is completely filled too. Sometimes large volumes may be necessary, but a large cavity appended to the flow path is not effective, because

Table 1.2: Scaling of the parameters governing diffusion and depletion in a cube. <sup>1</sup>The volume is a cube here. <sup>2</sup>The volume of a water molecule is  $3.1 \text{ \AA}^3$ , and a cubic shape was assumed for this calculation. <sup>3</sup>The diffusion coefficient is  $D_n = 40 \mu\text{m}^2 \text{ s}^{-1}$ . <sup>4</sup>The number of monolayers that can be formed on one face of the cube if all molecules adsorb on it. The area of 1 molecule was fixed as  $10 \times 10 \text{ nm}^2$ , which is of the same order than an IgG antibody.

dimension	volume	surf./vol <sup>1</sup>	surf./vol.	time for	number of	number of
<b>d</b>	<b>d<sup>3</sup></b>	<b>d<sup>-1</sup></b>	water	diffusion <sup>3</sup>	molecules	monolayers <sup>4</sup>
	[mm <sup>3</sup> ]	[mm <sup>-1</sup> ]	molecules <sup>2</sup>	of <b>d</b> [s]	at 1 $\mu$ M	at 1 $\mu$ M
1 m	1 10 <sup>9</sup>	0.006	1.9 10 <sup>-9</sup>	2.5 10 <sup>10</sup>	6 10 <sup>17</sup>	60000
1 dm	1 10 <sup>6</sup>	0.06	1.9 10 <sup>-8</sup>	2.5 10 <sup>8</sup>	6 10 <sup>14</sup>	6000
1 cm	1 10 <sup>3</sup>	0.6	1.9 10 <sup>-7</sup>	2.5 10 <sup>6</sup>	6 10 <sup>11</sup>	600
1 mm	1	6	1.9 10 <sup>-6</sup>	2.5 10 <sup>4</sup>	6 10 <sup>8</sup>	60
0.1 mm	1 10 <sup>-3</sup>	60	1.9 10 <sup>-5</sup>	2.5 10 <sup>2</sup>	6 10 <sup>5</sup>	6
0.01 mm	1 10 <sup>-6</sup>	600	1.9 10 <sup>-4</sup>	2.5	6 10 <sup>2</sup>	0.6
1 $\mu$ m	1 10 <sup>-9</sup>	6000	1.9 10 <sup>-3</sup>	2.5 10 <sup>-2</sup>	6 10 <sup>-1</sup>	0.06
100 nm	1 10 <sup>-12</sup>	60'000	1.9 10 <sup>-2</sup>	2.5 10 <sup>-4</sup>	6 10 <sup>-4</sup>	0.006

the capillary pressure it generates is too low to draw the liquid through the small conduits upflow with high flow resistance. To increase the capillary pressure it becomes necessary to substructure the flow promotion unit which is also termed capillary pump. When there are several reaction chambers and CSs placed close to each other, an arborescent structure provides an optimal solution that maximizes the volume versus the surface occupied, Fig. 1.9.

On the other hand, partial replenishment at controlled flow speed can be tuned to create the desired gradient of surface coverage of adsorbed molecules and is described in Chapter 4.

## 1.6 Design of capillary microfluidic systems

The parameters that determine the efficiency of a specific bio/chemical process are: (i) the volume, (ii) the concentration, (iii) the depletion, (iv) the diffusion coefficients of the reactants, and (v) the reaction constants, the relations of which have been resumed in table 1.2. A capillary microfluidic system can be optimized for a specific process by tuning the (i) geometry and the (ii) surface chemistry of the conduits, which will define (iii) the capillary pressure and (iv) the flow resistance, and implicitly determine (iv) the flow rate as well as (v) the flow profile for a particular solution delivered to the system and drawn through the reaction cham-

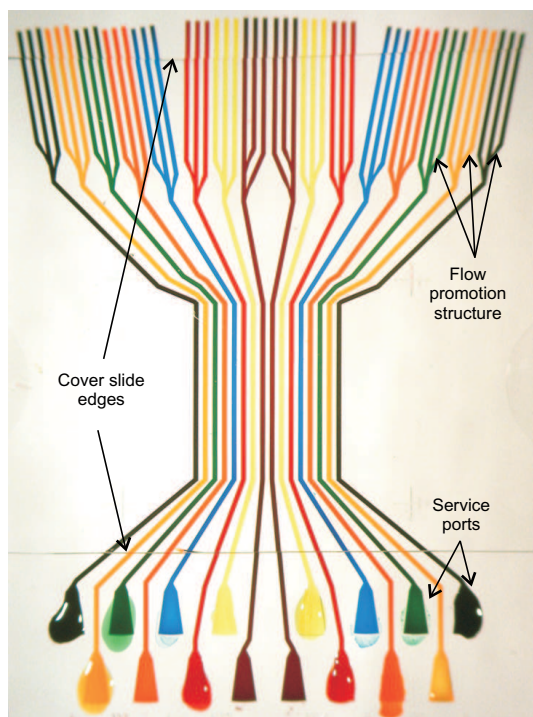


Figure 1.9: Photograph of an array of 16 microfluidic systems. The colored aqueous solutions that were supplied with a pipette to their service ports were drawn into the microchannels, the reaction chambers (defined as the zone where the channels run in parallel), and into the flow promotion structures by capillary action. These structures are composed of threefold branches that generate both a large volume and considerable capillary pressure, and are optimized to occupy as little area as possible around the reaction zone. The capillary structures can continuously resupply the reaction zones of the microsystem with liquid until the structures are completely filled.

bers. The fundamental relations linking these parameters have been resumed in table 1.1. The optimization of a CS for a particular bio/chemical process necessitates the consideration of all of the above-mentioned parameters.

The fabrication and the basic properties and possibilities of our microfluidic CSs are illustrated in Chapter 2 and 3, whereas advanced patterning applications are described in Chapter 4 and 5.

### 1.6.1 Advanced capillary systems

Equation 1.11 of the flow rate ( $D \equiv$  liquid current) is reminiscent of the fundamental electrical relation linking electrical current  $I$ , tension  $U$ , and resistance  $R$ :  $I = U/R$ . In analogy to electrical circuits, a  $R_{FR}$  can also be attributed to an arbitrary section of the microfluidic system. The total  $R_{FR}$  of several sections in a series can be calculated by simply adding the  $R_{FR}$  of each individual one. The resistance of different sections running in parallel can, like in the electrical case, be calculated as  $1/R_{A//B} = (1/R_A) + (1/R_B)$ . This allows the  $R_{FR}$  of a complex system to be calculated [31, 77, 112, 113], and, importantly, this analogy evidently also holds for systems made up of interconnected microfluidic networks. The synchronization of capillary pressure and resistance – both are linked but can be tailored independently (within a limited range) by subdividing a channel or by varying its length for example – of different parts of a capillary system should open the possibility of advanced microfluidic operations.

In Chapter 6, we introduce advanced microfluidic operations, namely the autonomous transport of multiple liquids, and demonstrate it. This demonstration is extended to a basic interconnection scheme where four autonomous microfluidic CSs are linked to a single capillary structure that acts as a secondary pump.

# Bibliography

- [1] Manz, A., Graber, N. & Widmer, H.M. Miniaturized total chemical analysis systems: a novel concept for chemical sensing. *Sens. Actuators B* **10**, 244-248 (1990).
- [2] Manz, A. & Becker, H. *Microsystem technology in chemistry and life science* (Springer, Berlin, 1998).
- [3] van den Berg, A., Olthuis, W. & Bergveld, P. *Proceedings of the  $\mu$ TAS 2000 symposium*, Enschede, NL. *Micro total analysis systems 2000* (Kluwer Academic Publishers, Dordrecht, 2000).
- [4] Ramsey, M. & van den Berg, A. *Proceedings of the  $\mu$ TAS 2001 symposium*, Monterrey, USA. *Micro total analysis systems 2001* (Kluwer Academic Publishers, Dordrecht, 2001).
- [5] Stryer, L. *Biochemistry* (W. H. Freeman and Company, New York, 4th. Ed., 1995).
- [6] Senturia, S.D. *Microsystem design* (Kluwer Academic Publishers, Dordrecht, 2001).
- [7] Gad-el-Hak, M. *The MEMS handbook* (CRC Press, Boca Raton, 2001).
- [8] Vickers, L. *Guide to diagnostic rapid test device components*, 2nd. Ed. (Schleicher & Schuell, Keene, USA, 2000).
- [9] See <http://www.clearblue.org.uk/>
- [10] Columbus, R. & Palmer, H.J. "Architextured" fluid management of biological liquids. *Clin. Chem.* **33**, 1531-1537 (1987).
- [11] Lilja, J.E. & Lennart, S.E. Apparatus for sampling, mixing the sample with a reagent and making particularly optical analysis. US patent no 4 088 448, filed 1976.
- [12] Columbus, R. Liquid transport device and method. US patent no 4 233 029, filed 1979.
- [13] Bassous, E., Taub, H.H. & Kuhn, L. Ink jet printing nozzle arrays etched in silicon. *Appl. Phys. Lett.* **31**, 135-137 (1977).
- [14] Terry, S.C., Jerman, J.H. & Angell, J.B. A gas chromatographic air analyzer fabricated on a silicon wafer. *IEEE Electron Device Lett.* **ED-2**, 126-129 (1979).
- [15] Hosokawa, K., Fujii, T. & Endo, I. Handling of picoliter liquid samples in a poly(dimethylsiloxane)-based microfluidic device. *Anal. Chem.* **71**, 4781-4785 (1999).

- [16] Schena, M., Shalon, D., David, R.W. & Brown, P.O. Quantitative monitoring of gene expression patterns with a complementary DNA microarray. *Science* **270**, 467-470 (1995).
- [17] Brenner, S. *et al.* Gene expression analysis by massively parallel signature sequencing (MPSS) on microbead arrays. *Nat. Biotech.* **18**, 632-634 (2000).
- [18] Adessi, C., Matton, G., Ayala, G., Turcatti, G., Mermoud, J.-J., Mayer, P. & Kawashima, E. Solid phase DNA amplification: characterisation of primer attachment and amplification mechanisms. *Nucleic Acids Res.* **28**, e87.
- [19] Zhu, H. *et al.* Global analysis of protein activities using proteome chips. *Science* **293**, 2101-2105 (2001).
- [20] Whitesides, G.M. & Stroock, A.D. Flexible methods for microfluidics. *Physics Today*, June 2001, 42-48.
- [21] Dertinger, S.K.W., Chiu, D.T., Jeon, N.L., & Whitesides, G.M. Generation of gradients having complex shapes using microfluidic networks. *Anal. Chem* **73**, 1240-1246 (2001).
- [22] Ruciszka, J. Microflow analysis based on sequential and bead injection. In Ref. [3], pp. 1-10.
- [23] Kopf-Sill, A. Commercializing lab-on-a-chip technology. In Ref. [3], pp. 233-238.
- [24] Knapp, R., Kopf-Sill, A., Dubrow, R., Chow, A., Chien, L.-R., Chow, C., Parce, W. Commercialized and emerging lab-on-a-chip applications. In Ref. [4], pp. 7-9.
- [25] van Lintel, H.T.G., van de Pol, F.C.M. & Bouwstra, S.A. Piezoelectric micropump based on micromachining of silicon. *Sens. Actuators* **15**, 153-167 (1988).
- [26] van der Schoot, B.H., van den Berg, A., Jeanneret, S., de Rooij, N. & Grisel, A.A. A miniaturized chemical analysis system using two silicon micropumps. *Proceedings IEEE Transducers 91* San Francisco, CA (New York IEEE, 1991), pp. 789-791.
- [27] Manz, A., Fettingner, J.C., Verpoorte, E., Harrison, D.J., Ludi, H. & Widmer, H.M. Design of integrated electroosmotic pumps and flow manifolds for total chemical analysis systems. *Proceedings MME 90* (Berlin, 1990), pp. 127-132.
- [28] Guenat, O.T., Ghiglione, D., Morf, W.E., & de Rooij, N.F. Partial electroosmotic pumping in complex capillary systems: Part 2: Fabrication and application of a micro total analysis system (TAS) suited for continuous volumetric nanotitrations. *Sens. Actuators B* **72**, 273-282 (2001).
- [29] McKnight, T.E., Culbertson, C.T., Jacobson, S.C. & Ramsey J.M. Electroosmotically induced hydraulic pumping with integrated electrodes on microfluidic devices *Anal. Chem.* **73**, 4045-4049 (2001).

- [30] Takamura, Y., Onoda, H., Inokuchi, H., Adachi, S., Oki, A. & Horiike, Y. Low-voltage electroosmosis pump and its application to on-chip linear stepping pneumatic pressure source. In Ref. [4], pp. 230-231.
- [31] Weigl, B.H., Bardell, R., Schulte, T. & Williams, C., Passive microfluidics – ultra-low-cost plastic disposable lab-on-a-chips. In Ref. [3], pp. 299-302.
- [32] Hats, A., Kamholly, A.E., Hawkins, K.R., Munson, M.S., Schilling, E.A., Weigl, B.H. & Yager, P. A rapid diffusion immunoassay in a T-sensor. *Nat. Biotech.* **19**, 461-465 (2001).
- [33] Lemoff, A.V., Lee, A.P., Miles, R.R. & McConaghy, C.F. An AC magnetohydrodynamic pump. *Proceedings Transducers'99* (Sendai, Japan, 1999).
- [34] Leventis, N. & Gao, X. Magnetohydrodynamic electrochemistry in the field of Nd-Fe-B magnets. Theory, experiment, and application in self-powered flow delivery systems. *Anal. Chem.* **73**, 3981-3992 (2001).
- [35] Pérez-Castillejos, R., Estece, J., Acero, M.C. & Plaza, J.A. Ferrofluids for disposable microfluidic systems. In Ref. [4], pp. 492-494.
- [36] Böhm, S., Timmer, B., Olthuis, W. & Bergveld, P. A closed-loop controlled electrochemically actuated micro-dosing system. *J. Micromech. Microeng.* **10**, 498-504 (1998).
- [37] Rife, J.C. & Bell, M.I. Acousto- and electroosmotic microfluidic controllers. SPIE Conference on microfluidic devices and systems (Santa Clara, California, 1998). *Proc. SPIE* **3515**, 125-134 (1998).
- [38] Ajdari, A. Pumping liquids using asymmetric electrode arrays. *Phys. Rev. E* **61**, 45-48 (2000).
- [39] Beebe, D.J. Moore, J.S., Bauer, J.M., Yu, Q., Liu, R.H., Devadoss, C. & Jo, B.-H. Functional hydrogel structures for autonomous flow control inside microchannels. *Nature* **404**, 588-590 (2000).
- [40] Beebe, D.J., Moore, J.S., Yu, Q., Liu, R.H., Kraft, M.L., Jo, B.-H. & Devadoss, C. Microfluidic tectonics: A comprehensive construction platform for microfluidic systems. *Proc. Natl. Acad. Sci.* **97**, 13488-13493 (2000).
- [41] Aussillous, P. & Quéré, D. Liquid marbles. *Nature* **411**, 924-927 (2001)
- [42] Sundberg, S.A., Parce, J.W., Chow, C.Y.H. Microfabricated structures for facilitating fluid introduction into microfluidic devices. US patent no. 6 090 251, filed 1997.
- [43] Laurell, T., Wallman, L. & Nilsson, J. Design and development of a silicon microfabricated flow-through dispenser for on-line picolitre sample handling. *J. Micromech. Microeng.* **9**, 369-376 (1999).
- [44] Kim E., Xia Y., Whitesides G.M. Polymer microstructures formed by

- moulding in capillaries *Nature* **376**, 581-584 (1995)
- [45] Kim E., Xia Y., Whitesides G.M. Micromolding in capillaries: applications in materials science. *J. Am. Chem. Soc.* **118**, 5722-5731 (1996).
- [46] Yang, P., Rizvi, A.H., Messer, B., Chmelka, B.F., Whitesides, G.M. & Stucky, G.D. Patterning porous oxides within microchannel networks. *Adv. Mater.* **13**, 427-431 (2001).
- [47] Delamarche E., Bernard A., Schmid H., Michel B. & Biebuyck H. Delivery of immunoglobulins to surfaces using microfluidic networks. *Science* **276**, 779-781 (1997).
- [48] Delamarche E., Bernard A., Schmid H., Bietsch A., Michel B. & Biebuyck H. Microfluidic networks for chemical patterning of substrates: design and application to bioassays. *J. Am. Chem. Soc.* **120**, 500-508 (1998).
- [49] Bernard, A., Michel, B. & Delamarche, E. Micromosaic immunoassays. *Anal. Chem.* **73**, 8-12 (2001).
- [50] Burns, M. A. *et al.* An integrated nanoliter DNA analysis device. *Science* **282**, 484-487 (1998)
- [51] Andersson, H., van der Wijngaart, W., Griss, P., Niklaus, F. & Stemme, G. Hydrophobic valves of plasma deposited octafluorocyclobutane in DRIE channels. *Sens. Actuators* **75**, 136-141 (2001).
- [52] Zhao, B., Moore, J. S. & Beebe, D. J. Surface-directed liquid flow inside microchannels. *Science* **291**, 1023-1026 (2001).
- [53] Lam, P., Wynne, K.J. & Wnek, G.E. Surface-tension-confined microfluidics. *Langmuir* **18**, 948-951 (2002).
- [54] Johnson, R.D., Badr, I.H.A., Barrett, G., Lai, S., Lu, Y., Madou, M.J. & Bachas, L.G. Development of a fully integrated analysis system for ions based on ion-selective optodes and centrifugal microfluidics. *Anal. Chem.* **73**, 3940-3946 (2001).
- [55] Duffy, D.C., Gillis, H.L., Lin, J., Sheppard, N.F. & Kellogg G.J. Microfabricated centrifugal microfluidic systems: characterization and multiple enzymatic assays. *Anal. Chem.* **71**, 4669-4678 (1999).
- [56] McNeely, M.R., Spute, M.K. & Oliphant, A.R. Fluid circuit components based upon passive fluid dynamics. PCT international patent application number WO 00/22436, filed 1999.
- [57] Prins, M. W. J., Welters, M. W. J. & Weekamp, J. W. Fluid control in multichannel structures by electrocapillary pressure. *Science* **291**, 277-280 (2001).
- [58] Gallardo, B.S., Gupta, V.K., Eageron, F.D., Jong, L.I., Craig, V.S., Shah, R.R. & Abbot, N.L. Electrochemical principles for active control of liquids on submillimeter scales. *Science* **283**, 57-60 (1999).
- [59] Ichimura, K., Oh, S.K. & Nakagawa, M. Light-driven motion of liquids on



- a photoresponsive surface. *Science* **288**, 1624-1626 (2000).
- [60] Daniel, S., Chaudhury, M.K. & Chen, J. C. Fast drop movements resulting from phase change on a gradient surface. *Science* **291**, 633-636 (2001).
- [61] Kataoka, D.E. & Troian, S.M. Patterning liquid flow on the microscopic scale. *Nature* **402**, 794-797 (1999).
- [62] Darhuber, A.A., David, J.M., Reisner, W.W. & Troian, S.M. Thermo-capillary migration of liquids on patterned surfaces: Design concept for microfluidic delivery. In Ref. [4], pp. 244-245.
- [63] Goedecke, N. & Manz, A. Towards evaporation-driven HPLC on a chip: an alternative transport process for micro analysis systems. In Ref. [4], pp. 375-376.
- [64] Vykoukal, J., Schwartz, J.A., Becker, F.F. & Gascoyne, P.R.C. A programmable dielectrophoretic fluid processor for droplet-based chemistry. In Ref. [4], pp. 72-74.
- [65] Cho, S.K., Fan, S.-K., Moon, H. & Kim, C.-J. Towards digital microfluidic circuits: Creating, transporting, cutting and merging liquid droplets by electrowetting-based actuation. *Proceedings IEEE MEMS-02* conference (Las Vegas, NV, 2002), pp. 32-35.
- [66] See <http://www.advalytix.com>.
- [67] Taggi, A.J. & Walker, P. "Printing Processes" in *Encyclopedia of Chemical Technology*, Vol 20, Ed. Kirk, R.E. & Othmer, D.F. (New York: Wiley, 1996) p. 62.
- [68] Kipphan, H. *Handbuch der Printmedien: Technologien und Printverfahren* (Springer, Berlin, 2002).
- [69] Wong, P.Z., Flow in porous media: permeability and displacement patterns. *MRS Bulletin*, May 1994, 32-38.
- [70] Lenormand, R. & Zarcone, C. Role of roughness and edges during imbibition in square capillaries. *Tech. digest* 59th Annual tech. conf. and exhibition of the Society of Petroleum Engineers of AIME (Houston, Texas, 1984), SPE-13264.
- [71] Parker, A.R. & Lawrence, C.R. Water capture by a desert beetle. *Nature* **414**, 33 - 34 (2001).
- [72] Barthlott, W. & Neinhuis, C. Purity of the sacred lotus, or escape from contamination in biological surfaces. *Planta* **202**, 1-8 (1997).
- [73] Oertli, J.J. Der Saftaufstieg in Bäumen. *Vierteljahresschrift der Naturforschenden Gesellschaft in Zürich* **183/3**, 169-190 (1993).
- [74] Lösch, R. *Wasserhaushalt der Pflanzen* (Quelle & Meyer Verlag, Wiebelsheim, 2001).
- [75] Kramer, P.J. *Water relations of plants* (Academic Press, New York, 1983).
- [76] Kramer, P.J. & Boyer, J.S. *Water Relations of Plants and Soils* (Academic Press, San Diego, 1995).

- [77] West, G.B., Brown, J.H. & Enquist, B.J. A general model for the structure and allometry of plant vascular systems. *Nature* **400**, 664-667 (1999).
- [78] Rossel, J. *Physique générale* (Édition du Griffon, Neuchâtel, Switzerland, 1970), pp. 260-266.
- [79] Israelachvili, J. *Intermolecular & surface forces*, 2nd. Ed. (Academic Press, London, 1991).
- [80] de Gennes, G. Wetting: Statics and dynamics. *Rev. Mod. Phys.* **57**, 827-863 (1985).
- [81] Öner, D. & McCarthy. T.J. Ultrahydrophobic surfaces: effects of topography length scales on wettability. *Langmuir* **16**, 7777-7782 (2000).
- [82] Jackman, R.J., Duffy, D.C., Ostuni, E., Willmore, N.D & Whitesides, G.M. Fabricating large arrays of microwells with arbitrary dimensions and filling them using discontinuous dewetting. *Anal. Chem.* **70**, 2280-2287 (1998).
- [83] Ostuni, E., Chen, C.S., Ingber, D.E. & Whitesides, G.M. Selective deposition of proteins and cells in arrays of microwells. *Langmuir* **17**, 2828-2834 (2001)
- [84] Michel, B., Bernard, A., Bietsch, A., Delamarche, E., Geissler, M., Juncker, D., Kind, H., Renault, J.-P., Rothuizen, H., Schmid, H., Schmidt-Winkel, P., Stutz, R., and Wolf, H. Printing meets lithography: Soft approaches to high-resolution patterning. *IBM J. Res. & Dev.* **45**, 697-719 (2001) .
- [85] Whitesides, G.M., Ostuni, E., Shuichi, T., Jiang, X. & Ingber, D. Soft lithography in biology and biochemistry. *Annu. Rev. Biomed. Eng.* **3**, 335-373 (2001).
- [86] Wapner, P.G. & Hoffman, W.P. Partial wetting phenomena on non-planar surfaces and in shaped microchannels. *Langmuir* **18**, 1225-1230 (2002).
- [87] Peters, R.-P., Osterloh, D.K. & Backes, H. Sample support. PCT international patent application number WO 99/46045, filed 1998.
- [88] Spurk, J.H. *Strömungslehre*, 4th Ed. (Springer, Berlin, 1996), pp. 160-167.
- [89] Middleman, S. *An introduction to fluid dynamics*(John Wiley & Sons, Inc., New York, 1998), pp. 39-64.
- [90] Hoffman, R.L. A study of the advancing interface. 1. Interface shape in liquid-gas systems. *J. Colloid Interface Sci.* **50**, 228-241 (1974).
- [91] Sobolev, V.D., Churaev, N.V., Velarde, M.G. & Zorin, Z.M. Surface tension and dynamic contact angle of water in thin quartz capillaries. *J. Colloid Interface Sci.* **222**, 51-54 (2000).
- [92] Rye, R.R., Yost, F.G. & Mann, J.A. Wetting kinetics in surface capillary grooves. *Langmuir* **12**, 4625-4627 (1996).
- [93] Rye, R.R., Yost, F.G. & O'Toole, E.F. Capillary flow in irregular surface grooves. *Langmuir* **14**, 3937-3943 (1998)

- [94] Dong, M. & Chatzis, I. The imbibition and flow of a wetting liquids along the corners of a square capillary tube. *J. Colloid Interface Sci.* **172**, 278-288 (1995).
- [95] Weislogel, M.M., Capillary flow in containers of polygonal section. *J. Am. Inst. Aeronautics Astronautics* **39**, 2320-2326 (2001).
- [96] Bird, R.B., Stewart, W.E. & Lightfoot, E.N. *Transport phenomena*, 2nd. Ed. (John Wiley & Sons, Inc., New York, 2002), pp. 11-39.
- [97] Rossel, J. *Physique générale* (Édition du Griffon, Neuchâtel, Switzerland, 1970), pp. 182-191.
- [98] Streeter, V.L., Wylie, E.B. & Bedford, K.W. *Fluid mechanics*, 9th. Ed. (McGraw-Hill, Boston, 1998).
- [99] Washburn, E. The dynamics of capillary flow. *The Physical Review* **XVII**, 273-283 (1921).
- [100] Bird, R.B., Stewart, W.E. & Lightfoot, E.N. *Transport phenomena*, 2nd. Ed. (John Wiley & Sons, Inc., New York, 2002), pp. 531.
- [101] Atkins, P.W. *Physikalische Chemie*, 2nd Ed. (VCH Verlagsgesellschaft, Weinheim, 1996), pp. 798-807.
- [102] Craig, V.S.J., Neto, C. & Williams, D.R.M. Shear-dependent boundary slip in an aqueous newtonian liquid. *Phys. Rev. Lett.* **87**, 054504 (2001).
- [103] Frank, P. & v. Mises, R. *Die Differential- und Integralgleichungen*, Part II, 2nd Ed. (Dover Publications, Inc, NY, 1961), pp. 553-559.
- [104] Bird, R.B., Stewart, W.E. & Lightfoot, E.N. *Transport phenomena*, 2nd. Ed. (John Wiley & Sons, Inc., New York, 2002), pp. 612-648.
- [105] Glaser, R.W. Antigen-antibody binding and mass transport by convection and diffusion to a surface: a two-dimensional computer model of binding and dissociation kinetics. *Anal. Biochem.* **213**, 152-161 (1993).
- [106] Chen, R., Weng, L., Sizto, N.C., Osorio, B., Hsu, C.-J., Rodgers, R. & Litman, D.J. Ultrasound-accelerated immunoassay, as exemplified by enzyme immunoassay of choriogonadotropin. *Clin. Chem.* **30**, 1446-1451 (1984).
- [107] Lettieri, G.-L., Dodge, A., Boer, G., Lichtenberg, J., Verpoorte, E. & de Rooij, N. Consequences of opposing electrokinetically and pressure-induced flows in microchannels of varying geometries. In Ref. [3], pp. 351-354.
- [108] Oddy, M.H., Santiago, J.G. & Mikkelsen, J.C. Electrokinetic instability mixing. *Anal. Chem.* **73**, 5822-5832 (2001).
- [109] Liu, R.H., Stremler, M.A., Sharp, K.V., Olsen M.G., Santiago, J.G., Adrian, R.J., Aref, H. & Beebe, D.J. Passive mixing in a three-dimensional serpentine microchannel. *J. Microelectromech. Syst.* **9**, 190-197 (2000).
- [110] Stroock, A.D., Dertinger, S.K.W., Ajdari, A., Mezić, I., Stone, H.A. & Whitesides, G.M. Chaotic mixer for

microchannels. *Science* **295**, 647-651 (2002).

- [111] He, B., Burke, B.J., Zhang, X., Zhang, R. & Regnier, F.E. A picoliter-volume mixer for microfluidic analytical systems. *Anal. Chem.* **73**, 1942-1947 (2001).
- [112] Zimmermann, M.H. *Xylem structure and the ascent of sap* (Springer, Berlin, 1983), pp. 66-95.
- [113] Kramer, P.J. *Water relations of plants* (Academic Press, New York, 1983), pp. 187-214.

## Chapter 2

# Fabrication and use of capillary microfluidic systems

**Soft and rigid two-level microfluidic networks for patterning surfaces**

David Juncker, Heinz Schmid, André Bernard, Isabelle Caelen, Bruno Michel, Nico de Rooij, and Emmanuel Delamarche

*Journal of Micromechanics and Microengineering* **11**, 532-541 (2001).



# Soft and rigid two-level microfluidic networks for patterning surfaces

David Juncker<sup>1,2</sup>, Heinz Schmid<sup>1</sup>, André Bernard<sup>1</sup>,  
Isabelle Caelen<sup>3</sup>, Bruno Michel<sup>1</sup>, Nico de Rooij<sup>2</sup> and  
Emmanuel Delamarche<sup>1,4</sup>

<sup>1</sup> IBM Research, Zurich Research Laboratory, Säumerstrasse 4, 8803 Rüschlikon, Switzerland

<sup>2</sup> University of Neuchâtel, Institut de Microtechnique, Rue Jaquet-Droz 1, 2000 Neuchâtel, Switzerland

<sup>3</sup> CSEM, Rue Jaquet-Droz 1, 2000 Neuchâtel, Switzerland

E-mail: emd@zurich.ibm.com

Received 19 March 2001, in final form 14 May 2001

Published 19 July 2001

Online at [stacks.iop.org/JMM/11/532](http://stacks.iop.org/JMM/11/532)

## Abstract

We describe the microfabrication and use of elastomeric and rigid two-level microfluidic networks ( $\mu$ FNs), made of poly(dimethylsiloxane) (PDMS) or Si, for patterning surfaces. The first level corresponds to microchannels and the second to via holes through the  $\mu$ FNs serving as filling and venting ports.  $\mu$ FNs in PDMS are manufactured using a ‘sandwich’ replication from a microfabricated four inch mold structured with SU-8 photoresist, which is planarized by mechanical polishing.  $\mu$ FNs in Si are microfabricated using deep reactive ion etching. Both types of  $\mu$ FNs can be positioned onto a substrate, creating sealed microchannels, filled with different liquids, flushed, removed and reused. These two-level  $\mu$ FNs allow us to access the ports from the rear, minimize interchannel crosstalk, and are economic of solutions. The channels are made wettable so that the liquids can flow spontaneously into the conduits, but stop at the venting ports. The sealing of the conduits usually requires that either the  $\mu$ FN or the substrate be soft. A strategy for using hard two-level  $\mu$ FNs, in Si, for patterning hard substrates is presented: despite voids in-between the  $\mu$ FN and the substrate, a water-based solution can be guided by hydrophilic microchannels over a hydrophobic surface. Adjusting the wetting properties of the various surfaces is key to preventing undesired spreading of solutions. We illustrate our concepts by micromolding colored photocurable polymers on glass and patterning proteins as lines on a polystyrene surface.

## 1. Introduction

Surface patterning relies on a broad range of classical contact-mediated techniques [1] such as screen and stencil printing, offset printing and electrophotography. For higher resolution, radiation-mediated patterning such as optical, UV, x-ray and e-beam lithographies are widely used. Soft lithography [3, 4] is a recent high-resolution patterning technique that uses the contact between a structured elastomer and a substrate to confine a chemical reaction at the surface of the substrate. It can therefore be regarded as an enhancement of the classical patterning techniques.

In this paper, we focus on a variant of soft lithography called the microfluidic networks ( $\mu$ FNs) [5–9]: a  $\mu$ FN is a structured elastomer placed onto a substrate, forming conduits at the interface. Akin to screen and stencil printing, the exposed surface areas of the substrate (within the conduits) are chemically processed, whereas the sealed areas are not. In  $\mu$ FNs, the channels are generally small in size (a few to several hundred micrometers) and can guide liquids and reactants to where desired. Using a  $\mu$ FN is simple, see figure 1. Firstly, the substrate is placed onto the  $\mu$ FN ((a) and (b)). Then, the patterning solutions are loaded into the filling ports (c); they flow into the microchannels, and a reaction can take place on the part of the surface exposed in the channels (d). Finally, the patterned substrate is separated from the  $\mu$ FN (e).

<sup>4</sup> Author to whom correspondence should be addressed.

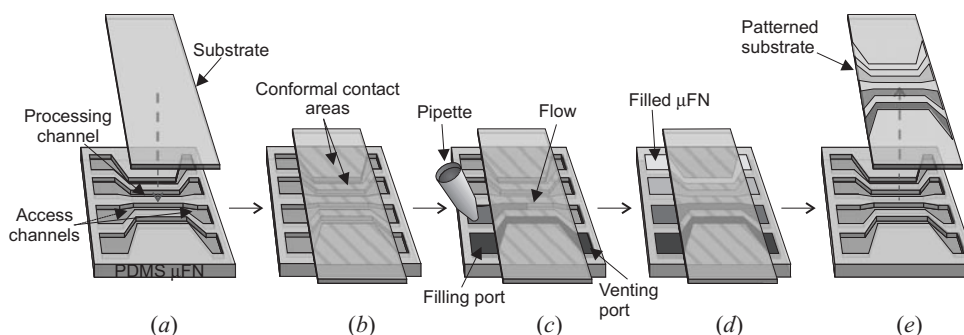


**Figure 1.** The procedure for patterning a substrate using a single-level  $\mu$ FN. (a) A  $\mu$ FN featuring open conduits is partially closed with a flat substrate. (b) The contact areas produce leak-free joints. (c) The filling pads (or ports) are individually addressed with different solutions that fill the channels up to the venting ports by capillary pressure. After completion of the reactions (d), the patterned substrate is separated from the  $\mu$ FN (e).

Applying the concepts of microfluidics [10] to the patterning of surfaces is particularly attractive for several reasons.

- (i)  $\mu$ FNs can guide fluids from distant reservoirs along microchannels to target zones of a substrate with high resolution, depending on the size of the microchannels.
- (ii) These devices can transport a wide range of liquids such as acids and bases [11], solutions of proteins [8], cells [12] or polymers over a substrate [6].
- (iii) They require only minute amounts of reagents [13].
- (iv) They feature fast reactions because in the small dimensions of the microchannels, the time needed for the diffusion of the reactants to the substrate is reduced.
- (v) A potent enhancement introduced to surface patterning by  $\mu$ FNs is the transfer of distinct reagents with inherent alignment, performed by loading the chemicals into different filling ports.

This capability eliminates the need for both iterative processing steps and precise alignment of successive masks. It paves the way for routinely using contact lithographies to transfer distinct, possibly fragile, molecules onto a substrate—in a single patterning step. Applications currently envisaged range from patterning colored dyes for displays [14] to patterning biomolecules for sensing and screening of biochemical interactions [15–17].

In this paper, we explain the benefits of using capillary pressure to transport the reagents, and discuss the properties of poly(dimethylsiloxane) (PDMS) as a material for fabricating  $\mu$ FNs as well as the limitations of single-level  $\mu$ FNs. We introduce two-level  $\mu$ FNs, having many microchannels and openings for rear access, that can be made either in PDMS or Si. Their fabrication and utilization are explained in detail, and we illustrate how a hard  $\mu$ FN can be reversibly sealed onto a hard substrate. We demonstrate surface patterning with both types of  $\mu$ FNs. Finally, we discuss the use of soft and hard two-level  $\mu$ FNs in light of their figures of merit.

### 1.1. Capillary pressure for filling $\mu$ FNs

If a liquid is confined within a small capillary, the liquid front is curved proportionally to its angles of contact with the walls and the size of the conduit [8]. This curvature gives rise to pressure, which in the case of a wettable conduit draws the liquid into

the microchannel (a non-wettable surface would generate an equivalent positive pressure acting against filling). Capillary pressure is especially useful to transport liquids for surface patterning. Firstly, it generates a pressure sufficient to fill small conduits, which scales favorably and therefore is particularly appropriate for filling micrometer-sized channels.  $\mu$ FNs using capillary pressure for filling are passive systems, not requiring any external pump connected to the network, in which each microchannel has, and is, its own pumping device, enabling a high degree of integration for these devices. Passive  $\mu$ FNs do not require ‘strong’ seals with the substrate because no pressure is added to force liquid into the channels. In contrast, a light vacuum can be used to help emptying filled channels. Secondly, the design of a  $\mu$ FN can tailor the capillary pressure produced by its various parts (filling port, open and closed sections of the microchannel and venting port, see figure 1) and thus ‘control’ the filling. For example, the flow stops autonomously at the venting port when the geometry of the channel reduces the capillary pressure.  $\mu$ FNs are ideal for handling scarce and precious materials because an optimum design can efficiently reduce the overall volume of the device; a 1 cm long channel with a  $100 \times 100 \mu\text{m}^2$  section has a 100 nl volume. It is worth noting that in small capillaries the flow is typically laminar (Reynold’s number  $\ll 2000$ ). However, driving liquids within  $\mu$ FNs using capillary pressure has some limitations. A liquid loaded into a port will quickly fill the entire microchannel, but cannot be stopped before it reaches the venting port. The filling speed is governed by the size of the channel, its wetting properties and the properties of the liquid, and cannot be interactively controlled.

### 1.2. $\mu$ FNs made of PDMS

A seal between an open microchannel and a substrate is required to create closed, individual capillary pathways (figure 2). It is easy to obtain a liquid-tight seal if either the open microfluidic system or the substrate is an elastomer such as PDMS [18]: PDMS (Sylgard 184) spontaneously conforms to relatively smooth surfaces by adhesion forces, producing a seal.  $\mu$ FNs made of PDMS are simple to fabricate by replication of a mold. Structuring a Si wafer using photolithography and etching techniques can provide the ‘master’ on which PDMS is then poured as a liquid and cured.



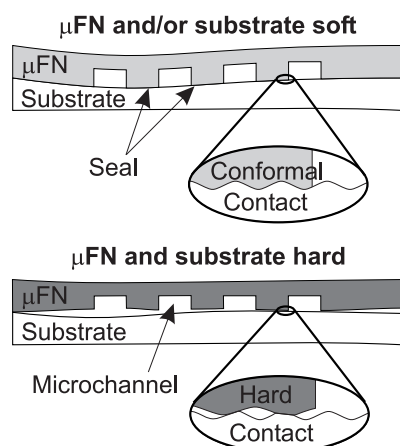


**Figure 2.** Conformal contact between a  $\mu$ FN and a substrate is *a priori* necessary to keep the patterning well localized to the areas of the substrate exposed in the microchannels. Using a soft  $\mu$ FN on a hard substrate or a hard  $\mu$ FN on a soft substrate can provide a tight sealing of the microchannels. There is *a priori* no seal when both the  $\mu$ FN and the substrate are hard because roughness of the surface and long-range curvature of the substrate produce voids.

The PDMS replica can easily be cut to yield many individual  $\mu$ FNs, and the mold can be reused many times.

PDMS is now widely used for microfluidic applications [5–9, 19]. It is a transparent material, which allows monitoring displacement of liquids inside the networks; it is slightly permeable to gases such as  $O_2$  and  $N_2$ , which can help in filling microchannels without vents. The surface of  $\mu$ FNs in PDMS is hydrophobic. Such  $\mu$ FNs can be filled directly with nonpolar polymers or liquids or, alternatively, with water-based solutions but only after hydrophilization of the microchannels. An  $O_2$ -based plasma is useful for this purpose because it can create a thin, glassy oxide at the PDMS surface. As hydrophilized PDMS exposed to air reverts to a hydrophobic state within a few minutes [20], oxidized  $\mu$ FNs have to be used directly after hydrophilization or stored under water to keep the surface indefinitely hydrophilic.

### 1.3. Single-level $\mu$ FNs in PDMS

Individual  $\mu$ FNs comprise macroscopic zones, the filling ports, which are open reservoirs serving as interfaces for users to handle and pipette liquids to fill each microchannel. They also have venting ports to prevent the trapping of air inside the channels during filling. Although straightforward to fabricate because all structures of single-level  $\mu$ FNs have the same depth, these  $\mu$ FNs are limited by several constraints.

The filling, and preferably also venting, ports must be open, i.e.  $\mu$ FNs must extend beyond the substrate (figure 3(a)). The contact line between substrate,  $\mu$ FN and air is wettable because either the  $\mu$ FN or the substrate has to be wettable for the network to be filled entirely. Hence, the liquid might follow this border line and cross-contaminate adjacent microchannels. This can be obviated by opening vias through the PDMS layer to create deep ports at the beginning and the end of the channels, e.g. by either fixing rods onto the mold or by piercing openings after demolding the  $\mu$ FN. Although simple, these procedures are cumbersome and not compatible with the fabrication of highly integrated  $\mu$ FNs. In the following, we shall present

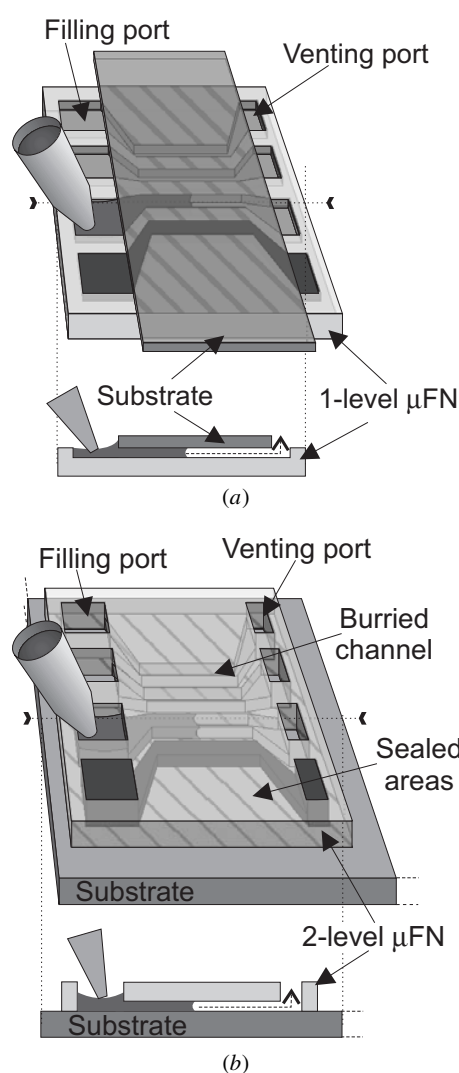


**Figure 3.** Single-level and two-level  $\mu$ FNs for patterning surfaces. (a) The single-level  $\mu$ FN is placed below the substrate and needs to extend beyond the substrate for filling and venting. (b) Placing the two-level  $\mu$ FN on top of the target area eases the constraints on the substrate size. It can help reduce the length of channels and the overall footprint size, economizing both reagents and filling time. Moreover, the deep filling ports and the novel design of the  $\mu$ FN minimize the risk of cross-contamination between microchannels.

microfabricated, compact two-level  $\mu$ FNs that are convenient to use.

## 2. Two-level $\mu$ FNs for surface patterning

The two-level  $\mu$ FNs we design and fabricate allow the simultaneous patterning of surfaces with distinct chemicals (figure 3(b)). They feature openings through the layer [21, 22], permitting rear access for loading solutions and for venting the channels being filled. These networks possess enhanced patterning properties: they can be placed directly over the target area, which allows the filling ports to be close to the target area. Such  $\mu$ FNs entail a smaller footprint, fill faster, and economize reagents by having shorter channels. Moreover, they can accommodate substrates having topographical structures outside the target area. Finally, the

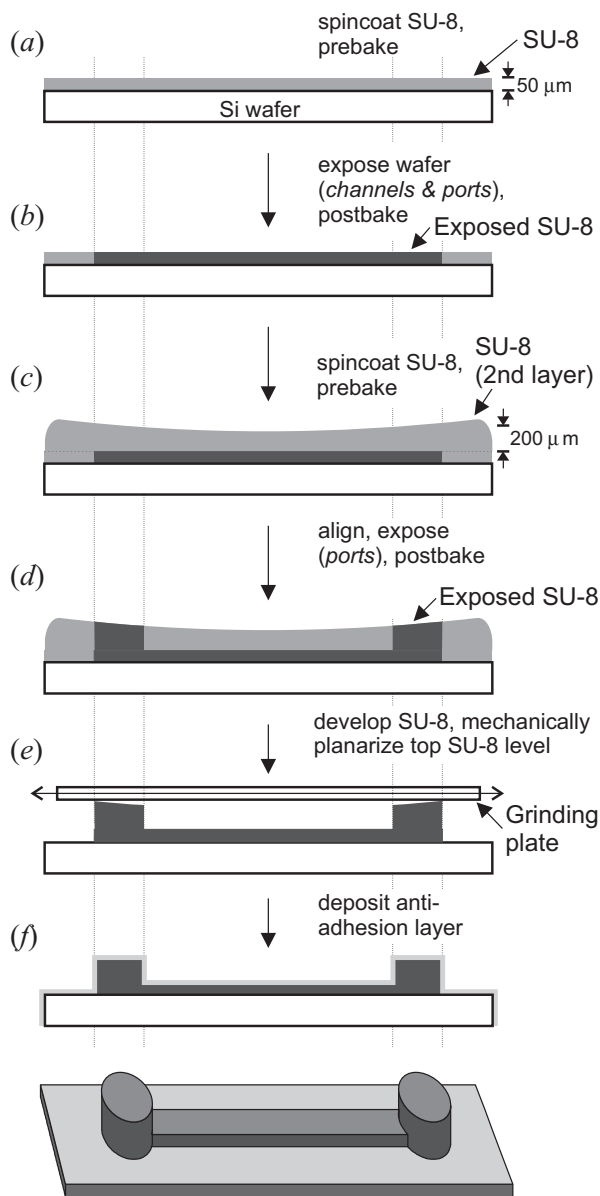


**Figure 4.** Microfabrication of a two-level mold in SU-8 photoresist. (a)–(d) An SU-8 resist is spin-coated onto a Si wafer, photoexposed after alignment, and baked. These steps are repeated for the second level, and both patterns are then developed simultaneously. (e) Mechanical polishing planarizes the SU-8 resist. Alternatively, the SU-8 can be planarized before development, which might be useful for protecting a high-aspect-ratio structure from buckling. PDMS is spread onto the planarized mold, cured and peeled off to remove dust particles. (f) An anti-adhesion layer is deposited on the mold.

deeper ports and the suppression of a border line minimize the risk of cross-contamination between adjacent microchannels.

### 2.1. Microfabrication of two-level PDMS $\mu$ FNs

The PDMS  $\mu$ FNs are replicated from a two-level mold. This mold can either be micromachined into Si using deep reactive ion etching (DRIE) [12] or structured by patterning a thick photoresist. We present the latter method using SU-8 as the photoresist (figure 4). Other groups [21, 22] have used similar

fabrication techniques for producing microfluidic systems. The main differences are that these microfluidic systems are closed, permanently sealed and rely on a pump for displacing liquids.

Molding of vias through the PDMS  $\mu$ FN is achieved by pressing a flat and rigid plate onto the PDMS curing on the patterned mold. Eventually all raised structures have to contact this plate so that the PDMS is squeezed out completely. On the scale of a wafer, the thickness of the spin-coated SU-8 photoresist typically varies by up to 20% which, for layers that are several hundred micrometers thick, translates into tens of micrometers in height difference. The SU-8 elasticity can only compensate for slight variations, thus some PDMS may remain in place over the shorter ‘pillars’ of the mold (the ‘pillars’ are the placeholders for the access ports of the  $\mu$ FN). An overall flatness of the top surface of the SU-8 is necessary, as otherwise a thin PDMS membrane will form and obstruct the via holes.

We have established a novel process to planarize the SU-8 mold that relies on mechanical polishing and we present two variants of this. The first starts by patterning the wafer with the photoresist in a standard way. After development of the pattern, the photoresist structures are mechanically polished on an abrasive paper affixed to a flat plate (figure 4(e)). This method is straightforward, prevents the embedding of polishing particles into the resist, and is effective for fabricating the microfluidic structures presented here. For higher-aspect-ratio structures, buckling during polishing can be a problem. Additionally, the dust produced during polishing can stick to the wafer and has to be removed. This first variant process and the associated issues will be described and illustrated in greater detail later.

The second process consists of exposing the SU-8 photoresist, postbaking, and then polishing it prior to development and removal of any unexposed photoresist. The unpolymersed SU-8 is liquid at higher temperatures, but solid at room temperature, although relatively soft. This unexposed resist can nevertheless be polished along with the exposed and polymerized hard structures. In this case, the polishing plate needs to be microstructured. If both substrate and working piece are completely flat, wet polishing is not so accurate because either a water film can prevent contact between the surfaces or the surfaces tend to ‘stick’ together. The unexposed resist on the other hand protects the mold from the dust produced during polishing and can help stabilize high-aspect-ratio structures (results not shown).

We believe that these processes are appealing for making multilayer structures in resists where flatness is critical or where a precisely defined thickness of each layer is desired.

**2.1.1. Microfabrication of the mold in the photoresist.** A four inch Si wafer, 525  $\mu$ m thick, is spin-coated with SU-8 photoresist (Microchem Corp., Newton, MA, USA) to a thickness of 50  $\mu$ m. The resist is prebaked at 95  $^{\circ}$ C for 1 h, and exposed with a contact mask aligner (MA 4, Karl Süss) to broadband UV light (6.5 mW cm $^{-2}$ ) for 50 s through a Cr mask featuring all network elements (access ports and microchannels). The resist is postbaked for 15 min at 95  $^{\circ}$ C to crosslink the exposed areas. A second SU-8 layer, with a thickness of 200–300  $\mu$ m, is spin-coated on top of the first and prebaked for 3 h at 95  $^{\circ}$ C on a hot plate. The contrast

of the ‘latent’ image in the first layer allows the alignment of a mask having only filling and venting ports, which is then exposed for 140 s. For thicker layers, this alignment method can become ineffective owing to the limited focal depth of the mask aligner. In that case, marks on the rear of the wafer can be used for alignment. A second postbake for 15 min at 95 °C crosslinks the exposed zones of the second layer. The pattern in both layers is developed in 1,2-propanediol monomethyl ether acetate (PGMEA) in about 20 min with ultrasonification.

The SU-8/Si wafer is attached to a precision-machined vacuum chuck, which also serves as a handle, to prevent bending of the thin wafer. The protruding SU-8 structures are manually abraded and polished on a lapping paper (Imperial lapping paper, 3M) attached to a flat and rigid glass plate. The lapping paper is wetted continuously. For this, water containing a surfactant (1% sodium dodecylsulfate) is used because it does not swell the glue of the lapping paper and wets both paper and wafer. At first, only the highest structures are affected, and the progression of the abrasion is shown by the contour line of the nonabraded zone. The grain size of the lapping paper is decreased from 15  $\mu\text{m}$  nominal granularity to 9, 3, and finally 1  $\mu\text{m}$ . The final polishing step results in a slightly reflective surface. Some of the particles abraded stick to the SU-8/Si surface. The surface tension agent can only partly prevent this. However, these particles can be removed by pouring PDMS onto the wafer, curing it, and peeling it off along with the embedded particles. Finally, a 50 nm thick fluorinated layer is deposited using a DRIE process (Surface Technology Systems, Bristol, UK) to facilitate the subsequent removal of cured  $\mu\text{FNs}$  in PDMS.

**2.1.2. Replica molding of  $\mu\text{FNs}$  in PDMS.** Figure 5 delineates the replication procedure of a two-level mold for making PDMS  $\mu\text{FNs}$  with openings for access to the filling and venting ports from the rear. An Al block serving as flat support is covered with a thin, transparent foil to prevent PDMS from spilling over the block during the process. The two PDMS components A and B (Sylgard 184, Dow Corning, Midland, MI, USA) are mixed in a 10:1 ratio using an automatic dispenser (DOPAG MICROMIX E, Cham, Switzerland). The viscous mixture is degassed for  $\approx 5$  min under a vacuum ( $\approx 1$  mbar) to remove and prevent the formation of bubbles, and is then poured over the mold. A 250  $\mu\text{m}$  thick polycarbonate (PC) foil (Europlex, Röhm, Darmstadt, Germany) is sandwiched between the PDMS and a flat glass cover plate. The top plate is pushed down manually until the PC foil touches the upper part of the mold; the plate is then slid smoothly sideways to expel any PDMS left between the SU-8 pillars and the plate. The ensemble is placed on a hot plate, loaded with a 2.5 kg weight, and heated to 85 °C for 3 h to cure the PDMS. The top glass plate and the PC foil are removed, and the PDMS replica is peeled off the mold after cooling. Using a smooth PC foil is not essential to this process, but helps to keep the top surface flat and thus the  $\mu\text{FNs}$  transparent. In some cases, the mold does not touch the PC foil, but if the gap is sufficiently small, the obstructing PDMS membranes tear spontaneously upon separation or during subsequent preparation steps (figures 6(a) and (b)). One replication operation typically generates 20  $\mu\text{FNs}$ . An individual network can be cut to size prior to using it for patterning.

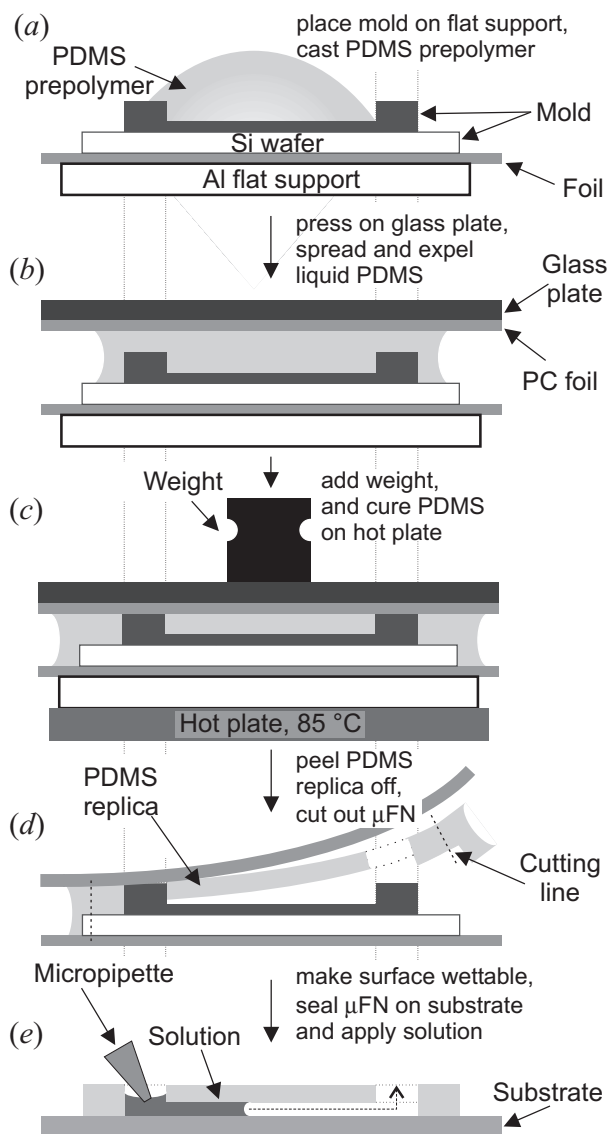


**Figure 5.** Replica molding of PDMS  $\mu\text{FNs}$  having rear access from a two-level mold. (a) Liquid PDMS prepolymer is cast onto the mold, and (b) enclosed with a polycarbonate foil and a flat, rigid glass plate. (c) The setup is slightly pressurized before and during curing on the hot plate to expel excess PDMS. (d) Glass plate and foil are removed after cooling, then the PDMS replica is peeled off, and finally the individual  $\mu\text{FNs}$  are cut to a convenient size for further use (e).

## 2.2. Patterning of glass with PDMS $\mu\text{FNs}$

The utilization of a two-level  $\mu\text{FN}$  in PDMS is illustrated by patterning three polymers having similar composition but different colors on a substrate. The  $\mu\text{FNs}$  prepared here have 16 independent fluidic zones, each comprising a filling port and a venting port 290  $\mu\text{m}$  wide and 3 mm long, and two connection channels between the ports and the microchannel that are 50  $\mu\text{m}$  wide and 2.3 mm long. The microchannels are 120  $\mu\text{m}$  wide and 3.7 mm long. The depth of all structures in this network is determined by the local thickness of the resist on the Si wafer forming the mold.



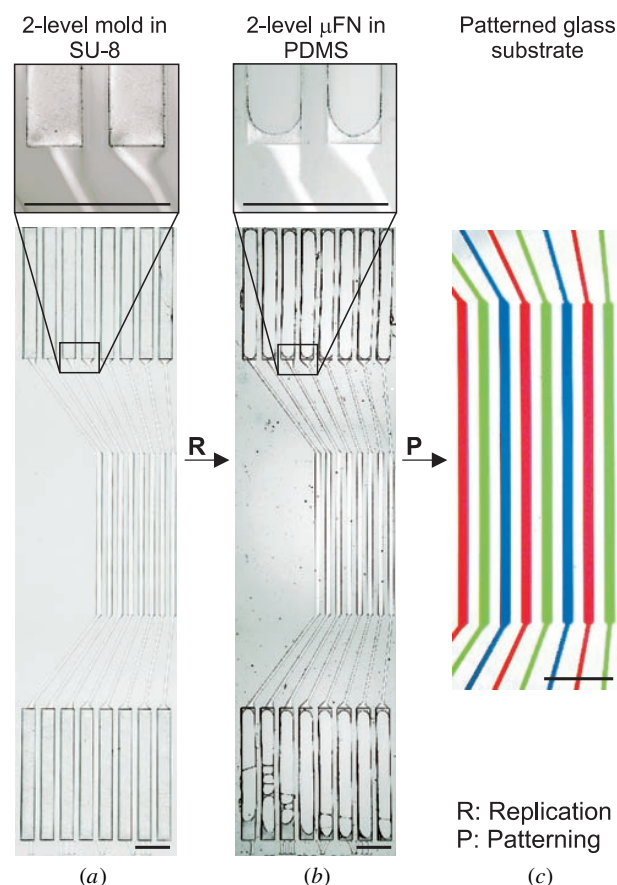


**Figure 6.** (a) Optical microscope images of the left-most eight channels of a planarized SU-8 mold, (b) the corresponding replicated PDMS μFN, and (c) the patterned substrate. (b) The PDMS network is an accurate replica of the mold; all ports are open but thin membranes of PDMS remain in some areas. (c) The 120 μm wide lines of red, green and blue polymers patterned on a glass substrate using the microchannels of the μFN as templates. The scale bar is 800 μm.

**2.2.1. Application.** The PDMS μFN is placed on a glass substrate by hand without applying pressure. Three aliquots of polymers colored with red, green or blue pigments (Color Mosaic 7001, Olin Microelectronics Materials, Zwijndrecht, Belgium) are mixed with a UV adhesive carrier (UV 15, Master Bond Inc, Hackensack, NJ, USA) in a ratio of 1:3, and degassed in vacuum (<1 mbar) for 15 min to eliminate some of the volatile solvents. This adhesive was selected as the carrier because it has a relatively low viscosity (150 cps), and can easily be hardened in UV. It does not swell PDMS noticeably, and filling the microchannels with this material can prevent solvent evaporation at the filling front. A few microliters of each of the three colored polymers are applied sequentially with a 'stretched' Pasteur pipette (glass capillary) into the filling ports under an ocular. It takes ≈1 min to fill the 8 mm long microchannels. The colored polymers inside the μFNs are cured *in situ* with UV flood-curing light (ELC-4001, Electro-Lite Corp., Danbury, CT, USA) for 15 min. The PDMS μFN is separated from the substrate, and the pattern post-exposed with UV for an additional 5 min.

**2.2.2. Results and discussion.** The lines of polymers patterned with the PDMS μFN [5, 6] can be seen in figure 6(c).

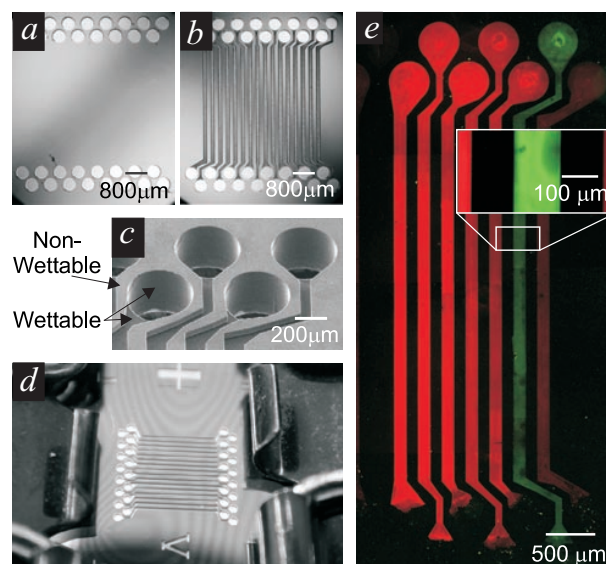


**Figure 7.** Microscope images of: (a)–(c) a two-level Si μFN; (d) the μFN clipped onto a hard substrate; and (e) a fluorescence image of the substrate patterned with lines of proteins. (a) The rear of the μFN comprises the filling and venting ports. (b) The side in contact with the substrate contains both the channels and the ports. (c) A scanning electron microscope image emphasizes the difference in depth between the channels and the ports. (d) The μFN is clipped onto a polystyrene-covered glass slide but Newton's rings reveal that most of the areas are not in contact. (e) The colored lines correspond to fluorescently-tagged BSA proteins deposited from solutions using the μFN clipped to the substrate as shown in (d). The fluorescence intensity correlates to the concentration of the solution filled into each channel. There is no crosstalk between the channels, and the pattern has high contrast.

When the μFN is used to pattern a substrate with a material that solidifies in the microchannel, removing the μFN necessitates separating the molded material from all three channel walls. In this case, the adhesion forces between the material and the walls may lift the patterned material off the substrate. PDMS is an advantageous material in this respect because it has a surface with low free energy and because it can be bent and simply peeled off the substrate. Some materials may shrink and dewet the microchannels during the curing step, which can also help in removing the μFN from the substrate without damaging the pattern. The sharp edge of the colored lines suggests that the formation of patterns at higher resolution with such two-level μFNs is achievable.

Designing μFNs in PDMS must allow for the limited stability of large covers and narrow supports in PDMS, which are prone to sagging and collapsing, respectively [24]. The use of μFNs in PDMS is also restricted to solvents that do not excessively swell PDMS. Hard materials, such as glass or Si, provide an alternative for μFN fabrication and can avoid the above-mentioned problems. In the following section, we present a method for fabricating two-level μFNs in Si and using them without the need for a conformal contact to obtain a seal.

### 3. Two-level Si μFNs

μFNs in Si [25] can be manufactured using standard microfabrication processes such as wet, dry and, in particular,

deep reactive ion etching [26]. Si is a rigid material, supports high-aspect-ratio structures, and permits precise registration of  $\mu$ FNs with a substrate. Such Si  $\mu$ FNs can be made wettable with nonpolar liquids by removing the native Si oxide with buffered HF acid or grafting alkylsilanes [27]. Conversely, a  $\mu$ FN in Si can be cleaned with an O<sub>2</sub> plasma to make its surface wettable by polar solutions such as water.

So far, using Si  $\mu$ FNs has been restricted to soft substrates, which can provide conformal contact to seal the various parts of the network. The reason for this lies in the difficulty of achieving tight seals between two hard surfaces: imperfections such as long-range curvature and surface roughness as well as dust particles compromise a large area of contact (figure 2). In bonding processes, these problems are circumvented by working in a clean-room environment and by applying high pressure to the two substrates. Heat, high voltage or chemical activation are options for achieving a durable seal [28, 29]. However, as these techniques can only create permanent seals, they are not suitable for surface patterning, where it is desirable to remove the substrate from the  $\mu$ FN after processing. Permanently bonded microfluidic systems, moreover, can neither be easily cleaned nor reused.

### 3.1. Wettability patterns to produce seals

Our technique to confine liquids (aqueous solutions) to the channels is to pattern wetting and non-wetting zones [30]: the interior walls of the microchannels are made wettable, whereas the raised surfaces are made non-wettable. Water is particularly well suited as a reactant carrier for the patterning of hard substrates with hard  $\mu$ FNs because of its low viscosity (1 mPa s at 20 °C) and high surface tension ( $\approx 70$  mN m<sup>-1</sup>). It is thus possible to control the wetting properties of a surface with water using standard chemical treatments of this surface.

Here, we render the channels of the Si  $\mu$ FN hydrophilic and the outer surfaces hydrophobic. A solution of water in-between two surfaces that face each other in close proximity will not spread if both surfaces are hydrophobic. A microchannel with three hydrophilic walls can promote the displacement of an aqueous solution along a hydrophobic substrate. Thus, the simple clipping of a hard  $\mu$ FN with hydrophilic channels and a hydrophobic surface onto a hydrophobic substrate can create both self-filling channels and liquid-tight ‘barriers’ separating the channels. These barriers can resist a pressure defined by the surface tension of the liquid, the contact angles between liquid and surfaces, and the gap size. Such an assembly can effectively prevent uncontrolled spreading of the solutions and enable the use of hard  $\mu$ FNs with hard substrates. The reversible sealing process makes it possible to pattern a substrate, and then simply remove and reuse the  $\mu$ FN. Next, we describe the microfabrication of such two-level  $\mu$ FNs in Si and explain how to use them for the patterning of proteins on surfaces.

### 3.2. Fabrication of two-level Si $\mu$ FNs

We fabricate the Si  $\mu$ FNs using photolithography, wet etching, DRIE, and microcontact printing ( $\mu$ CP) techniques (figure 8).

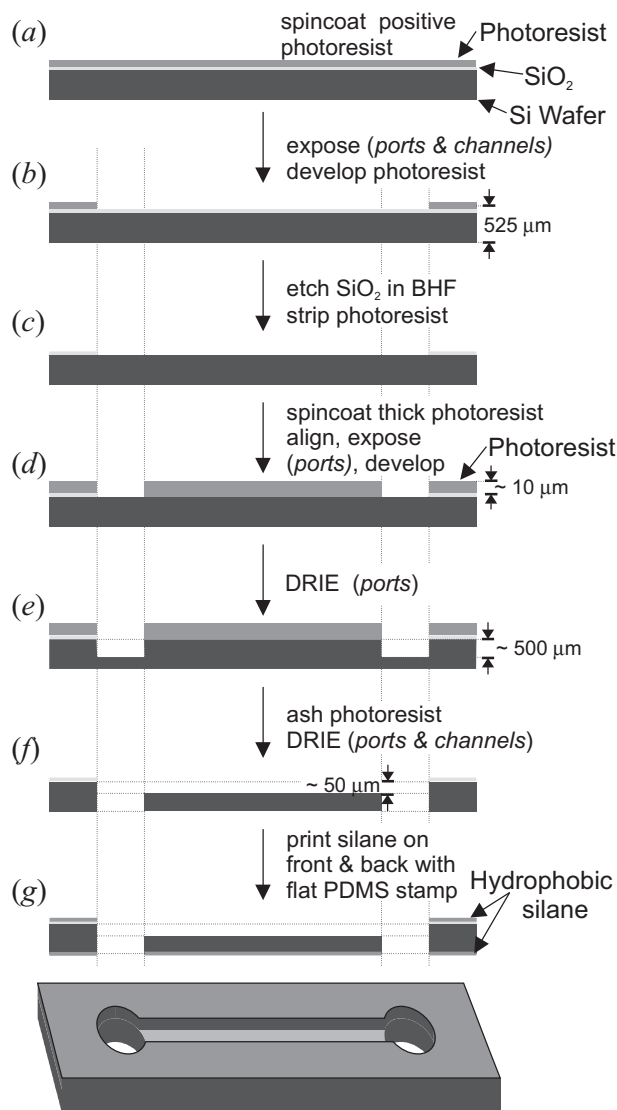


**Figure 8.** The fabrication process of two-level  $\mu$ FNs in Si. (a)–(c) The pattern featuring microchannels and access ports (for filling and venting) is transferred into a SiO<sub>2</sub> pattern on a Si wafer. (d) A second spin-coated photoresist layer is exposed through a mask having only the access ports. (e) and (f) First the patterned resist and then the SiO<sub>2</sub> layer act as masks for DRIE of the Si wafer. Only the access ports are etched through the wafer. (g) Hydrophobic silanes are printed and grafted onto the front and the back of the wafer using a flat PDMS stamp.

**3.2.1. Micromachining of the topography.** A Si{100} wafer (Siltronic, Geneva, Switzerland), four inches in diameter, 525  $\mu$ m thick, with a 1  $\mu$ m thick thermal SiO<sub>2</sub> layer is spin-coated with a photoresist (PR) (AZ6612, Hoechst, Strasbourg, France) for 45 s at 4000 rpm. The PR is prebaked at 110 °C for 50 s, and exposed through a mask featuring all the elements (ports and microchannels) for 5 s, developed in AZ400K (Hoechst), diluted 1:4 with deionized water (DI), and rinsed in DI. The uncovered SiO<sub>2</sub> is etched away in a 1:7 buffered hydrofluoric acid (BHF) solution in  $\approx 15$  min (dewetting of the substrate where SiO<sub>2</sub> has been etched indicates completion of the etch). An O<sub>2</sub> plasma or acetone is used to ash or strip the remaining PR. A second PR layer (AZ4562, Hoechst) is spin-coated at 1500 rpm for 45 s, yielding a thick overlayer of

$\approx 10 \mu\text{m}$  [31]. The  $\text{SiO}_2$  pattern underneath this PR layer is still visible and is used to align the wafer with a second mask featuring the ports only. After exposure and development of the PR, the wafer is rinsed, dried, and heated at  $95^\circ\text{C}$  for 20 min for postbaking. The Si wafer is glued onto a support wafer with melted white wax to protect the chuck. An inductively coupled plasma (ICP) DRIE (Surface Technology Systems, Bristol, UK) is used to transfer the PR and embedded  $\text{SiO}_2$  patterns into wafer topography in a three-step process [32]:

- (i) DRIE to make  $\approx 500 \mu\text{m}$  deep ports into Si (pattern defined by the thick PR).
- (ii) Without unloading the wafer from the DRIE machine, the PR is ashed using a plasma.
- (iii) The exposed  $\text{SiO}_2$  pattern acts as mask for a second dry-etch process of about  $50 \mu\text{m}$  in depth, creating  $50 \mu\text{m}$  deep channels, and opening the filling and venting ports through the wafer. After unloading, the support wafer is detached under a stream of warm water. The micromachined wafer is then cleaned with acetone, ethanol and DI, and cleaved into individual  $\mu\text{FN}$ s.

**3.2.2. Surface treatments.** The Si  $\mu\text{FN}$ s are cleaned using an  $\text{O}_2$  plasma ( $\approx 1$  min at 400 W; Technics Plasma 100-E GmbH, Kirchheim, Germany), rendering the  $\text{SiO}_2$  surfaces hydrophilic and reactive for chemical derivatization. The raised surfaces are hydrophobized using  $\mu\text{CP}$  [27] as follows. A flat PDMS used as inker pad is impregnated with a 2 mMol solution of 1H,1H,2H,2H-perfluorodecyltrichlorosilane (Gelest, Karlsruhe, Germany) in heptane for 5 s and blown dry under a flow of  $\text{N}_2$ . A flat PDMS stamp is inked by pressing it firmly onto the PDMS pad for 5 s. The flat stamp is applied to one face of the  $\mu\text{FN}$  for 3 s to graft a layer of silanes to the  $\text{SiO}_2$  surface. These processing steps are applied three times to both the front and rear sides of the  $\mu\text{FN}$  to increase the hydrophobicity of the coating. With this procedure, the parts of the  $\mu\text{FN}$  that should be non-wettable have advancing and receding contact angles with water of  $\approx 125^\circ$  and  $\approx 70^\circ$ , respectively. We ink the stamp using a PDMS inker pad to minimize swelling of the stamp by heptane. Alternatively,  $\mu\text{FN}$ s can be covered with gold and then patterned with thiols exhibiting different wettabilities [33].

The fabricated  $\mu\text{FN}$  (figures 7(a)–(c)) has identical filling and venting ports,  $400 \mu\text{m}$  in diameter, aligned in two rows with a pitch of  $600 \mu\text{m}$  between the ports and a separation distance of  $400 \mu\text{m}$  between the rows (figure 7(a)). Two adjacent ports are separated by  $100 \mu\text{m}$ . The processing zone comprises straight, parallel channels  $120 \mu\text{m}$  wide,  $50 \mu\text{m}$  deep and  $3.7$  mm long (figure 7(b)). The total length of the flowing zone is  $\approx 4.7$  mm, 1 mm of which is occupied by the filling and venting ports. The entire footprint of the 16-channel system is  $29.7 \text{ mm}^2$  for a processing area of  $13.7 \text{ mm}^2$ . We believe that this design offers a good compromise between having convenient access to the filling ports and having as large a ratio of active to total area as possible.

### 3.3. Patterning of hard substrates with Si $\mu\text{FN}$ s

The ability to pattern a hard substrate using a Si  $\mu\text{FN}$  is illustrated by the deposition of lines of proteins on

a polystyrene surface. Proteins are fragile biomolecules that have to be dissolved in water-based buffers for handling; different proteins cannot be easily patterned on a single substrate using conventional lithographic techniques. Polystyrene is prone to the deposition of proteins from solution, is widely used as a substrate for biological assays, and it is hydrophobic (it has advancing and receding contact angles with water of  $100^\circ$  and  $90^\circ$ , respectively). These characteristics allow the use of a ‘wettability barrier’ to guide and pattern proteins dissolved in water on a polystyrene surface. As proteins, we used bovine serum albumin (BSA) tagged with tetramethyl rhodamine isothiocyanate (TRITC, red,  $\lambda_{\text{FE}} = 570 \text{ nm}$ ) or fluorescein isothiocyanate (FITC, green,  $\lambda_{\text{FE}} = 525 \text{ nm}$ ) to visualize the patterns with fluorescence microscopy.

**3.3.1. Application.** The Si  $\mu\text{FN}$  is pressed onto a PS spin-coated glass using paper clips (figure 7(d)). A gap of a few micrometers between the  $\mu\text{FN}$  and the substrate, due to surface contamination and/or curvature, is revealed by the presence of numerous Newton’s rings. The filling ports of the Si  $\mu\text{FN}$  are loaded with solutions of TRITC–BSA in PBS with concentrations of 1000, 500, 250, 125, 62, and  $31 \mu\text{g ml}^{-1}$ , except for one port that is not loaded (negative control) and one that is loaded with FITC–BSA at a concentration of  $50 \mu\text{g ml}^{-1}$ . A pipetting robot (Probot, BAI GmbH, Lautertal, Germany) is used to take 160 nl of a solution of proteins from a titerplate and dispense 80 nl of it into two filling ports ( $n$ th and  $(n + 8)$ th). The robot rinses its pipetting capillary with DI and repeats the loading operation until 14 ports of the  $\mu\text{FN}$  have been loaded. The seven solutions are dispensed in 7 min and are allowed to react with the surface for an additional 2 min. A milliliter of PBS is deposited over all filling ports to flush the protein solutions from the channels to the venting ports. It is possible to actively remove all solutions at once from the venting ports using a silicone tubing connected to a water pump to better flush the channels with PBS and then DI. The clips are removed, and the polystyrene-covered glass is separated from the Si  $\mu\text{FN}$ , rinsed with DI and blown dry under a flow of  $\text{N}_2$ .

**3.3.2. Results and discussion.** The result of the patterning process can be seen in figure 7(e). The intensity of the fluorescence on the surface reflects the concentration of biomolecules in the solution; the rightmost channel is, as expected, the least fluorescent. The surface coverage of adsorbed BSA is constant along the entire channel. The  $50 \mu\text{m}$  depth of the Si microchannel helps to keep the surface-to-volume ratio relatively small, minimizing the depletion of proteins in the solution, which could lead to coverage density gradients on the substrate along the lines of proteins [25, 34]. The liquid confined in the microchannel has a small area exposed to ambient, which strongly reduces its evaporation. Drying of the solution would be detrimental to an homogeneous patterning of the substrate and could lead to denaturation of the proteins. We observed that the microchannels remained filled during the relatively long patterning process. In contrast, 80 nl aqueous droplets on a surface vanish within seconds. The properties described above make such  $\mu\text{FN}$ s well suited for use in combination with optical sensors to detect biochemical interactions, e.g. antibody recognition [34–36].

**Table 1.** Comparison of the main requirements and attributes of three fundamental strategies for surface patterning by  $\mu$ FNs.

	Si $\mu$ FN/hard substrate	Si $\mu$ FN/PDMS substrate	PDMS $\mu$ FN/flat substrate
Confinement of the liquid	Wetting pattern	Conformal seal	Conformal seal
Substrate wettability	Non-wetting	No requirements	No requirements
Possible processing solutions	Liquids with high surface tension (water)	Liquids compatible with PDMS	Liquids compatible with PDMS
Possible surface treatments of the $\mu$ FN	Stable surface modification by standard processes, e.g. deposition, dry or wet chemistry	Stable surface modification by standard processes, e.g. deposition, dry or wet chemistry	Surface modification by plasma, grafting, and UVO; difficult
Patterning properties	Inherent alignment	Inherent alignment, high resolution	Inherent alignment, high resolution, but lateral distortions possible
$\mu$ FN separation from substrate	Rinse step required first	Peeling of the PDMS layer under a rinsing solution	Peeling of the PDMS layer under a rinsing solution
Applications	Patterning of biomolecules	Patterning of biomolecules, molding of polymers	Patterning of biomolecules, cells, crystals, polymers, colored materials

#### 4. Concluding Remarks

$\mu$ FNs are convenient and versatile devices for patterning surfaces with distinct chemicals in a single step. There is a large number of possibilities to employ  $\mu$ FNs for patterning substrates, depending on the  $\mu$ FN and substrate properties and the liquid and reactants used. Here, we sought to fabricate  $\mu$ FNs with two levels to minimize crosstalk between independent flowing zones and to achieve a higher integration of the device. We developed efficient microfabrication techniques and processes to make such  $\mu$ FNs in soft elastomers such as PDMS or hard materials such as Si.  $\mu$ FNs in PDMS are easy to seal on substrates, but have limited mechanical stability and necessitate ‘custom’ fabrication techniques, whereas  $\mu$ FNs in Si can be structured using microfabrication technology. For patterning hard substrates, hard  $\mu$ FNs require an additional method to create a seal by superposing a wettability pattern onto the channel topography. This strategy only works on non-wettable substrates, however. Which  $\mu$ FN is the most practical should be evaluated on a case-by-case basis. We outline the requirements and attributes of a few combinations for  $\mu$ FNs, substrates and applications in table 1.

Patterning of elastomeric substrates with rigid  $\mu$ FNs is advantageous because it combines the refined fabrication processes for hard materials with substrates capable of conformal contact, such as PDMS. This strategy can be further extended; once patterned, a PDMS substrate can be used as a stamp to transfer the original pattern to another substrate, similarly to offset printing [37,38].

An application of two-level networks with openings and reversible sealing approaches could be the stacking of layers with matching patterns for obtaining three-dimensional networks [21, 22]. Both soft and hard  $\mu$ FNs may be used for making multilayered systems. Such a microfluidic device could be assembled and disassembled several times to allow the microfluidic sub-components to be cleaned and reused multiple times. In addition, sealing between hard surfaces could possibly be used to fabricate microfluidic

systems relying on electrokinetically-driven flow [39]. In summary, the fabrication technologies and reversible sealing approaches presented here can improve the reliability, degree of complexity and integration of passive  $\mu$ FNs, and extend their scope of utilization to novel, possibly even nonpatterning, applications.

#### Acknowledgments

D Juncker, A Bernard, B Michel and E Delamarche acknowledge partial financial support from the Swiss Federal Office for Education and Science within the BIOTECH European project BIOPATT (BIO4CT980536). I Caelen acknowledges financial support from the Swiss National Foundation NFP36 project. We thank A Bietsch, J P Renault, M Geissler, H Wolf, P Schmidt-Winkel and M Despont for useful discussions, G Genolet, R Widmer and U Drechsler for their help in preparing the microfluidic networks and H Ott for making the vacuum chuck/handle. We are grateful to P F Seidler (IBM) for his continuous support.

#### References

- [1] Taggi A J and Walker P 1996 Printing Processes *Encyclopedia of Chemical Technology* vol 20, ed R E Kirk and D F Othmer (New York: Wiley) p 62
- [2] 1997 Special issue on optical lithography *IBM J. Res. Dev.* **41** (1/2)
- [3] Xia Y and Whitesides G M 1998 *Angew. Chem., Int. Ed. Engl.* **37** 550
- [4] Michel B, Bernard A, Bietsch A, Delamarche E, Geissler M, Juncker D, Kind H, Renault J-P, Rothuizen H, Schmid H, Schmidt-Winkel P, Stutz R and Wolf H 2001 *IBM J. Res. Dev.* at press
- [5] Kim E, Xia Y and Whitesides G M 1995 *Nature* **376** 581
- [6] Kim E, Xia Y and Whitesides G M 1996 *J. Am. Chem. Soc.* **118** 5722
- [7] Delamarche E, Bernard A, Schmid H, Michel B and Biebuyck H 1997 *Science* **276** 779
- [8] Delamarche E, Bernard A, Schmid H, Bietsch A, Michel B and Biebuyck H 1998 *J. Am. Chem. Soc.* **120** 500

- [9] McDonald J C, Duffy D C, Anderson J R, Chiu D T, Wu H, Schueller O J A and Whitesides G M 2000 *Electrophoresis* **21** 27
- [10] Manz A and Becker H (eds) 1998 *Microsystem Technology in Chemistry and Life Sciences (Topics in Current Chemistry)* vol 194 (Berlin: Springer)
- [11] Kenis P J A, Ismagilov R F and Whitesides G M 1999 *Science* **285** 83
- [12] Folch A, Ayon A, Hurtado O, Schmidt M A and Toner M 1999 *Trans. ASME, J. Biomech. Eng.* **121** 28
- [13] Hosokawa K, Fujii T and Endo I 1999 *Anal. Chem.* **71** 4781
- [14] Pardo D A, Jabbour G E and Peyghambarian N 2000 *Adv. Mater.* **12** 1249
- [15] Southern E M, Case-Green S C, Elder J K, Johnson M, Mir K U, Wang L and Williams J C 1994 *Nucleic Acids Res.* **22** 1363
- [16] Rowe C A, Tender L M, Feldstein M J, Golden J P, Scruggs S B, MacCraith B D, Cras J J and Ligler F S 1999 *Anal. Chem.* **71** 3846
- [17] MacBeath G and Schreiber S L 2000 *Science* **289** 1760
- [18] Bietsch A and Michel B 2000 *J. Appl. Phys.* **88** 4310
- [19] Duffy D C, Schueller O J A, Brittain S T and Whitesides G M 1999 *J. Micromech. Microeng.* **9** 211
- [20] Fritz J L and Owen M J 1995 *J. Adhes.* **54** 33
- [21] Jo B-H, Van Lerberghe L M, Motsegood K M and Beebe D J 2000 *J. Microelectromech. Syst.* **9** 76
- [22] Anderson J R, Chui D T, Jackman R J, Cherniavskaya O, McDonald J C, Wu H, Whitesides S H and Whitesides G M 2000 *Anal. Chem.* **72** 3158
- [23] Lorenz H, Despont M, Fahrni, N, Brugger J, Vettiger P and Renaud P 1998 *Sensors Actuators A* **64** 33
- [24] Delamarche E, Schmid, H, Michel B and Biebuyck H 1997 *Adv. Mater.* **9** 741
- [25] Caelen I, Bernard A, Juncker D, Michel B, Heinzelmann H and Delamarche E 2000 *Langmuir* 9125
- [26] Hynes A M, Ashraf H, Bhardwaj J K, Hopkins J, Johnston I and Shepherd J N 1999 *Sensors Actuators A* **74** 13
- [27] John P M St and Craighead H G 1996 *Appl. Phys. Lett.* **68** 1022
- [28] Gösele U, Tong Q-Y, Schumacher A, Kräuter G, Reiche M, Plöbl A, Kopperschmidt P, Lee T-H and Kim W-J 1999 *Sensors Actuators A* **74** 161
- [29] Stjernström M and Roeraade J 1998 *J. Micromech. Microeng.* **8** 33
- [30] Handique K, Burke D T, Mastrangelo C H and Burns M A 2000 *Anal. Chem.* **72** 4100
- [31] Roth S, Dellmann L, Racine G-A and de Rooij N F 1999 *J. Micromech. Microeng.* **9** 105
- [32] Mita Y, Mita M, Tixier A, Gouy J-P and Fujita H 2000 *Proc. IEEE 13th Annual Int. Conf. on MicroElectroMechanical Systems 'MEMS 2000' (Miyazaki, Japan)* (Piscataway, NJ: IEEE) p 300
- [33] Papra A, Bernard A, Juncker D, Larsen N B, Michel B and Delamarche E 2001 *Preprint* at press
- [34] Rabbany S Y, Marganski W A, Kusterbeck A W and Ligler F S 1998 *Biosens. Bioelectron.* **13** 939
- [35] Bernard A and Bosshard H R 1995 *Eur. J. Biochem.* **230** 416
- [36] Wiki W and Kunz R E 2000 *Opt. Lett.* **25** 463
- [37] Geissler M, Bernard A, Bietsch A, Schmid H, Michel B and Delamarche E 2000 *J. Am. Chem. Soc.* **122** 6303
- [38] Bernard A, Renault J P, Michel B, Bosshard H R and Delamarche E 2000 *Adv. Mater.* **12** 1067
- [39] Ceriotti L, Verpoorte E and de Rooij N F 2000 *Micro Total Analysis Systems 2000* ed A van den Berg *et al* (Dordrecht: Kluwer) p 225



## Chapter 3

# Engineering of the surface chemistry of capillary systems

Microfluidic networks made of poly(dimethylsiloxane), Si, and Au coated with polyethylene glycol for patterning proteins onto surfaces

Alexander Papra, André Bernard, David Juncker, Niels B. Larsen, Bruno Michel and Emmanuel Delamarche

*Langmuir* **17**, 4090-4095 (2001).



# Microfluidic Networks Made of Poly(dimethylsiloxane), Si, and Au Coated with Polyethylene Glycol for Patterning Proteins onto Surfaces

Alexander Papra,<sup>†</sup> André Bernard,<sup>‡</sup> David Juncker,<sup>‡</sup> Niels B. Larsen,<sup>†</sup>  
Bruno Michel,<sup>‡</sup> and Emmanuel Delamar<sup>\*‡</sup>

Risø National Laboratory, P.O. Box 49, 4000 Roskilde, Denmark, and IBM Research, Zurich  
Research Laboratory, Säumerstrasse 4, 8803 Rüschlikon, Switzerland

Received December 4, 2000. In Final Form: April 17, 2001

Microfluidic networks ( $\mu$ FNs) are passive (self-filling) devices incorporating microchannels for guiding minute volumes of fluids over surfaces.  $\mu$ FNs can be employed to localize the deposition of proteins from aqueous solutions onto substrates, for example. The walls of the channels must be hydrophilic for this purpose and should ideally resist the adsorption of proteins. We made  $\mu$ FNs using poly(dimethylsiloxane) (PDMS), Si/SiO<sub>2</sub>, and Au-covered Si and derivatized them with poly(ethylene glycol)s (PEGs) to fulfill both of these requirements. The grafting of the PEG molecules is optimized for either type of  $\mu$ FN: the networks from PDMS and silicon are derivatized using PEG-silanes and the Au-coated networks are derivatized with a thiolated PEG. Additionally, the zones of the Au-covered Si  $\mu$ FNs separating the channels are selectively covered with a hydrophobic thiol using microcontact printing. X-ray photoelectron spectroscopy and contact angle measurements indicate that all grafted layers have the expected chemical composition and are thin, homogeneous, and hydrophilic where desired. Finally, using fluorescently labeled antibodies we show that these  $\mu$ FNs are more effective for patterning, with high positional accuracy and edge resolution on PDMS substrates, than conventional O<sub>2</sub>-plasma-treated  $\mu$ FNs made from PDMS. Overall, our approach should help in making and using  $\mu$ FNs made from different materials but having similar surface properties.

## Introduction

Patterned deposition of biomolecules onto surfaces is a prerequisite for the development of array-based biosensing devices.<sup>1,2</sup> Microfluidic networks ( $\mu$ FNs) represent a compelling approach for the patterning of biological molecules,<sup>3,4</sup> because these devices can guide solutions of proteins conveniently over regions of a substrate to localize the adsorption of proteins.<sup>5–10</sup> There are several requirements concerning substrates and  $\mu$ FNs for a successful patterning of proteins:<sup>4,6</sup> (i)  $\mu$ FNs must be sufficiently hydrophilic to promote filling of the microchannels by capillary action, (ii) the contact between the substrate and  $\mu$ FN should be good enough to seal the channels, (iii) promoting the flow of a large volume of solution inside the microchannels can be necessary to guarantee a sufficient supply of proteins, and (iv) the  $\mu$ FN should have protein-

repellent surfaces to prevent unproductive loss of proteins to the walls of the microchannels. The first two requirements are mandatory, whereas the latter two are desirable.

In this article, we present a method for tailoring the surface properties of several types of  $\mu$ FN to fulfill the above-mentioned requirements. This extends the possible scope of applications of  $\mu$ FNs and makes them more convenient to use. Several combinations of materials for the substrate and for the  $\mu$ FN are possible, to ensure conformal contact between them and thus effective sealing of the channels. Either the  $\mu$ FN or the substrate can be an elastomer, for example. Figure 1 illustrates three of these possibilities, which we have investigated in detail and discuss here.  $\mu$ FNs made from poly(dimethylsiloxane) (PDMS) are soft and can be used on many substrates, regardless of their mechanical properties. Conversely,  $\mu$ FNs made in "hard" Si and Au can be used to pattern proteins onto PDMS substrates.<sup>9</sup> Harder  $\mu$ FNs are advantageous because they are mechanically more stable than  $\mu$ FNs in PDMS<sup>11</sup> and hence offer greater design possibilities. None of these three materials has ideal chemical surface properties to be readily used as  $\mu$ FNs, however. PDMS is a hydrophobic material, and therefore a  $\mu$ FN in PDMS must be hydrophilized before its channels can be filled by capillary action.<sup>4</sup> A brief oxygen-plasma treatment can be sufficient for this purpose. But in this case, the  $\mu$ FN must be used immediately after the plasma treatment or kept under water; the hydrophilized surface is not stable in ambient but reconstructs or contaminates toward a hydrophobic surface.<sup>12,13</sup> Si, with its native oxide, and Au have polar, wettable surfaces when they are clean,

\* To whom correspondence should be addressed.

<sup>†</sup> Risø National Laboratory.

<sup>‡</sup> IBM Research.

(1) Xia, Y.; Whitesides, G. M. *Angew. Chem., Int. Ed. Engl.* **1998**, *37*, 550–575.

(2) Yang, S.; Pérez-Luna, V. H.; López, G. P. Two-dimensional patterning of proteins. In *Protein Architecture*; Lvov, Y., Möhwald, H., Eds.; Marcel Dekker: New York, 1999.

(3) Delamarche, E.; Bernard, A.; Schmid, H.; Michel, B.; Biebuyck, H. *Science* **1997**, *276*, 779–781.

(4) Delamarche, E.; Bernard, A.; Schmid, H.; Bietsch, A.; Michel, B.; Biebuyck, H. *J. Am. Chem. Soc.* **1998**, *120*, 500–508.

(5) Patel, N.; Sanders, G. H. W.; Shakesheff, K. M.; Cannizzaro, S. M.; Davis, M. C.; Langer, R.; Roberts, C. J.; Tendler, S. J. B.; Williams, P. M. *Langmuir* **1999**, *15*, 7252–7257.

(6) Caelen, I.; Bernard, A.; Juncker, D.; Michel, B.; Heinzlmann, H.; Delamarche, E. *Langmuir* **2000**, *16*, 9125–9130.

(7) Rowe, C. A.; Scruggs, S. B.; Feldstein, M. J.; Golden, J. P.; Ligler, F. S. *Anal. Chem.* **1999**, *71*, 433–439.

(8) Bernard, A.; Renault, J. P.; Michel, B.; Bosshard, H. R.; Delamarche, E. *Adv. Mater.* **2000**, *12*, 1067–1070.

(9) Geissler, M.; Bernard, A.; Bietsch, A.; Schmid, H.; Michel, B.; Delamarche, E. *J. Am. Chem. Soc.* **2000**, *122*, 6303–6304.

(10) Bernard, A.; Michel, B.; Delamarche, E. *Anal. Chem.* **2001**, *73*, 8–12.

(11) Delamarche, E.; Schmid, H.; Michel, B.; Biebuyck, H. A. *Adv. Mater.* **1997**, *9*, 741–746.

(12) Owen, M. J.; Smith, P. J. *J. Adhes. Sci. Technol.* **1994**, *8*, 1063–1075.

(13) Donzel, C.; Geissler, M.; Bernard, A.; Wolf, H.; Michel, B.; Hilborn, J.; Delamarche, E. *Adv. Mater.* **2001**, in press.

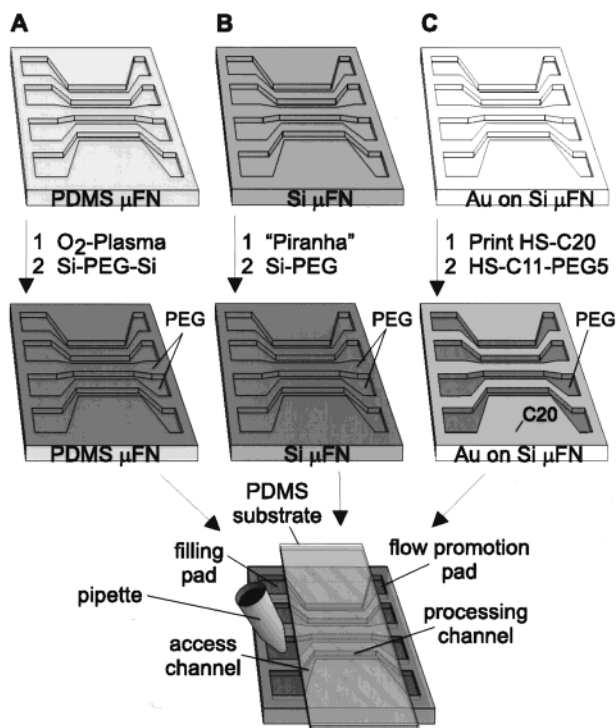


**Figure 1.** Strategies for coating  $\mu$ FNs made from different materials with poly(ethylene glycol)s. (A) The surface of  $\mu$ FNs in PDMS is oxidized in a  $O_2$ -based plasma and grafted with a PEG-disilane. (B)  $\mu$ FNs in silicon are cleaned with a strong oxidizing solution and silanized with PEGs. (C) HS-C20 is microcontact-printed on the raised parts of Au-coated  $\mu$ FNs, and the channels are derivatized with PEGs to control selectively the protein repellency and wetting characteristics of this type of  $\mu$ FN. All  $\mu$ FNs have the same design and are used in a similar way by placing a PDMS substrate across the channels.

but in practice these materials tend to contaminate under ambient conditions to become hydrophobic and chemically less defined. The possible loss of proteins because of their adsorption onto the walls of the  $\mu$ FNs during the patterning step is a second concern. Ideally, proteins should be spent only to derivatize the substrate, especially because, typically, a limited amount of proteins is displaced through the microchannel.

We choose to derivatize either type of  $\mu$ FN with functionalized poly(ethylene glycol) (PEG) polymers to yield  $\mu$ FNs with wettable and protein-repellent surfaces.<sup>13–16</sup> Derivatizing PDMS and Si/SiO<sub>2</sub> was done in an analogous manner.  $\mu$ FNs in PDMS were treated first with an  $O_2$  plasma before grafting a poly(ethylene glycol) di(triethoxy)silane (Si-PEG-Si) layer to it (Figure 1A), and  $\mu$ FNs in Si/SiO<sub>2</sub> were cleaned with a strong oxidizing solution and grafted with 2-[methoxy-(polyethyleneoxy)<sub>6–9</sub>-propyl]-trimethoxysilane (Si-PEG)<sup>17</sup> (Figure 1B). In the case of Au-coated Si  $\mu$ FNs, we combined self-assembly and microcontact printing of thiols:<sup>18</sup> Eicosanethiol (HS-C20) was printed<sup>9,19</sup> onto the raised

structures (gaps separating the channels) of the  $\mu$ FNs, which come into contact with the substrate during patterning.<sup>19</sup> Subsequent immersion of the printed  $\mu$ FNs in a solution of 11-penta(ethyleneoxy)undecanethiol (HS-C11-PEG5) localized the self-assembly of this hydrophilic, protein-repellent thiol<sup>20,21</sup> to the inner walls of the microchannels (Figure 1C).

## Experimental Section

**2.1. Proteins and Chemicals.** 2-[Methoxy-(polyethyleneoxy)<sub>6–9</sub>-propyl]-trimethoxysilane (Si-PEG, MW of 460–590, purity > 90%) from Gelest (Tullytown, PA), poly(ethylene glycol) di(triethoxy)silane (Si-PEG-Si, MW ~ 3400) from Shearwater Polymers (Huntsville, AL), and rabbit anti-guinea-pig IgG-TRITC from Sigma Chemie (Buchs, Switzerland) were used as supplied. Deionized water ( $R > 18.2 \text{ M}\Omega \text{ cm}^{-1}$ ) produced with a MilliQ purification unit (Millipore, Boston, MA) was used. All other chemicals were products of Aldrich (Milwaukee, WI).

**2.2. Fabrication of  $\mu$ FNs and Substrates.** PDMS  $\mu$ FNs resulted from curing PDMS (Sylgard 184, Dow Corning, Midland, MI) at 60 °C for at least 24 h against a fluorinated Si master. The fabrication of Si  $\mu$ FNs is described in detail elsewhere.<sup>22</sup> PDMS  $\mu$ FNs were oxidized in an oxygen plasma ( $P(O_2) \sim 0.36$  mbar, 140 W coil power, Technics Plasma 100-E, Florence, KY) for 10 s. The networks were immediately immersed in the Si-PEG-Si solution (1 mM Si-PEG-Si in water containing 0.8 mL concentrated HCl per liter) for 2 h at room temperature (RT). Afterward, the PDMS  $\mu$ FNs were washed twice in water and sonicated in water for 2 min. Si  $\mu$ FNs were sonicated in ethanol/water (1:1) for 5 min, dried, and then cleaned and oxidized with "piranha" solution (30% H<sub>2</sub>O<sub>2</sub> and concentrated H<sub>2</sub>SO<sub>4</sub>, 1:4 vol; caution: strong oxidizing agent) for 10 min. The networks were washed three times with water, sonicated in water for 10 min, blown dry and immediately immersed into the silane solution. The grafting was performed in a 3 mM solution of the Si-PEG in toluene containing 0.8 mL concentrated HCl per liter for 18 h at RT. The networks were washed in toluene (1 $\times$ ), ethanol (2 $\times$ ), and water (2 $\times$ ) and sonicated in water for 2 min to remove nongrafted material. Au-coated  $\mu$ FNs were fabricated by evaporating 1 nm of Ti and 100 nm of Au onto Si  $\mu$ FNs using an e-beam evaporator (Edwards FL 400). A hydrophobic monolayer was self-assembled on top of the raised structures of the Au-coated  $\mu$ FNs by printing for 10 s HS-C20 (0.5 mM solution in ethanol for the ink) using a (flat) PDMS stamp. These  $\mu$ FNs were immersed subsequently into a solution of HS-C11-PEG5 (5 mM in ethanol) for 10 s to form PEG monolayers exclusively inside the channels and pads. All  $\mu$ FNs were used with flat PDMS substrates. The PDMS substrates were cleaned with sonication in ethanol/water (1:1) for 3 min and then rinsed in water and dried under a stream of N<sub>2</sub> prior to their patterning.

**2.3. X-ray Photoelectron Spectroscopy (XPS).** XPS spectra were acquired on a Sigma Probe VG Scientific spectrophotometer operating at a base pressure of  $<10^{-9}$  mbar and equipped with a monochromatized Al K $\alpha$  source ( $E = 1486.6$  eV). The X-ray spot was focused down to 300  $\mu\text{m}$ . The analyzer had an angle of 45° to the sample, and samples were mounted on a multisample holder stage for examination under the same conditions. Spectra are referenced to the O 1s peak at 532 eV or to the Au 4f<sub>5/2</sub> peak at 84 eV, alternatively. For all samples, survey spectra were acquired first with a pass energy of 80 eV (0.2 eV steps for 40 ms), and two high-resolution spectra for N 1s taken with a pass energy of 40 eV were averaged (0.05 eV steps for 100 ms). The electron beam used to generate the X-rays had in all cases an intensity of 6.0 mA, which remained stable within <5% during the experiments. The intensity of the peaks from the substrates did not vary noticeably during the experiments, which indicated no particular damages on the surface of the grafted samples during the measurement. XPS on PDMS was done using a flood gun ( $\sim 0.6 \mu\text{A}$  emission current) at a partial pressure of Ar of

(14) Harris, J. M. In *Poly(ethylene glycol) chemistry. Biotechnological and biomedical applications*; Plenum Press: New York, 1992.

(15) Sofia, S.; Premnath, V.; Merrill, E. W. *Macromolecules* **1998**, *31*, 5059–5070.

(16) Malmsten, M.; Emoto, K.; Van Alstine, J. M. *J. Colloid Interface Sci.* **1998**, *202*, 507–517.

(17) Papra, A.; Gadegaard, N.; Larsen, N. B. *Langmuir* **2001**, *17*, 1457–1460.

(18) Kumar, A.; Whitesides, G. M. *Appl. Phys. Lett.* **1993**, *63*, 2002–2004.

(19) Libioulle, L.; Bietsch, A.; Schmid, H.; Michel, B.; Delamarche, E. *Langmuir* **1999**, *15*, 300–304.

(20) Prime, K. L.; Whitesides, G. M. *Science* **1991**, *252*, 1164–1167.

(21) Pale-Grosdemange, C.; Simon, E. S.; Prime, K.; Whitesides, G. M. *J. Am. Chem. Soc.* **1991**, *113*, 12–20.

(22) Juncker, D.; Schmid, H.; Bernard, A.; Caelen, I.; Michel, B.; de Rooij, N. F.; Delamarche, E. *J. Micromech. Microeng.* **2001**, in press.



$\sim 5 \times 10^{-8}$  mbar for charge compensation of these insulating samples. Charge compensation for measuring on the Si substrate was not necessary because the oxide of this substrate was relatively thin (2.0 nm as measured with ellipsometry). The sensitivity of the XPS is independent of the type of substrate when charge compensation is effective and when the experimental conditions are conserved between samples. All PDMS samples were cut to a size of  $<40$  mm<sup>2</sup> to minimize deterioration of the ultrahigh vacuum environment. The X-ray and flood guns were switched on, to warm them, before introducing the samples in the analysis chamber, and the X-ray gun was carefully degassed before acquiring the spectra to prevent contamination by the PDMS samples.

**2.4. Contact Angle Measurements.** Wettability of the modified surfaces by water was determined using a Krüss contact angle goniometer (Hamburg, Germany) equipped with a motorized pipet (Matrix Technology, Nashua, NH). Advancing and receding contact angles were measured at several spots on each sample and the respective values were averaged.

**2.5. Fluorescence Microscopy.** Fluorescence images of the tagged antibodies present on the surface were acquired with a fluorescence microscope (Nikon Labophot-2) equipped with a charge-coupled device camera (ST-8, SBIG, Santa Barbara, CA) cooled to  $-5$  °C. The fluorescence images were up to  $765 \times 510$  pixels (16 bits dynamic range) and were acquired with 4 s integration time and a magnification of  $\sim 10$ , using software designed for this camera (e.g., SkyPro, Software Bisque, Golden, CO).

**2.6. Protein Adsorption Assay.** PDMS substrates were placed onto the channels of the  $\mu$ FN. A 1  $\mu$ L drop of protein solution was pipetted onto the filling pad and transported through the channel by capillary action. After a 10 min incubation time, the substrate was removed under buffer (phosphate buffered saline, PBS) and rinsed with PBS and water.

## Results and Discussion

Our strategy to prepare wettable and protein-repellent  $\mu$ FNs is to graft a layer of PEGs onto the surface of PDMS, Si, and Au  $\mu$ FNs. This strategy is practical because PEGs are relatively chemically inert and thus compatible with a large variety of anchoring groups. Grafting PEG chains onto PDMS is the only case in this strategy requiring a pretreatment of the  $\mu$ FN surface with an O<sub>2</sub>-based plasma. This plasma treatment oxidizes the surface of PDMS and produces a thin, glassy silicate layer on the PDMS, which renders it suitable for the grafting of silane-derivatized PEGs. In the case of PDMS, the grafting of a PEG-disilane molecule prevented the strong loss of hydrophilicity of the O<sub>2</sub>-plasma-treated  $\mu$ FNs, by highly mobile silicon rubber chains.<sup>13</sup> This loss of hydrophilicity, termed "hydrophobicity recovery", has been studied in detail.<sup>23,24</sup> The possible causes for the hydrophobicity recovery of oxidized PDMS are mainly (i) the migration of low molecular weight siloxane chains and monomers from the bulk to the surface, (ii) the reorganization of the interface to expose less hydrophilic species at the PDMS-air interface in order to lower surface free energy, and (iii) accumulation of airborne hydrophobic contaminants. The possibility of having cross-linking between the silane anchoring groups did not seem to disturb the attachment of the PEG layer onto the surface, at least not in the concentration and under the conditions of grafting that we used. Furthermore, the relatively large molecular weight (3400 g mol<sup>-1</sup>) of the PEG molecule grafted onto  $\mu$ FNs made of PDMS may help to stabilize the grafted surface against reconstruction toward a more hydrophobic surface. We studied the hydrophobicity recovery of PDMS grafted with a series of PEGs with molecular weights

ranging from 500 to 5000 g mol<sup>-1</sup> and having one or two trialkoxysilanes<sup>25</sup> and found that Si-PEG-Si was probably the best type of PEG to graft to PDMS; this PEG is commercially available and preserves the hydrophilicity of the oxidized PDMS surface for over 3 weeks.<sup>13</sup>

The XPS survey spectrum in Figure 2 corresponding to this grafting reaction is largely consistent with previous work<sup>16</sup> and with the expected chemical composition of the PEG-PDMS surface. This spectrum and those obtained for the other types of  $\mu$ FNs were obtained by focusing the X-ray beam in the middle region of the filling pads and also between the two filling pads of the C20-coated part of the Au  $\mu$ FN; the C 1s peak reveals the presence of oxidized carbon atoms at 286.5 eV and represents  $\sim 30\%$  of the C 1s signal found in Au-PEG. Such oxidized carbon species are typically absent from PDMS surfaces treated with plasma conditions similar to ours.<sup>13,24,26</sup> The O 1s peak does not provide a major indication on the composition of the grafted layer because the oxidized PDMS substrate should contain oxygen atoms in a variety of chemical environments, which overlap with the oxygen signals from the PEG layer. As for oxygen, the Si peaks are dominated by the signals from the substrate. Importantly, the C 1s signal attributed to PEG is relatively small compared to that of PEG on Si/SiO<sub>2</sub> or Au, which suggests that the PEG layer on PDMS is thin or corresponds to an incomplete monolayer. This might result from a lower density of silanol anchoring groups on oxidized PDMS than on SiO<sub>2</sub> or from the condensation of silanols after the plasma treatment.<sup>23,26</sup> The recovery of hydrophobicity, starting after the plasma treatment, may also account for hiding some silanols from the anchoring groups of PEGs. The delay between plasma oxidation of PDMS and grafting with PEGs was kept to a minimum for this reason.

The oxide of a  $\mu$ FN made in Si reacts similarly with silanes as O<sub>2</sub>-plasma-treated PDMS, but the excellent homogeneity and chemical stability of this interface facilitates grafting silanes. For this reason, we used a relatively short monosilane having 6–9 PEG units in the case of Si/SiO<sub>2</sub>, for which the resulting grafted layer had the expected chemical composition, as shown in Figure 2. Two species for Si are visible, which correspond to Si from the bulk of the wafer and, at a slightly higher binding energy, to Si from the thin native oxide. These signals mask the signal associated to the Si anchoring group, which is otherwise attenuated by the presence of the monolayer. The O 1s peak from the PEG is similarly overwhelmed by the oxygen from the substrate. The C 1s signal at 287 eV corresponds to carbon from the PEG layer.<sup>21</sup> The intensity of this C 1s peak suggests the presence of a thicker PEG layer on Si than on Au. This is consistent with the work by Papra et al.,<sup>17</sup> in which the same compound was grafted onto Si/SiO<sub>2</sub> wafers under equivalent conditions and in which the PEG had a measured thickness of  $\sim 1.6$  nm, whereas the type of PEG that we grafted to Au is composed of an alkyl chain  $\sim 1.2$  nm long and has a PEG moiety of  $\sim 1.3$  nm.<sup>21</sup>

Au-coated  $\mu$ FNs offer an advantage over  $\mu$ FNs in PDMS or Si/SiO<sub>2</sub>: Au can be selectively microcontact printed with one type of alkanethiol, leaving unprinted regions of the  $\mu$ FN available for the chemisorption from solution of a second type of alkanethiol. HS-C20 was selected because it is simple to microcontact print onto Au and it forms a highly hydrophobic surface thereupon. We note that the

(23) Hillborg, H.; Gedde, U. W. *IEEE Trans. Dielectr. Electr. Insul.* **1999**, *6*, 703–717.

(24) Owen, M. J.; Smith, P. J. *J. Adhes. Sci. Technol.* **1994**, *8*, 1063–1075.

(25) Donzel, C. et al. Manuscript in preparation.

(26) Kim, J.; Chaudhury, M. K.; Owen, M. J. *J. Colloid Interface Sci.* **2000**, *226*, 231–236.

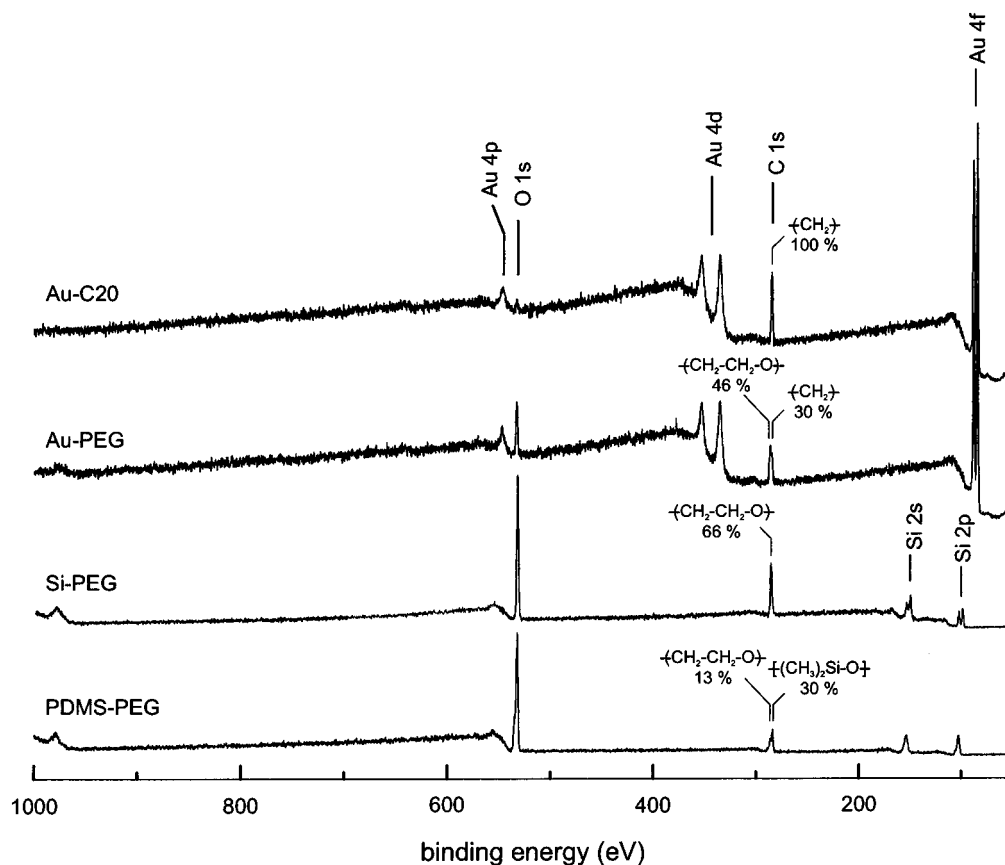


**Figure 2.** XPS overview spectra measured on the surface of  $\mu$ FNs derivatized with specific films. The XPS spectra on the Au  $\mu$ FNs were obtained inside the filling pad (Au-PEG) and between two filling pads (Au-C20). Information on the C 1s peaks obtained from high-resolution spectra are reported on the survey and compared to the C 1s signal measured on Au-C20, which can serve as a reference.

small O 1s peak in the Au-C20 spectrum (Figure 2) was the only unexpected element detected in the XPS spectra. This oxygen might correspond to a small quantity of HS-C11-PEG5 molecules that were possibly exchanged with some of the printed HS-C20 molecules during the self-assembly from the solution of the PEG-derivatized monolayer. We used a relatively high concentration of HS-C11-PEG5 solution and a short reaction time when chemisorbing those PEG molecules, to minimize this exchange of thiols.<sup>27</sup> The C 1s and O 1s peaks are both associated with the grafted PEG layer. The C 1s peak has one component at 284.6 eV, corresponding to carbons from the alkyl chains, and a second component at 286.8 eV, corresponding to the carbon atoms linked to the oxygen forming the PEG units.<sup>27</sup>

Contact angle measurements with water as the probe liquid were used to measure the hydrophilicity of the  $\mu$ FNs and are reported in Figure 3. The advancing contact angles of water reflect the susceptibility of either type of  $\mu$ FN for filling, whereas the hysteresis between advancing and receding contact angles gives an indication of the chemical and/or topological heterogeneity of the  $\mu$ FN surface and therefore indirectly reveals the quality of the coating.<sup>28,29</sup> All contact angles were measured on zones of the  $\mu$ FNs that were planar and large enough to avoid contact

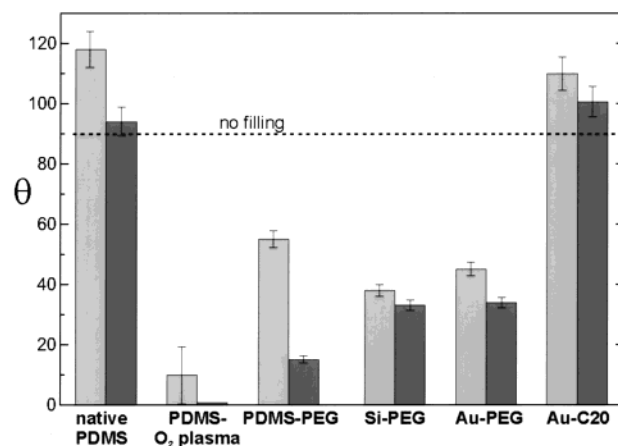


**Figure 3.** Advancing (bright columns) and receding (dark columns) contact angles of water (captive drop method) on surface-treated  $\mu$ FNs. All contact angles were stable in time, except those of PDMS treated only with an  $O_2$  plasma, and measured 5 min after the plasma treatment. Advancing contact angles must be lower than  $90^\circ$  to permit filling of the microchannels with solutions of proteins, owing to capillary pressure. Capillary pressure increases with diminishing contact angles.

between water droplets and microstructures, which would have influenced the wetting behavior of the probe liquid. Native PDMS is evidently a hydrophobic material; thus, untreated PDMS microchannels cannot be filled by aqueous protein solutions. In contrast, PDMS, Si, and Au  $\mu$ FNs each with grafted PEG have a comparable hydrophilicity. The advancing contact angles of  $\sim 40$ – $50^\circ$  observed for these surfaces indicate that it will be easy

(27) Mixed monolayers on Au comprising PEG and hydrocarbon chains remain protein-repellent depending on the length of the PEG chains and the molar fractions of the thiols. See also: Prime, K.; Whitesides, G. M. *J. Am. Chem. Soc.* **1993**, *115*, 10714–10721.

(28) Bain, C. D.; Whitesides, G. M. *J. Am. Chem. Soc.* **1995**, *117*, 3882–3893.

(29) Atre, S. V.; Liedberg, B.; Allara, D. L. *Langmuir* **1988**, *4*, 3665–3666.

to fill these  $\mu$ FNs with solutions of proteins. The larger hysteresis between the advancing and the receding contact angle observed for the PDMS-PEG surface reveals that this  $\mu$ FN has a less chemically homogeneous and/or morphologically smooth surface than  $\mu$ FNs in Si or Au; PDMS is the product of a chemical reaction involving prepolymers of various chain lengths and degree of functionality, filler materials, catalysts, and modulators, and the plasma treatment creates microcracks on the surface of the oxidized polymer.<sup>30</sup> PDMS freshly treated with O<sub>2</sub> plasma only is more hydrophilic than PDMS grafted with PEG. We observed, however, that the microcracks produced by the plasma on the surface of the oxidized PDMS accelerate the hydrophobicity recovery when  $\mu$ FNs are stressed too much during handling.<sup>30,31</sup> Alternatively, the very low advancing contact angle with water of plasma-treated  $\mu$ FNs in PDMS might lead to the excursion of some sample solutions to adjacent channels during filling of the  $\mu$ FN pads.<sup>22</sup> HS-C20 self-assembled on Au has a similar hydrophobicity to that of PDMS and is very effective in preventing the excursion of liquid away from the fillable parts of the network.

The PEG-coated  $\mu$ FNs were used to pattern fluorescently tagged IgGs from solution onto PDMS substrates (Figure 4). The concentration of proteins ranged from 400 down to 2  $\mu$ g mL<sup>-1</sup>. This range of concentrations was selected to evaluate the practical limits for patterning proteins onto PDMS using these  $\mu$ FNs. The patterning parameters (duration of deposition, substrate, and rinsing steps, for example) and the geometry of the  $\mu$ FNs were kept the same during all experiments to facilitate comparing the performances of either type of  $\mu$ FN. We examined the fluorescence and the N 1s XPS signal associated to the proteins on the substrate as well as on the walls of the  $\mu$ FNs (unproductive deposition). No fluorescence signal could be recorded from the hard  $\mu$ FNs because of quenching (n.a. in Figure 4). As can be seen for all the  $\mu$ FNs, the amount of proteins deposited on the substrate is proportional to their concentration in solution, and for the detection conditions of the fluorescence used here, a significant amount of proteins is detected on the surface even for the 20  $\mu$ g mL<sup>-1</sup> solution. The contrast and resolution of the pattern are high in all cases but are probably the best for the Si and Au  $\mu$ FNs. The images obtained on the PDMS  $\mu$ FNs hydrophilized with an O<sub>2</sub> plasma and coated with PEG reveal a loss of IgGs in the microchannel which was filled with the most concentrated solution of proteins. When considering the fluorescence signal on the PDMS substrates, it becomes clear that these losses are only moderate and that these  $\mu$ FNs were overall efficient in repelling proteins from their walls. As a complement to the fluorescence experiments, we studied the loss of protein on all the  $\mu$ FNs by recording the regions corresponding to N 1s peaks using XPS (Figure 4). The PDMS  $\mu$ FN treated with an O<sub>2</sub> plasma and the PEG-coated PDMS  $\mu$ FN feature an important difference: the surface of the plasma-hydrophilized  $\mu$ FN is not stable<sup>26</sup> but recovers its original hydrophobicity of PDMS over time. This hydrophobicity recovery poses practical problems because it is easily accelerated by flexing and handling the  $\mu$ FN and because some time is needed to position the  $\mu$ FN over the substrate and to fill it. As a result, the  $\mu$ FN can quickly become less protein-repellent while it recovers its hydrophobicity. We estimate from the N 1s XPS signals that the amount of proteins deposited onto the  $\mu$ FN in PDMS, used 1 min after the plasma treatment, corre-

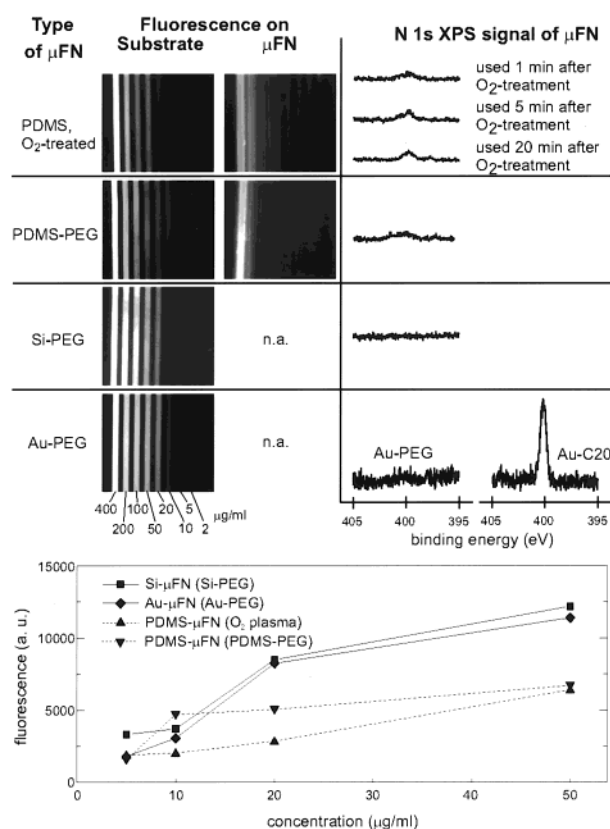


**Figure 4.** Fluorescence microscopy and XPS reveal the amount of TRITC-tagged antibodies deposited from solutions with decreasing concentrations on a PDMS substrate (images in left column) or lost on the walls of the  $\mu$ FNs (images in right column) used for this patterning. Fluorescence signals could not be measured on the Au and Si  $\mu$ FNs because of strong quenching of the fluorescence, but the N 1s XPS signals reveal the quantities of proteins lost on all types of  $\mu$ FNs. The XPS signals measured on the Au  $\mu$ FN are displayed enlarged compared to the other signals. The amount of protein lost on the O<sub>2</sub>-plasma-treated  $\mu$ FN increases with the delay between the plasma treatment and use of the  $\mu$ FN. The lower graph quantifies the surface fluorescence signal associated to the deposited IgGs depending on their concentration in solution and the type of  $\mu$ FN used.

sponds to  $\sim$ 9% of a full monolayer of IgGs. This amount increases up to  $\sim$ 16% and  $\sim$ 20% when the delay between the plasma treatment and use of the  $\mu$ FNs increases to 5 and 20 min, respectively. In contrast, we found that the PEG-treated  $\mu$ FNs remained hydrophilic for more than 3 days,<sup>25</sup> while conserving a high degree of protein repellency. The amount of IgG lost to this type of  $\mu$ FN is between 6% and 8% of a full monolayer. The XPS N 1s regions for the Si and Au PEG-coated  $\mu$ FNs corroborate the indications given by Figures 2 and 3: grafting a PEG layer on these surfaces was not only simpler than grafting it on a PDMS elastomer, but it resulted in an even better protein-repellent layer. There is no trace of nitrogen found by XPS in the N 1s region of the PEG-Si  $\mu$ FN, and although there seems to be a trace of nitrogen in the N 1s signal for the Au-PEG type of  $\mu$ FN, this signal is too small to be quantified.

The overall amount of protein lost to the walls of the different types of  $\mu$ FN might not appear very critical, at least not for depositing proteins from concentrated solutions. This may not be the case when the solutions of proteins are diluted and flow in relatively long microchannels.<sup>6</sup> The graph in Figure 4 which shows the surface fluorescence associated with the immobilized IgGs, depending on their concentration in solution and the type

(30) Fritz, J. L.; Owen, M. J. *J. Adhes.* **1995**, *54*, 33–45.

(31) Hillborg, H.; Gedde, U. W. *Polymer* **1998**, *38*, 1991–1998.



of  $\mu$ FN used, corroborates the previous observations: for a concentration equal to or less than  $50 \mu\text{g mL}^{-1}$ , the amount of protein deposited onto the substrate using  $\mu$ FNs in PDMS is already significantly lower than when Si-PEG and Au-PEG  $\mu$ FNs are used. Finally, all fluorescence values for even lower concentrations converge toward the background level for this surface fluorescence assay.

### Conclusion

The networks of three types of  $\mu$ FNs including an elastomer (PDMS replica), an oxide (micromachined Si/SiO<sub>2</sub>), and an oxide covered with a metal (Au) were made hydrophilic and protein-repellent by derivatizing their channels with PEG moieties. This expands the scope of applications of  $\mu$ FNs for the patterning of proteins onto substrates without requiring very specific surface treatments of the different types of  $\mu$ FNs. As PEG molecules are protein-repellent in general, we think that our grafting strategies can be successful for a large variety of proteins. Preventing or minimizing losses of proteins because of

their deposition onto the channels of a  $\mu$ FN adds to the versatility of PEG-coated  $\mu$ FNs. Because it is possible to use an elastomer such as PDMS for the substrate to pattern the deposition of proteins, the preparation of "hard"  $\mu$ FNs in Si might prove particularly attractive. Indeed, the coating of such  $\mu$ FNs with an evaporated Au film seems ideal, because it opens the possibility to tailor independently the surface properties of the  $\mu$ FN inside the channels and in the sealing regions.

**Acknowledgment.** We thank H. Wolf, C. Donzel, I. Caelen, J. Ph. Renault, H. Schmid, F. Kamounah, and K. Schaumburg for their help and discussions, R. Widmer and U. Drechsler for their help in preparing the microfluidic networks, and P. F. Seidler for his continuous support. This work was supported in part by the Swiss Federal Office of Education and the BIOTECH European project BIOPATT (BIO4CT980536).

LA0016930



## Chapter 4

# Patterning of density-gradients of adsorbed proteins

**Formation of gradients of proteins on surfaces with microfluidic networks**

Isabelle Caelen, André Bernard, David Juncker, Bruno Michel, Harry Heinzelmann and Emmanuel Delamarche

*Langmuir* **16**, 9125-9130 (2000).



## Formation of Gradients of Proteins on Surfaces with Microfluidic Networks

Isabelle Caelen,<sup>†</sup> André Bernard,<sup>‡</sup> David Juncker,<sup>‡</sup> Bruno Michel,<sup>‡</sup>  
Harry Heinzelmann,<sup>†</sup> and Emmanuel Delamarche<sup>\*,‡</sup>

Centre Suisse d'Electronique et de Microtechnique SA (CSEM), rue Jaquet-Droz 1,  
2007 Neuchâtel, Switzerland, and IBM Research, Zurich Research Laboratory,  
8803 Rüschlikon, Switzerland

Received June 19, 2000. In Final Form: August 23, 2000

The capability of microfluidic networks to pattern substrates with proteins is extended to create density gradients of proteins on surfaces. The networks are micromachined in Si, and the substrates are hydrophobic poly(dimethylsiloxane) (PDMS) elastomers. The gradients result from the progressive depletion of proteins in the fluids due to their adsorption onto the PDMS substrate as the solution travels along the microchannel. Forming gradients of rhodamine-tagged antigens on PDMS and binding the antigens with fluorescein-tagged antibodies from solution enable us to study the binding behavior of these partners on a surface: Detection of the fluorescence associated with either partner suggests that recognition of the surface-immobilized antigens by an antibody from solution is more effective for a low density of antigens on the surface.

### Introduction

Biological processes rely on molecular interactions between ligands and receptors, including enzymes and their substrates or inhibitors, adhesion factors and cell receptors, and antigens and antibodies, for example, all of which fulfill vital functions in organisms. The specificity and occurrence of ligand–receptor interactions must be exquisitely tuned to the needs of organisms for this reason. A particular and important use of ligand–receptor interactions in vitro is for immunodiagnosics where the interaction between an antigen and its antibody often occurs at a solid–liquid interface.<sup>1</sup>

A binding event at a solid–liquid interface is not comparable to one in solution, however. Proteins tend to alter their native conformation<sup>2,3</sup> as they adsorb onto liquid–solid interfaces and onto hydrophobic surfaces in particular. The binding properties of antibodies to antigens depend for both on their native three-dimensional structure; thus conformational changes of these proteins upon adsorption can affect their binding characteristics.<sup>4,5</sup> Steric access to the binding sites, orientation of the immobilized protein, and the proximity between these proteins are additional factors that affect interactions between ligands and receptors near a surface.<sup>6–8</sup>

Simultaneous control over the position and density of proteins on a surface could constitute a powerful means to investigate the binding properties between two partners

on a surface.<sup>9–14</sup> We propose in this Letter that microfluidic networks ( $\mu$ FNs)<sup>15,16</sup> be used to create gradients of immobilized proteins on a surface to investigate how the density of the immobilized proteins on the surface influences their recognition by antibodies from solution. Specifically, we prepared gradients of proteins on PDMS which served as antigens to bind antibodies from solution. The advantage of this method compared to previous studies that investigated the effect of the density on the binding properties of immobilized proteins<sup>6,7</sup> is that (i) forming gradients of proteins with  $\mu$ FNs is simple, fast, and uses small amounts of reagents, (ii) it provides a large ensemble of adjacent zones of a substrate with varying density of deposited proteins, which facilitates screening the results, and (iii) fluorescence tagging can be used to reveal the presence of both binding partners on the surface simultaneously.

Figure 1 summarizes our approach in which a PDMS substrate is placed across the channels of a Si micromachined  $\mu$ FN to pattern lines of proteins onto the substrate. The  $\mu$ FN comprises two macroscopic pads ( $2 \times 3 \text{ mm}^2$ ) separated by an array of 5-mm-long microchannels, Figure 1B. Capillary forces between a solution containing proteins and the hydrophilized walls of the  $\mu$ FN induce filling of the channels,<sup>17</sup> leading to deposition of proteins over the hydrophobic regions of the PDMS substrate exposed to the filled channels, Figure 1C.<sup>16</sup> The gradient of proteins on the PDMS substrate forms during this step: by flowing into the channels, the solution of protein is gradually

\* To whom correspondence should be addressed, e-mail: emd@zurich.ibm.com.

<sup>†</sup> Centre Suisse d'Electronique et de Microtechnique SA (CSEM).

<sup>‡</sup> IBM Research, Zurich Research Laboratory.

(1) *Immunoassay*, Diamandis, E. P., Christopoulos, Th.-K., Eds.; Academic Press: San Diego, 1996.

(2) Lyklema, J. *Colloids Surf.* **1983**, *10*, 33.

(3) Sandwick, R. K.; Schray, K. J. *J. Colloid Interface Sci.* **1987**, *115*, 130.

(4) Ngai, P. K. M.; Ackermann, F.; Wendt, H.; Savoca, R.; Bosshard, H. R. *J. Immunol. Methods* **1993**, *158*, 267.

(5) Schwab, C.; Bosshard, H. R. *J. Immunol. Methods* **1992**, *147*, 125.

(6) Schramm, W.; Paek, S.-H. *Anal. Biochem.* **1992**, *205*, 47.

(7) Wimalasena, R. L.; Wilson, G. S. *J. Chromatogr.* **1991**, *572*, 85.

(8) Butler, J. E.; Ni, L.; Nessler, R.; Joshi, K. S.; Suter, M.; Rosenberg, B.; Chang, J.; Brown, W. R.; Cantarero, L. A. *J. Immunol. Methods* **1992**, *150*, 77.

(9) Lin, Y. S.; Hlady, V.; Gölander, C.-G. *Colloids Surf., B: Biointerfaces* **1994**, *3*, 49.

(10) Herbert, C. B.; McLernon, T. L.; Hypolite, C. L.; Adams, D. N.; Pikus, L.; Huang, C.-C.; Fields, G. B.; Letourneau, P. C.; Distefano, M. D.; Hu, W.-S. *Chem. Biol.* **1997**, *4*, 731.

(11) Lee, J. H.; Kang, G. S.; Lee, J. W.; Lee, H. B. *Macromol. Symp.* **1997**, *118*, 571.

(12) Lee, J. H.; Jeong, B. J.; Lee, H. B. *J. Biomed. Res.* **1997**, *34*, 105.

(13) Ruardy, T. G.; Schakenraad, J. M.; van der Mei, H. C.; Busscher, H. J. *Surf. Sci. Rep.* **1997**, *29*, 1.

(14) Liedberg, B.; Tengvall, P. *Langmuir* **1995**, *11*, 3821.

(15) Delamarche, E.; Bernard, A.; Schmid, H.; Michel, B.; Biebuyck, H. *Science* **1997**, *276*, 779.

(16) Delamarche, E.; Bernard, A.; Schmid, H.; Bietsch, A.; Michel, B.; Biebuyck, H. *J. Am. Chem. Soc.* **1998**, *120*, 500.

(17) Kim, E.; Xia, Y.; Whitesides, G. M. *J. Am. Chem. Soc.* **1996**, *118*, 5722.

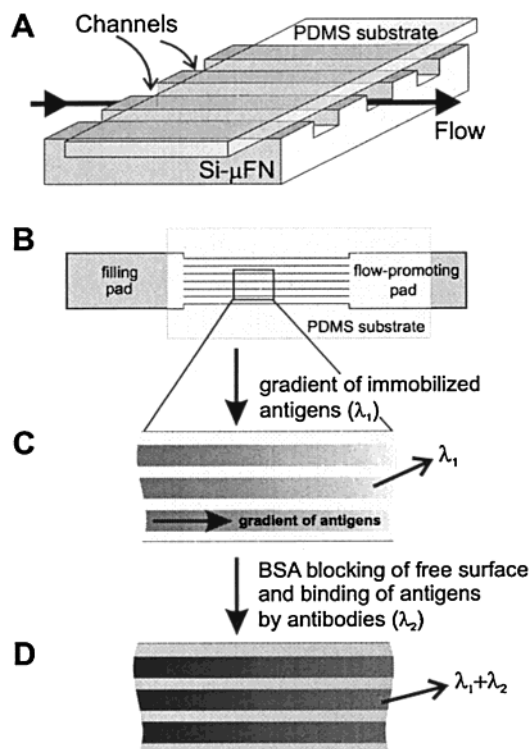


**Figure 1.** Si  $\mu$ FNs can pattern a PDMS substrate with a gradient of immobilized biomolecules. (A) The seal between the network and the elastomeric substrate confines the deposition of biomolecules from solution onto the PDMS regions exposed to the microchannels. (B) The PDMS substrate is placed across an array of microchannels and covers only a fraction of the filling- and flow-promoting pads to enable filling of the channels and displacement of air by the liquid, respectively. (C) The geometry of the  $\mu$ FN and the limited amount of proteins (antigens) flowing through the channels lead to a depletion gradient of immobilized antigens on the surface. These antigens can be tagged for example with a fluorophore  $\lambda_1$ . (D) After removal of the  $\mu$ FN and blocking the surface against nonspecific binding with BSA, the immobilized antigens are bound by fluorescently labeled ( $\lambda_2$ ) antibodies from bulk solution. The two different fluorophores allow for their simultaneous, yet individual, detection by fluorescence microscopy.

depleted by fast adsorption of the proteins to the PDMS. Blocking the underivatized areas of PDMS with bovine serum albumine (BSA) is done after separating the PDMS layer from the  $\mu$ FN structures. Binding the immobilized antigens with antibodies from solution is the last step of this assay, and "simultaneous" detection of the binding partners proceeds when both proteins are tagged with a different fluorophore, Figure 1D.

The  $\mu$ FNs used here were made in a Si wafer because Si is a convenient material to micromachine: many geometries for the  $\mu$ FN patterns are possible without compromising the stability of the microchannels;<sup>18</sup> the SiO<sub>2</sub> layer present at the surface of the  $\mu$ FN can be readily cleaned and hydrophilized. PDMS was used as a substrate because this elastomer establishes conformal contact<sup>19</sup> with the raised structures of the  $\mu$ FN and effectively seals the channels. The surface of PDMS is hydrophobic and promotes deposition of proteins from solution.<sup>20–22</sup> It is

transparent and has little interfering fluorescence at the standard wavelengths of excitation of common fluorescent tags.

## Experimental Section

**2.1. Fabrication of Microfluidic Networks.** Standard photolithography was used to pattern microchannels and pads in Si wafers. The wafers were first spin-coated at 4000 rpm with  $\sim 1.2 \mu\text{m}$  of AZ6612 photoresist (Hoechst), photoexposed through a Cr mask (Photronics, Dresden, Germany) and developed for 30 s in AZ400/H<sub>2</sub>O (1:4; Hoechst). The photoresist acted as a mask for an inductively coupled plasma (reactive ion etcher from Surface Technology Systems, Cambridge, U.K.) to pattern the silicon wafer. Three different geometries for the  $\mu$ FNs were used in this work. A first geometry consisted of two  $3 \times 2 \text{ mm}^2$  pads (a filling and a flow-promoting pad) connected via an array of 30 channels, which were 5 mm long,  $15 \mu\text{m}$  wide, and separated by  $20 \mu\text{m}$ . Both pads and microchannels had a depth of  $6.5 \mu\text{m}$ . The second type of  $\mu$ FNs was  $1.5 \mu\text{m}$  deep. The third one had 16 parallel channels (5 mm long,  $20 \mu\text{m}$  wide, and separated by  $20 \mu\text{m}$ ) that were each connected to a filling and flow-promoting pad ( $1.5 \times 1.5 \text{ mm}^2$ ). For this geometry, all structures were  $20 \mu\text{m}$  deep.

**2.2. Preparation of Substrates.** PDMS substrates were obtained by curing the prepolymer components of Sylgard 184 (Dow Corning, Midland, MI) at  $60^\circ\text{C}$  for at least 24 h against the bottom of a polystyrene dish; these components were mixed according to the recommendations of the manufacturer, using an automatic dispenser (DOPAG MICROMIX E, Cham, Switzerland).

**2.3. Proteins and Reagents.** Biomolecules, assay reagents, and immunoconjugates were obtained from Sigma (Sigma Chemie, Buchs, Switzerland). Deionized water or Millipore water ( $R > 18.2 \text{ M}\Omega \text{ cm}^{-1}$ ) produced with a Milli-Q purification unit (Millipore) was used in this work. Phosphate-buffer saline (PBS) was prepared with 150 mM NaCl, 4 mM KCl, 8.1 mM Na<sub>2</sub>HPO<sub>4</sub>, and 1.47 mM KH<sub>2</sub>PO<sub>4</sub> in deionized water and had a pH of 7.4.

**2.4.  $\mu$ FN Patterning of PDMS Substrates.** PDMS substrates were cut from a PDMS layer cured against the bottom of a Petri dish and placed by hand onto the  $\mu$ FN without applying pressure. Conformal contact between PDMS and the raised structures of the  $\mu$ FN was sufficient to ensure good sealing of the channels. Solutions of protein with a concentration in PBS ranging from 10 to  $1000 \mu\text{g mL}^{-1}$  were applied with an Eppendorf micropipet on the filling pad, from which the liquid entered and filled the hydrophilic channels of the  $\mu$ FN owing to capillary forces. This defined the starting time for the duration of the experiments. The fluid rapidly ( $1 \text{ mm s}^{-1}$ ) reached the flow-promoting pad. Removal of the PDMS substrate from the  $\mu$ FN was done quickly under a flow of BSA (1% in PBS). The PDMS substrates were then rinsed for 20 s under deionized water to remove partially bound proteins and were dried under a stream of N<sub>2</sub>. Each experiment for a given duration of immobilization and concentration of the protein solution was done in triplicate and with simultaneous use of at least three adjacent  $\mu$ FNs.

**2.5. Immunobinding Assays.** Sites of adsorption on the PDMS substrates that remained free after derivatization with the antigens were blocked by exposing the entire substrates to a  $100\text{-}\mu\text{L}$  solution of 1% BSA in PBS for 30 min at room temperature. The BSA solution was then pipetted back with care, and the PDMS substrates were covered with  $100 \mu\text{L}$  of diluted antispecies IgG solutions (1:200 in PBS). The substrates were not allowed to dry during removal of the BSA solution so as to use the remaining thin film of liquid to help cover the surface homogeneously with the antispecies solution. The recognition step was performed for 30 min and stopped by rinsing the substrate with deionized water for 20 s and then blow-dried with N<sub>2</sub>. Fluorescence images of the tagged proteins present on the surface were acquired with a fluorescence microscope (Nikon Labophot-2) equipped with band-pass filters, a 100-W Xe lamp, and a charge-coupled device camera (ST-8, SBIG, Santa Barbara,

(18) Delamarche, E.; Schmid, H.; Michel, B.; Biebuyck, H. *Adv. Mater.* **1997**, *9*, 741.

(19) Xia, Y.; Whitesides, G. M. *Angew. Chem., Int. Ed. Engl.* **1998**, *37*, 550.

(20) Lok, B. K.; Cheng, Y.-L.; Robertson, C. R. *J. Colloid Interface Sci.* **1983**, *91*, 104.

(21) Bernard, A.; Delamarche, E.; Schmid, H.; Michel, B.; Bosshard, H. R.; Biebuyck, H. *Langmuir* **1998**, *14*, 2225.

(22) Bernard, A.; Renault, J. P.; Michel, B.; Bosshard, H. R.; Delamarche, E. *Adv. Mater.* **2000**, *12*, 1067.

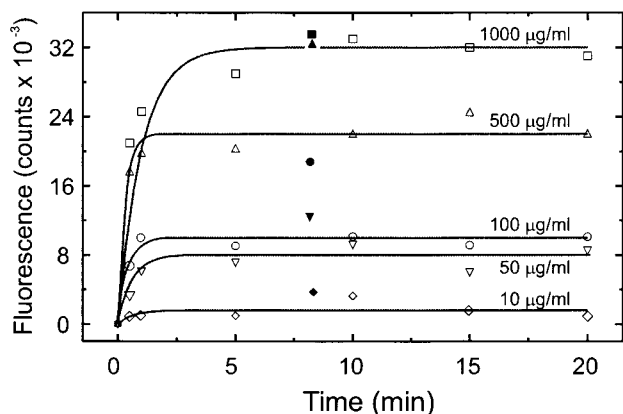


**Figure 2.** Fluorescence intensity of TRITC-labeled rabbit-IgGs deposited on PDMS as a function of protein concentration and incubation time. The comparison of protein adsorption from solution (filled symbols) and from a  $\mu$ FN (open symbols) having the same geometry as in Figure 1 as a function of the initial concentration revealed that the solutions of IgG were depleted in the channels (see text). A maximal coverage of IgG was reached for the highest protein concentration ( $1000 \mu\text{g mL}^{-1}$ ), corresponding here to 32 000 counts.

CA) cooled to  $0^\circ\text{C}$ . The fluorescence images were acquired with  $765 \times 510$  pixels (16 bits dynamic range), 4-s integration time, and a magnification of  $\sim 25$ , using SkyPro software (Bisque, Golden, CO). A series of images covering the gradient area was acquired under identical conditions, assembled with the software Photoshop (Adobe Systems, Inc., San Jose, CA), and analyzed with ImagePro (Media Cybernetics, Del Mar, CA).

### Results and Discussion

The first set of experiments characterizes the deposition of serum antibodies (rabbit) from solutions in PBS onto PDMS using a Si  $\mu$ FN having a geometry as shown in Figure 1. These antibodies are tagged with a rhodamine (TRITC) derivative so that the fluorescence intensity at the surface indicates how many proteins were immobilized for a given solution concentration and time of deposition, Figure 2. The profile of the curves reveals that initially deposition is fast but saturates at a certain protein coverage, which depends on the initial concentration of protein in the solutions that filled the  $\mu$ FN. For deposition from solution (filled symbols in Figure 2), maximum coverage is obtained using a concentration of antibodies in PBS of at least  $500 \mu\text{g mL}^{-1}$ .<sup>6,8,24</sup> In contrast, for solutions flowing in the  $\mu$ FNs (open symbols in Figure 2), reducing this concentration from 1000 to  $500 \mu\text{g mL}^{-1}$  already decreases the amount of antibodies immobilized on the PDMS surface. The curves in Figure 2 reveal that this observation is general: at equivalent concentrations and durations of reaction, fewer antibodies are deposited onto the substrate using a  $\mu$ FN than when a drop of solution of proteins was placed directly onto the PDMS substrate. We attribute this difference to the depletion of antibodies in the solutions filling the channels.<sup>16</sup> The site for assessing the amount of surface-adsorbed proteins by fluorescence was always the same distance from the filling pad of the  $\mu$ FN. The high surface-to-volume ratio of the microchannels provides a large area for derivatization per unit volume of protein solution. As a consequence, only the beginning of the channels is covered with proteins when the concentration of proteins in the solution is not high enough. Promoting the flow of the solution through the channels is in some cases important for ensuring the renewal of their content and for reducing or preventing this depletion effect when necessary.

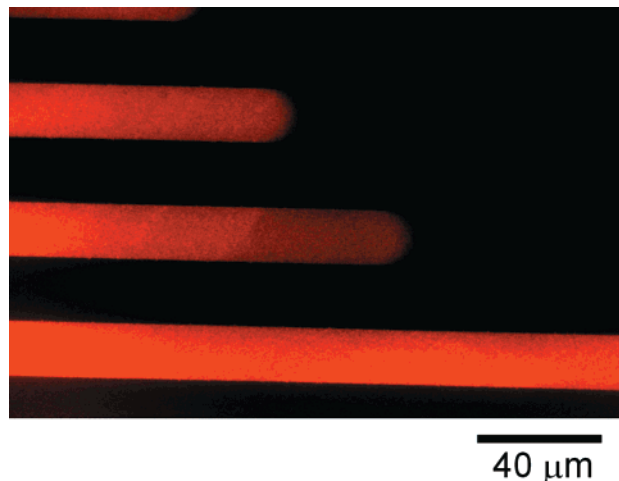


**Figure 3.** Short-scale gradient of a fluorescently labeled antibody deposited from a  $\mu$ FN onto a PDMS substrate. The protein solution had a concentration of  $100 \mu\text{g mL}^{-1}$  of TRITC-tagged IgGs in PBS, and the Si  $\mu$ FN had  $20\text{-}\mu\text{m}$ -wide and  $1.5\text{-}\mu\text{m}$ -deep channels. The Poiseuille flow profile and the sharp drop of surface coverage reflect the fast rate of deposition of the IgGs from the fluid, the laminar nature of the flow, and the high speed of filling.

In this work, the depletion of proteins in the fluids displaced along the microchannels enabled the formation of surface-density gradients of immobilized proteins. The small dimensions of the channels are desired and have an important influence on the creation of surface-density gradients. Depletion of reactants flowing in a microchannel is exacerbated when the characteristic diffusion length of the reactants attains the same order of magnitude of or becomes greater than the cross section of the conduits. In this case, deposition of proteins, for example, can occur rapidly because the adsorption process is not limited by the transport from the solution to the substrate. The fluorescence microscopy image in Figure 3 illustrates such a situation. The  $15\text{-}\mu\text{m}$ -wide and  $1.5\text{-}\mu\text{m}$ -thin channels used here were very efficient in guiding a solution of antibodies dissolved in PBS and favored the loss of antibodies from solution by deposition onto the PDMS substrate. In this example, the length scale of the gradient is only  $\sim 30 \mu\text{m}$ . The shape of this gradient is equally interesting: it reflects the profile of fluid velocity within the channel near the depletion zone. The flow was fastest in the middle of the channel (Poiseuille type of flow profile); hence proteins could be carried by the fluid a little bit farther along the channels before they were deposited.

Even though it is straightforward to create a gradient of proteins on a surface like the one displayed in Figure 3, we suggest that it is important to have the factors affecting the shape and the length scale of the gradient well under control. The gradient should not be too short in order to facilitate the evaluation of the results. The concentration of proteins in the fluid and the geometry of the channels can serve to "shape" the gradient; the wettability of the channels and the reactivity between the proteins and interfaces are not convenient parameters for controlling the formation of the gradient.

Figure 4 illustrates how it is possible to take advantage of an array of independent channels to pattern lines with different densities of proteins onto PDMS.<sup>23</sup> Solutions with decreasing concentration of rabbit antigens in PBS were drawn in each channel where their deposition was homogeneous and resulted in a decreasing amount of



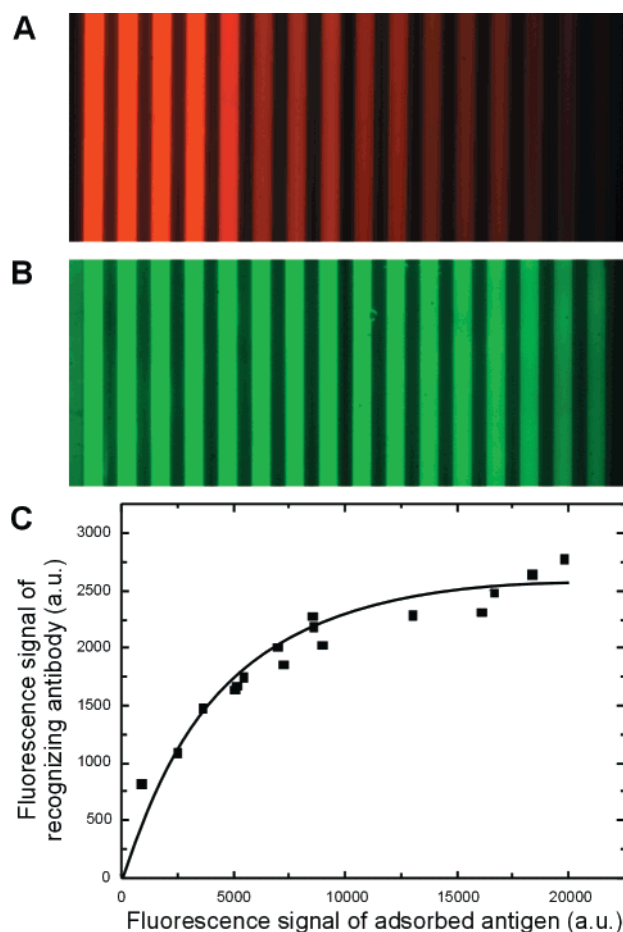


**Figure 4.** Detecting the antigens on a surface and their bound antibodies reveals the nonlinear binding behavior of these partners on the surface. (A) A 16-channel  $\mu$ FN was used to pattern 20- $\mu$ m lines of decreasing antigen coverage onto a PDMS substrate (left line to right line) using solutions ranging from 2 mg mL<sup>-1</sup> to 5  $\mu$ g mL<sup>-1</sup> in PBS. The  $\mu$ FN was 20  $\mu$ m high, and the antigen was labeled with rhodamine. (B) The deposited antigens were recognized by a specific antibody carrying a fluorescein label. Although the former pattern was reproduced accurately, the fluorescence of the recognizing species did not scale proportionally to the one of the immobilized antigen. (C) A plot of the amount of bound antibody versus the amount of surface-immobilized antigen corroborates the observation from (B): the line fitting the data deviate from a linear binding correlation.

proteins on the surface from the left line to the right line. No gradient has formed in the direction of the channels because the  $\mu$ FN used here had 20- $\mu$ m-deep channels (and thus had a less critical surface-to-volume ratio) that were connected to a "large" flow-promoting pad. Filling of each pad ensured at least an  $\sim$ 50-fold renewal of the content of the associated channel. In some sense, the substrate here is decorated with a "discontinuous" gradient in the direction across the lines of proteins. Such a pattern is useful to investigate the binding behavior of the immobilized antigens by antibodies from solution as a function of the antigen density on the surface in a discrete manner. Detection and quantitation of both partners on the surface are done simultaneously using fluorescence. This has the advantage that all the necessary information is present in a small region of the surface: the proteins forming the pattern are rigorously exposed to the same conditions for rinsing, blocking, and recognition, which provides a high level of self-consistency in this experiment.

The left line in Figure 4A has the highest coverage of antigens on the PDMS substrate and the right line the

lowest coverage. Immunocomplexation of the TRITC-tagged rabbit antigens was done, after a BSA blocking step, by exposing the patterned PDMS substrate to a solution containing FITC-labeled anti-rabbit antibodies (diluted 1:200 from the commercial solution). Detection of the second antibodies using fluorescent labels, Figure 4B, reveals that their presence on the surface matches the pattern of the rabbit antibodies immobilized in the regions corresponding to the channels. The microfluidic networks used here were optimized for manipulating minute amounts of protein and having a micrometer-scale pattern yet well within the reach of conventional fluorescence microscopes. The red and green fluorescences are proportional to the density of antigens and antibodies on the surface, respectively, but it is not possible to compare these signals directly because several factors contribute to their magnitude. A slightly different number of fluorophores per molecule, distinct spectral properties between TRITC and FITC labels, and the sensitivity of the detector for FITC and TRITC are the principal factors. This is the reason we calibrated the fluorescence signals with the amount of protein on the surface (see below). Plotting the fluorescence from the antigens versus the fluorescence associated with the antibodies, Figure 4C, reveals a nonlinear correlation between these two quantities. Apparently, proportionally more antibodies are present on the surface when their respective antigens have a lower coverage on the surface.<sup>6-8,24</sup>

Forming a continuous gradient of immobilized IgGs and recognizing them with their binding partners from solution should complement the previous experiment: such a gradient can offer a continuum of decreasing densities of immobilized proteins and should prove experimentally simpler than using a  $\mu$ FN with a series of independent channels. Figure 5 illustrates this situation. The fluorescence microscope image in Figure 5A corresponds to a gradient of rabbit IgGs deposited onto PDMS from a  $\mu$ FN having an array of channels connected to the same filling zone. The image covers the beginning of the channels from where the depletion phenomenon already started. We again evaluated binding between the immobilized antigens and their partners, after a BSA blocking step, with fluorescence microscopy, Figure 5B. The intensities of the fluorescence associated with either partner on the surface along the gradient are reported in Figure 5C. The red fluorescence from the immobilized antigens decreases along the channels due the depletion phenomenon. The green fluorescence does not evolve in a similar manner, however. As anticipated from Figure 4, the fluorescence from the antibodies (green curve in Figure 5C) decreases less quickly than that associated with the antigens (red curve).

It is possible to calculate the surface coverage for both proteins for a given fluorescence intensity measured on the surface. We assume that up to one layer of proteins can be deposited on the substrate. As a reference for full coverage we use the maximal fluorescence intensity measured after a long deposition time (1 h) from a high concentration of proteins (1 mg mL<sup>-1</sup>, see Figure 2). Another two important assumptions are that the simultaneous presence of the two fluorophores on the surface does not affect their emission (no fluorescence resonance energy transfer) and that their fluorescence is independent of their density on the surface (no self-quenching). Control experiments suggested that these latter assumptions are

(24) Delamarche, E.; Sundarababu, G.; Biebuyck, H.; Michel, B.; Gerber, Ch.; Sigrist, H.; Wolf, H.; Ringsdorf, H.; Xanthopoulos, N.; Mathieu, H. J. *Langmuir* **1996**, *12*, 1997.

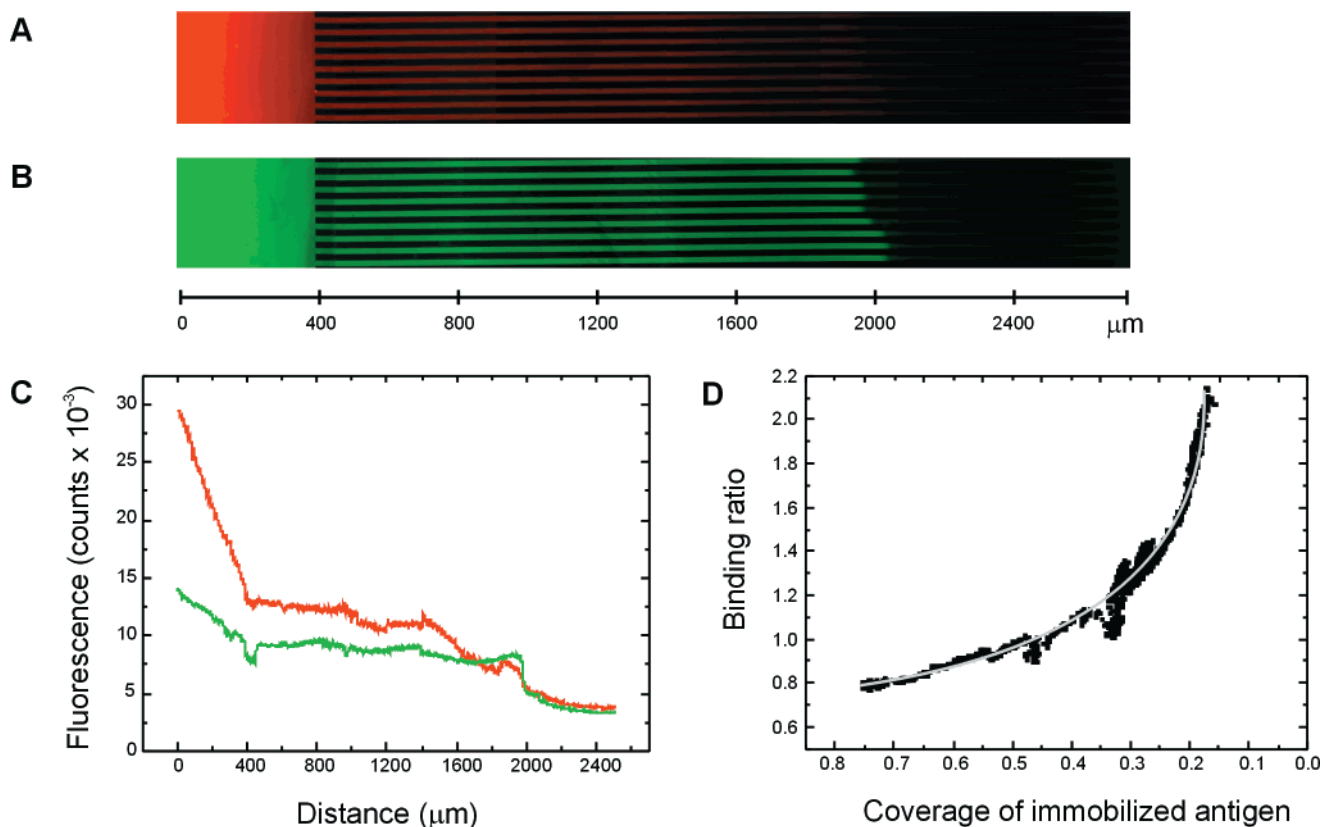


**Figure 5.** (A) Continuous gradients of antigens (rabbit IgGs) were produced by a  $\mu$ FN on a PDMS surface and (B) recognized by their antibodies (anti-rabbit IgGs) from solution. The gradient profiles in (C) were measured using the fluorescence associated with either protein and those in (D) were converted into monolayer quantities of immobilized proteins to give the binding behavior between the antigens and antibodies. The latter graph illustrates that binding of the immobilized antigen by its antibody from solution is more favorable for antigens dilute on the surface.

correct, at least for the density of fluorophores reported in the experiments. Exciting FITC while simultaneously monitoring light emission in the red wavelengths did not result in an observable signal. These results indicate that color conversion was not a path for loss of signal from FITC. In contrast, the loss of fluorescence by self-quenching is more difficult to estimate.<sup>25</sup> The limited amount of fluorophores per IgG (3.7 on average per antigen and  $\sim$ 3.9 per antibody), the relatively large size of IgGs compared to the fluorophores, and the strong dependence of fluorescence quenching with the distance between fluorophores suggest that fluorescence quenching should not be a problem, at least for intermediate and low-density coverage of the IgGs on the surface.

In consequence, the fluorescence signals indicate how much of a monolayer of antigens and antibodies is present on the surface and hence leads to the binding ratio between the partners. This binding ratio is reported in Figure 5D and, importantly, confirms the nonlinear binding behavior of the partners on the surface. For the conditions of recognition used here, one antibody from solution binds on average one antigen on the surface for an antigen coverage of up to  $\sim$ 0.5 of a monolayer. The binding efficiency then gradually increases to  $\sim$ 2 as progressively fewer antigens are present on the surface. This observation was expected because there are many causes that can affect the recognition of an antigen on a surface by its antibody from solution. Among these causes, steric hindrance seems to be a particularly important factor: proteins that form a dense monolayer on a surface are likely to be less accessible for binding partners than if

they are free in solution or adsorbed at a lower density on the surface. Orientation of the immobilized antigens, their conformation with respect to their density on the surface, the specificity of the immunocomplexation (monoclonal system vs polyclonal), and the relative sizes of the partners are also likely to influence their binding behavior at the solid–liquid interface.

### Conclusion

It has long been recognized that the binding between a partner from solution and another on a surface can be affected by the density of the immobilized partner. Several additional factors may also be of importance, such as the orientation of the partners on the surface, their relative size, and the distribution of their sites of interaction. In our work, we create gradients of biomolecules on surfaces using  $\mu$ FNs on length scales from micrometers up to millimeters with minute amounts of protein solutions. Our methodology uses fluorescence labeling with which the amount of deposited antigens is readily compared to the amount of bound antibodies from solution. The binding ratio of such partners is not linear with the density of the antigen on the surface but improves with decreasing density of antigens on the surface. We suggest that gradients of biomolecules on surfaces created by  $\mu$ FNs are an excellent means to study the binding behavior between ligands and receptors on surfaces in general.

**Acknowledgment.** I. Caelen acknowledges financial support from the Swiss National Foundation NFP36 project. A. Bernard, D. Juncker, B. Michel, and E. Delamarche acknowledge partial financial support from

(25) Ballerstadt, R.; Schultz, J. S. *Anal. Chim. Acta* **1997**, *345*, 203.

the Swiss Federal Office for Education and Science within the BIOTECH European project BIOPATT (BIO4CT980536). We thank H. Schmid, A. Bietsch, J.-Ph. Renault, M. Geissler, and H. Wolf for useful discussions and R. Widmer and U. Drechsler for their help in preparing

the microfluidic networks. We are grateful to P. F. Seidler (IBM) and H. R. Bosshard (University of Zurich) for their continuous support.

LA000851K



## Chapter 5

# Fabrication of “smart”-stamps for microarraying proteins *en masse*

**Fabricating microarrays of functional proteins using affinity contact printing**

Jean-Philippe Renault, André Bernard, David Juncker, Bruno Michel, Hans Rudolf Bosshard and Emmanuel Delamarche

*Angewandte Chemie International Edition* **41**, 2320-2323 (2002)



## Fabricating Microarrays of Functional Proteins Using Affinity Contact Printing\*\*

Jean Philippe Renault, André Bernard, David Juncker, Bruno Michel, Hans Rudolf Bosshard, and Emmanuel Delamarche\*

Phenomena involving the binding between biomolecules are ubiquitous in biology and are essential for cell growth, signal transmission, and immune defense. In the latter system, the binding between antibody and antigen has already been exploited technologically to perform affinity purifications on columns and immunoassays on surfaces.<sup>[1]</sup> Recently, the fabrication of microarrays of proteins which require the immobilization of a large number of receptors on a surface have fueled the invention of novel patterning techniques such as pin-spotting and drop-on-demand.<sup>[2]</sup> Microarrays of proteins may find utility in proteomics, immunoassays, or for screening libraries of (bio)chemicals. It is at present not clear which patterning method will be the one best suited to pattern proteins on surfaces, but classical lithography does not seem capable of fabricating microarrays of proteins. Soft lithography<sup>[3]</sup> offers the possibility of manipulating proteins and other biomolecules by printing them from a micropatterned stamp to a surface<sup>[4]</sup> or by depositing them from a liquid using microfluidic networks ( $\mu$ FNs).<sup>[5]</sup> Affinity microcontact printing ( $\alpha$ CP)<sup>[6]</sup> is a refined soft-lithographic technique that uses an elastomeric stamp made of polydimethylsiloxane (PDMS) and derivatized with binding biomolecules to extract corresponding binding partners from an impure, dilute source for placing them on a surface with spatial control.

Herein, we describe, by using one particular example, how specific binding between biomolecules provides a unique opportunity to make use of self-assembly processes in technology: we propose different variants of  $\alpha$ CP to pattern surfaces with ensembles of biomolecules where the pattern on the affinity stamp ( $\alpha$ -stamp) is not determined by its topography but by the position of various proteins covalently linked to a planar  $\alpha$ -stamp (Figure 1). This modified surface enables the simultaneous capture of different target proteins on the  $\alpha$ -stamp from a complex solution (Figure 1A). Thus, the capture step (Figure 1B) directs the assembly of an array of target molecules on the stamp (Figure 1C), which can be

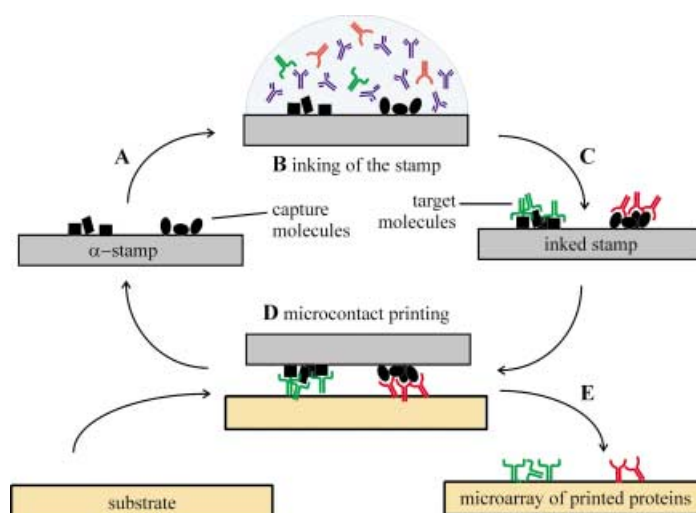


Figure 1. Microarrays of proteins on surfaces can be fabricated using an  $\alpha$ -stamp derivatized with various capture sites that can extract target biomolecules from a complex solution and release them on a surface in a single microcontact-printing step. The  $\alpha$ -stamp can be reused for several inking and printing cycles.

microcontact-printed onto a substrate in one step (Figure 1D). The  $\alpha$ -stamp is recovered at the end of this process, and can be reused.<sup>[6]</sup> We opted for protein antigens (entire immunoglobulin G) as capture molecules and antibodies as targets because these binding partners are very specific, can be readily conjugated with fluorescent markers, and of course play an important role in heterogeneous immunoassays.

Affinity stamps are prepared by immobilizing the capture molecules on an “activated stamp” that is reactive towards  $\text{NH}_2$  groups of proteins. An activated stamp is made in three steps from a planar layer of PDMS (see the Supporting Information for experimental details). First, silanol groups are created at the PDMS surface using an  $\text{O}_2$  plasma.<sup>[7]</sup> These silanol groups are subsequently treated with 3-aminopropyltriethoxysilane to create an amino-derivatized surface. These amines are then treated with a homo-bifunctional cross-linker ( $\text{BS}^3$ ) to produce the activated surface.<sup>[7]</sup> The stamps produced in this way are stable for several hours in a dry environment such as a dessicator, and can immobilize monolayers of proteins under mild chemical conditions.<sup>[8, 9]</sup> Activated stamps are hydrophilic, with an advancing contact angle with water of approximately  $30^\circ$ , and therefore cannot be locally derivatized at high resolution with solutions of proteins by pin-spotting or ink-jet methods.<sup>[2, 10]</sup> Our aim was to prepare  $\alpha$ -stamps having arbitrary patterns with dimensions as small as a few micrometers, and we developed various methods to achieve this goal. The first method relies on coupling proteins to small areas of an activated stamp using microwells<sup>[11]</sup> ( $\mu$ -wells; Figure 2). The microwells are anisotropically etched through a 525- $\mu\text{m}$ -thick Si wafer, and can be placed in contact with the activated stamp (Figure 2a). This contact is conformal and seals each microwell individually. Pipetting the desired amount of protein solution into all or a subset of the microwells determines the array of capture molecules formed on the  $\alpha$ -stamp (Figure 2b, c). The hydrophobization of the top and bottom faces of the array of

[\*] Dr. E. Delamarche, Dr. A. Bernard, D. Juncker, Dr. B. Michel  
IBM Research  
Zurich Research Laboratory  
Säumerstrasse, 4, 8803 Rüschlikon (Switzerland)  
Fax: (+41) 1-724-8952  
E-mail: emd@zurich.ibm.com

Dr. J. P. Renault, Prof. H. R. Bosshard  
Dept. of Biochemistry  
University of Zurich  
Winterthurerstrasse 190, 8057 Zurich (Switzerland)

[\*\*] This work was partially supported by the Swiss National Science Foundation NFP 36 (grant 31.55308.98) and by the Swiss Federal Office for Education and Science within the BIOTECH European project BIOPATT (BIO4CT980536). We thank I. Caelen and H. Schmid for their help and discussions.

Supporting information for this article is available on the WWW under <http://www.angewandte.org> or from the author.

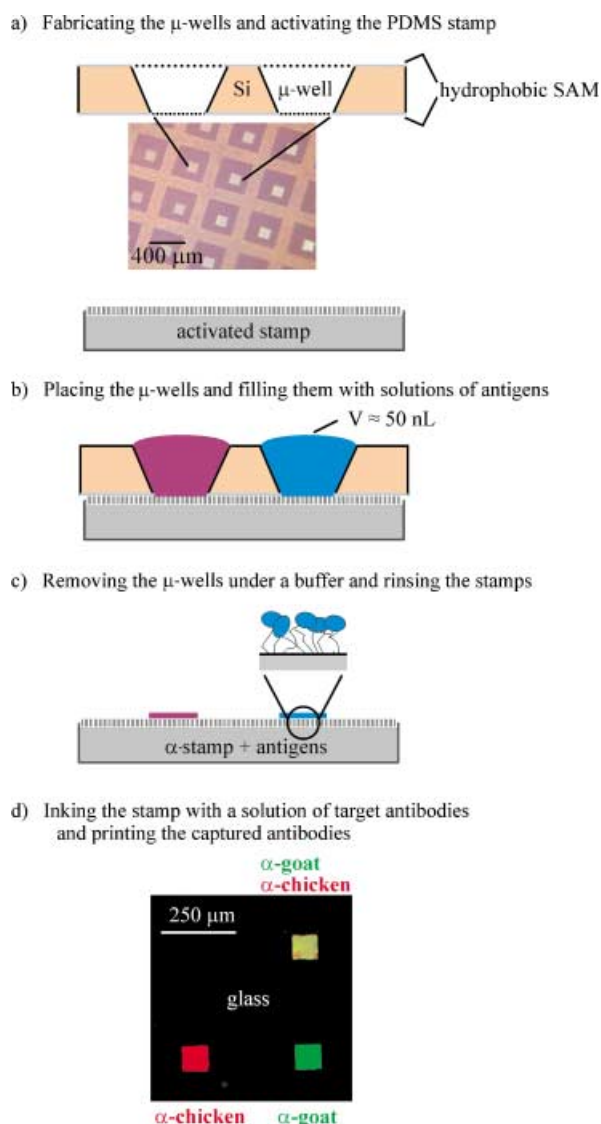


Figure 2. Preparation of a microarray of proteins using an  $\alpha$ -stamp patterned with microwells. a) The microwells are formed in a Si wafer, and the PDMS stamp is derivatized with cross-linkers for proteins. b) The contact of the microwells with the activated stamp localizes the attachment of capture molecules from solution to the area of the stamp exposed in each microwell. c) After separating it from the microwells, rinsing and drying, the  $\alpha$ -stamp is ready for use. d) The  $\alpha$ -stamp in this example had an empty capture site and sites with covalently attached anti-chicken antigens, anti-goat antigens, and protein A. Inking the  $\alpha$ -stamp consists of the binding of antibodies (here tagged fluorescently) from solution to their specific antigens on the surface of the stamp. After rinsing and drying the inked  $\alpha$ -stamp, the antibodies can be printed onto a glass surface and visualized by fluorescence microscopy.

microwells by using a perfluorinated silane prevents leakage of liquid across the wells.<sup>[12]</sup> In addition, the truncated pyramidal shape of the microwells makes it possible to fill them readily. The microwells used here can hold up to 50 nL of solution, and their drying could be controlled on the timescale needed for the coupling reaction. Affinity-capture sites based on the immobilization of protein A, and mouse, goat, and chicken antigens were patterned on an  $\alpha$ -stamp by using  $100 \times 100 \mu\text{m}^2$  wells (Figure 2d). This  $\alpha$ -stamp is inked with a solution of anti-species antibodies (fluorescein iso-

thiocyanate labeled (FITC) anti-goat and tetramethylrhodamine B isothiocyanate linked (TRITC) anti-chicken antibodies) containing a large amount of bovine serum albumin (BSA). Each type of antibody binds in parallel to its specific antigen on the  $\alpha$ -stamp during this inking step, and protein A captures both types of antibodies whereas BSA adsorbs elsewhere and prevents nonspecific adsorption on the  $\alpha$ -stamp. The target molecules are transferred from the  $\alpha$ -stamp to a glass slide during a printing step, and can be visualized as a result of their fluorescence label. The pattern in Figure 2d reveals the expected fluorescence pattern in which the target molecules are placed with high accuracy and contrast on their final substrate.

The preparation of the  $\alpha$ -stamp is probably the most critical part of the  $\alpha$ CP technique, and dispensing the solution of proteins into the microwells limits the practical resolution of  $\alpha$ CP. This limitation can be circumvented by using microfluidic networks ( $\mu$ FNs) to prepare the  $\alpha$ -stamp. We take advantage of the sealing between the channels of a  $\mu$ FN and a PDMS surface to deposit capture proteins on an intermediate stamp from the microchannels of the  $\mu$ FN (Figure 3a). This stamp is then contacted with the activated stamp for 10 min. The capture antigens transfer and bind covalently to the surface of the activated stamp in this step (Figure 3b). We verified that the transfer was complete and that it did not alter the pattern by using fluorescently tagged antigens. The fluorescence microscopy images in Figure 3c reveal that the  $\alpha$ -stamp prepared with this method can extract an ensemble of fluorescently tagged antibodies and then release them by printing onto a surface several times. The affinity site of line d in this example comprises protein A, for which we noticed that fewer FITC anti-goat antibodies were captured and printed after the third cycle. We speculate that during these consecutive cycles protein A captures both types of antibodies present in the ink with differing efficiencies. The high-resolution potential of  $\mu$ FNs<sup>[13]</sup> is conserved in the fabricated array of antibodies, and the investment in preparing the  $\alpha$ -stamp is compensated by reusing it for several cycles of capture and release.<sup>[6]</sup>

$\mu$ CP is an efficient and low-cost method for patterning proteins with submicrometer resolution.<sup>[14]</sup> Since  $\mu$ CP uses the deposition of proteins from bulk solution on stamps and prints them on a substrate, liquids can be handled simply by manual pipetting without the need for a particular dispensing device.  $\alpha$ CP can be extended by using  $\mu$ CP to form very high-resolution arrays of proteins in the following way. First, a layer of capture antigens is deposited from solution onto a hydrophobic PDMS stamp (Figure 4a). The contact between a patterned Si substrate and the inked stamp releases the proteins from the stamp to the Si surface in the areas of contact (Figure 4b).<sup>[15]</sup> This operation is a subtractive transfer of proteins, and does not require structured PDMS stamps; it is therefore insensitive to mechanical deformations as can occur in conventional  $\mu$ CP.<sup>[16]</sup> The patterned antigens are transferred to an activated PDMS stamp in a printing step (Figure 4c). Repeating these steps with careful alignment enables the formation of ensembles of arrays on the  $\alpha$ -stamp, each containing one type of capture protein (Figure 4d). The stability of the activating layer on the stamp means there is no

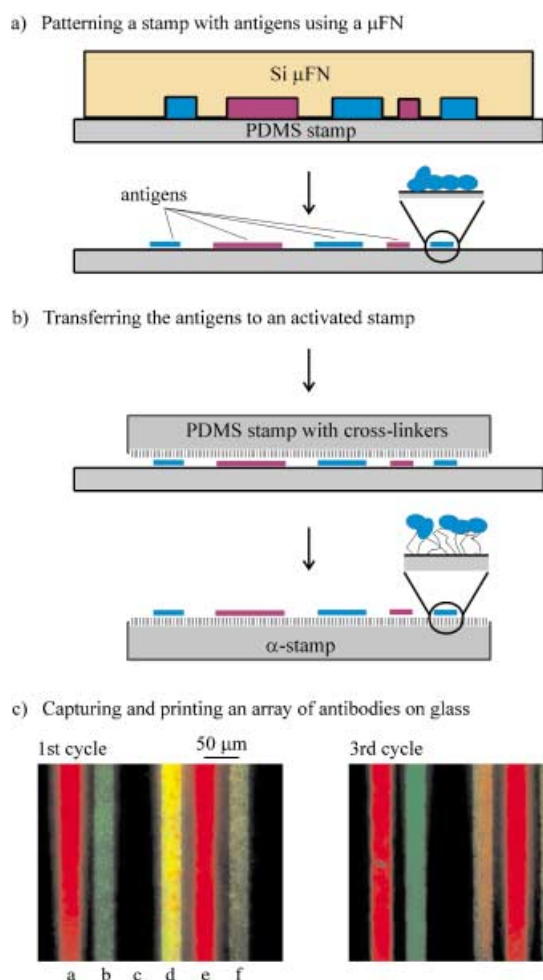


Figure 3. Patterning lines of proteins on a surface with an  $\alpha$ -stamp prepared using a  $\mu$ FN. The  $\mu$ FN localizes the deposition of capture antigens on an intermediate, nonmodified PDMS stamp (a), which can then transfer and attach the proteins to an activated PDMS stamp (b). The  $\alpha$ -stamp is used to capture fluorescently tagged antibodies, and print them as lines onto a glass surface (c). The captured molecules on the  $\alpha$ -stamp were chicken IgGs (lines a and e), goat IgGs (lines b and f), protein A (line d), and mouse IgGs (line c). Inking this stamp was done by exposing it to a solution containing BSA (1%), FITC-anti-goat antibodies, and TRITC-anti-chicken antibodies. The fluorescence microscope images reveal that the capture was specific, and the release efficient in providing a high-resolution pattern of printed antibodies even after the  $\alpha$ -stamp had been used several times.

need to reactivate the  $\alpha$ -stamp between printing steps of the capture proteins if the overall process is shorter than about 2 h. The pattern on the glass substrate in Figure 5a involved two printing steps (done manually) to prepare the  $\alpha$ -stamp, and one inking and printing cycle using the  $\alpha$ -stamp to yield the "microarray". Specifically, two different antigens (IgGs) from goat and chicken were immobilized on an activated stamp, and used as antigens to extract their respective target antibodies simultaneously from a solution containing FITC-anti-goat and TRITC-anti-chicken antibodies. The captured antibodies were then printed onto the glass substrate in  $3 \times 3 \mu\text{m}^2$  areas. This microarray has a density of approximately  $10^4$  spots of proteins per  $\text{mm}^2$  with two types of proteins. The ability of the printed anti-goat antibodies to bind to goat antigens is seen in the AFM image of Figure 5b.

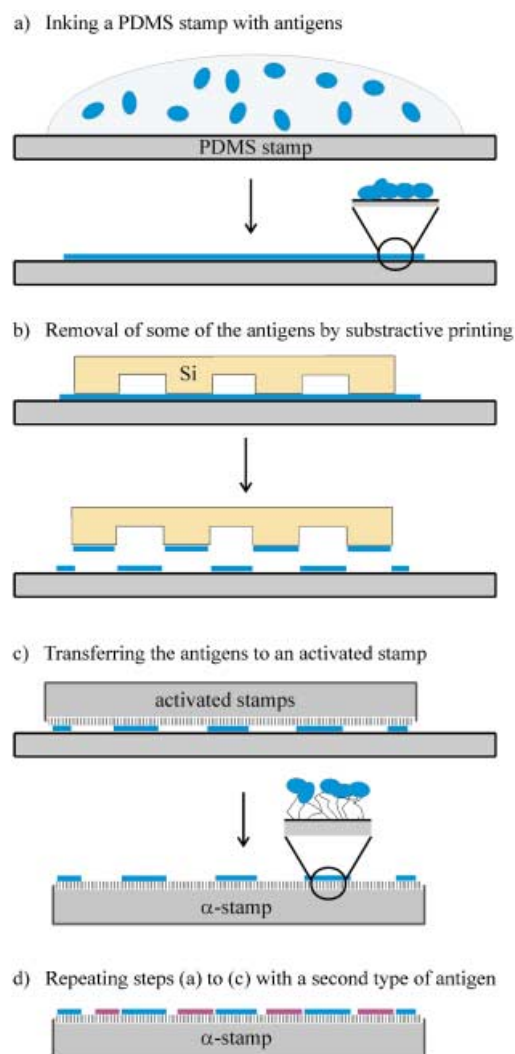


Figure 4. Preparation of an  $\alpha$ -stamp by using the deposition of capture proteins from solution and subtractive  $\mu$ CP. A layer of capture antigens is deposited from solution onto a PDMS stamp (a), and patterned by removing the antigens in some regions of the stamp by subtractive printing (b). The remaining capture antigens are transferred onto an activated stamp (c). Repeating these steps enables several arrays of capture proteins to be successively added to the  $\alpha$ -stamp (d).

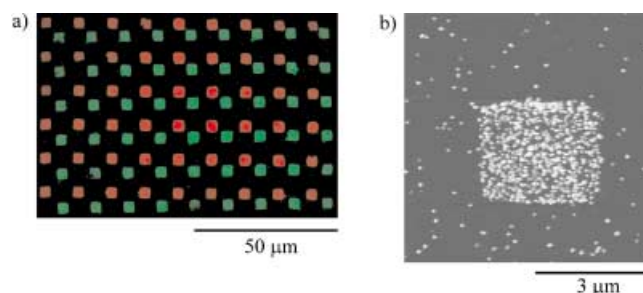


Figure 5. Arrays of anti-chicken antibodies and anti-goat antibodies printed using an  $\alpha$ CP having  $10^4$  equivalent capture sites per  $\text{mm}^2$  that consist of immobilized chicken and goat antigens. a) Fluorescence microscope image showing the placement of the TRITC-anti-chicken and FITC-anti-goat antibodies from a stamp onto a glass substrate. b) AFM image obtained on a spot of the array in which the printed anti-goat antibodies bound to Au-labeled goat antigens presented in solution. Detection of this binding was done by staining the Au labels with electroless-deposited silver particles of an average diameter of 80 nm.

The fluorescence data in our experiments indicated that the surface coverage of the final printed layer for each of the three patterning methods presented here is nearly equivalent and reaches about 60% of the surface coverage obtained by direct deposition of the antibodies from solution. As already described for  $\mu$ CP and  $\alpha$ CP of proteins, the printing process does not compromise the binding efficiency of the printed antibody. This strategy might not be suitable for patterning a large number of different proteins on a surface. However, it can place a few different proteins as adjacent high-density arrays on a surface. Such arrays could find an application for high-throughput screening in which a large number of analytes could be spotted using a subset of the patterned areas. Another possibility for creating high-density immunoassays on planar surfaces is by performing surface immunoassays using many different analytes and capture sites, such as shown in Figure 5. The main limiting factor in using the prepared microarrays for diagnostic purposes could be misplacement of target molecules during the inking of the  $\alpha$ -stamp. Such a misplacement, which may induce false positive reactions, can arise from cross-reactions of the target molecules with different capture proteins and/or from nonspecific adsorption on the  $\alpha$ -stamp. The former is limited by biological specificity of affinity extraction. The latter can be limited by the systematic use of blocking agents such as BSA. Indeed, for the recognition of goat antigen by the printed array shown in Figure 5a, the recognition signal in the areas with printed anti-chicken antibodies was only 5% of that in the areas with printed anti-goat antibodies.

In summary, we have illustrated how  $\alpha$ CP can complement different patterning methods to produce repeatedly, and in parallel, high resolution arrays of proteins in three simple steps: 1) "inking", 2) rinsing, and 3) printing the stamp on the substrate. Since  $\alpha$ -stamps carry the complementary pattern of binding partners specific to the target proteins on their surface, the proteins self-assemble into the predefined array on the stamp surface during inking in solution, and dissociate upon printing. Hence, the (re)production of the target protein arrays is fast and easy. The initial production of the  $\alpha$ -stamp is a one-time burden only. We thus believe that the methodology presented is powerful and versatile, and should be useful in detection and fabrication strategies that are based on arrays of proteins.

Received: January 30, 2002  
Revised: April 15, 2002 [Z18619]

- [1] *Immunassay* (Eds.: E. P. Diamandis, T. K. Christopoulos), Academic Press, San Diego, CA, **1996**.
- [2] *DNA Microarrays: A Practical Approach* (Ed.: M. Schena), Oxford University Press, Oxford, UK, **1999**.
- [3] a) Y. Xia, G. M. Whitesides, *Angew. Chem.* **1998**, *110*, 568–594; *Angew. Chem. Int. Ed.* **1998**, *37*, 550–575; b) G. M. Whitesides, E. Ostuni, S. Takayama, X. Jiang, D. E. Ingber, *Annu. Rev. Biomed. Eng.* **2001**, *3*, 335–373.
- [4] A. Bernard, E. Delamarche, H. Schmid, B. Michel, H. R. Bosshard, H. Biebuyck, *Langmuir* **1998**, *14*, 2225–2229.
- [5] E. Delamarche, A. Bernard, H. Schmid, B. Michel, H. Biebuyck, *Science* **1997**, *276*, 779–781.
- [6] A. Bernard, D. Fitzli, P. Sonderegger, E. Delamarche, B. Michel, H. R. Bosshard, H. Biebuyck, *Nat. Biotechnol.* **2001**, *19*, 866–869.

- [7] C. Donzel, M. Geissler, A. Bernard, H. Wolf, B. Michel, J. Hilborn, E. Delamarche, *Adv. Mater.* **2001**, *13*, 1164–1167.
- [8] S. C. Lin, F. G. Tseng, H. M. Huang, C. Y. Huang, C. C. Chieng, *Fresenius J. Anal. Chem.* **2001**, *371*, 202–208.
- [9] A. Bernard, H. R. Bosshard, *Eur. J. Biochem.* **1995**, *230*, 416–423.
- [10] a) G. MacBeath, S. L. Schreiber, *Science* **2000**, *289*, 1760–1763; b) H. Zhu, M. Bilgin, R. Bangham, D. Hall, A. Casamayor, P. Bertone, N. Lan, R. Jansen, S. Bidlingmaier, T. Houfek, T. Mitchell, P. Miller, R. A. Dean, M. Gerstein, M. Snyder, *Science* **2001**, *293*, 2101–2105.
- [11] a) J. Hyun, A. Chilkoti, *J. Am. Chem. Soc.* **2001**, *123*, 6943–6944; b) J. S. Hovis, S. G. Boxer, *Langmuir* **2001**, *17*, 3400–3405; c) U. Schobel, I. Coille, A. Brecht, M. Steinwand, G. Gauglitz, *Anal. Chem.* **2001**, *73*, 5172–5179.
- [12] D. Juncker, H. Schmid, A. Bernard, I. Caelen, B. Michel, N. de Rooij, E. Delamarche, *J. Micromech. Microeng.* **2001**, *11*, 532–541.
- [13] E. Delamarche, A. Bernard, H. Schmid, A. Bietsch, B. Michel, H. Biebuyck, *J. Am. Chem. Soc.* **1998**, *120*, 500–508.
- [14] A. Bernard, J. P. Renault, B. Michel, H. R. Bosshard, E. Delamarche, *Adv. Mater.* **2000**, *12*, 1067–1070.
- [15] Z. Yang, A. M. Belu, A. Liebmann-Vinson, H. Sugg, A. Chilkoti, *Langmuir* **2000**, *16*, 7482–7492.
- [16] A. Bietsch, B. Michel, *J. Appl. Phys.* **2000**, *88*, 4310–4318; M. Geissler, A. Bernard, A. Bietsch, H. Schmid, B. Michel, E. Delamarche, *J. Am. Chem. Soc.* **2000**, *122*, 6303–6304.

## Au-Nanoparticle Nanowires Based on DNA and Polylysine Templates

Fernando Patolsky, Yossi Weizmann,  
Oleg Lioubashevski, and Itamar Willner\*

The assembly of ordered nanoparticle architectures is a challenging topic in nanotechnology directed to the construction of nanoscale devices.<sup>[1]</sup> Within this broad subject, the conjugation of biomaterials and nanoparticles to yield ordered architectures is a promising route to tailor future sensing and catalytic devices, nanocircuitry, or nanodevices, for example transistors, and computing devices.<sup>[2]</sup> DNA is an attractive biomaterial for use as a template in programmed nanoparticle structures. The ability to synthesize nucleic acids of predesigned shapes and composition, the versatile biocatalytic transformations that can be performed on DNA, for example, ligation, scission, or polymerization, enable "cut and paste" procedures to be carried out on the template DNA, thus enabling us to design and manipulate the DNA "mold". Furthermore, the association of metal ions to the DNA phosphate units, or the intercalation of transition-metal complexes or molecular substrates into the DNA provide a means to functionalize the DNA-template and to initiate further chemical transformations on the mold. Nanoparticle–DNA assemblies were organized by the hybridization of nucleic-acid-functionalized metal<sup>[3]</sup> or semiconductor nano-

[\*] Prof. I. Willner, F. Patolsky, Y. Weizmann, O. Lioubashevski  
Institute of Chemistry  
The Hebrew University of Jerusalem  
Jerusalem 91904 (Israel)  
Fax: (+972) 2-652-7715  
E-mail: willnea@vms.huji.ac.il

# Chapter 6

## The autonomous transport of liquids

### Autonomous microfluidic capillary system

David Juncker, Heinz Schmid, Ute Drechsler, Heiko Wolf, Marc Wolf, Bruno Michel, Nico de Rooij and Emmanuel Delamarche.

Manuscript.

### Supplementary material

### Supplementary material II





## Autonomous Microfluidic Capillary System

David Juncker,<sup>1,2\*</sup> Heinz Schmid,<sup>1</sup> Ute Drechsler,<sup>1</sup> Heiko Wolf,<sup>1</sup> Marc Wolf,<sup>3</sup> Bruno Michel,<sup>1</sup>  
Nico de Rooij,<sup>2</sup> and Emmanuel Delamarche<sup>1\*</sup>

The transport of minute amounts of liquids using microfluidic systems has opened avenues for higher throughput and parallelization of miniaturized bio/chemical processes combined with a great economy of reagents. In this report we present a microfluidic capillary system (CS) that autonomously transports aliquots of different liquids in sequence: liquids pipetted into the service port of the CS flow unidirectionally through an access channel, a capillary retention valve, a 15- $\mu\text{l}$  reaction chamber and finally into a capillary pump, without the need for external power supply nor control device because the pumping and valving functions are integrated into the device by means of capillary phenomena. For this reason, a CS is simple to use and can easily be cloned into arrays. We illustrate the power of such CSs by conducting a surface immunoassay, within 25 min, on an area of  $100 \times 100 \mu\text{m}^2$ , using 16 sequential filling steps.

<sup>1</sup>IBM Research, Zurich Research Laboratory, 8803 Rüschlikon, Switzerland

<sup>2</sup>Institut de Microtechnique, Université de Neuchâtel, 2000 Neuchâtel, Switzerland

<sup>3</sup>Departement Forschung, Universitätskliniken Basel, 4031 Basel, Switzerland

\*To whom correspondence should be addressed: E-mail (D.J.): jun@zurich.ibm.com; (E.D.): emd@zurich.ibm.com.

Miniaturization of biological and chemical processes requires transporting and mixing liquids at microscopic scale; this is the realm of microfluidics. Here, the motion of liquids is dominated by different phenomena than at macroscopic scale, and it therefore necessitates devising microfluidic systems with novel and tailored liquid handling capabilities. Such microfluidic systems can in principle be integrated, but up to now still require external macroscopic actuators, cumbersome fluidic connections and electro-mechanical interfaces, which limits their scaling down and portability (1–3). An ideal microfluidic system should be straightforward to fabricate, self-contained and simple to use, yet flexible, robust, free of dead volumes, and easily duplicated to form arrays. Here, we present a concept for microfluidic systems that integrates all of these attributes. All actions necessary to supply and flush a reaction chamber with multiple solutions — including pumping, valving and synchronization — are effected by the capillary pressure, which is “coded” into the design of the flow path. Such a microfluidic capillary system (CS) is autonomous. Its liquid transport mechanism is reminiscent of the one used by trees (4–6): the most distal elements are the main contributors to the flow, and there is no need for moving parts.

The spontaneous motion of a tiny drop of liquid deposited on a structured surface is governed by

capillary phenomena resulting from the interplay between the surface tension of the liquid and the chemistry and geometry of the solid interfaces, and leads to the overall minimization of the free energies between the solid, liquid and vapor interfaces (7). These capillary phenomena can be exploited to fill microstructures spontaneously (8–12), valve (2, 12, 13), guide (14, 15), and actively displace (16–20) liquids along surfaces.

The capillary pressure  $P_c$  of a liquid-air meniscus in a rectangular microchannel is (8, 21)

$$P_c = -\gamma \left( \frac{\cos \alpha_b + \cos \alpha_t}{d} + \frac{\cos \alpha_l + \cos \alpha_r}{w} \right), \quad (1)$$

where  $\gamma$  is the surface tension of the liquid,  $\alpha_{b,t,l,r}$  are the contact angles of the liquid on the bottom, top, left, and right wall, respectively, and  $d$  and  $w$  are the depth and width of the channel, respectively. Each wettable ( $\alpha < 90^\circ$ ) wall of the CS contributes to having a negative pressure in front of the liquid and to drawing it into the channel. Washburn (22) derived the hydrodynamic solution of capillary filling for conduits of constant cross section. If the cross section varies, however, smaller cross sections will produce a correspondingly higher differential capillary pressure. Thus, it is possible to calculate precisely from Eq. (1) how to vary the cross section of a channel to drain a finite volume of liquid from one region to another, and further to predict the flow rate between these regions. By

adopting an arborescent structure for the flow path (23), large quantities of liquid can be displaced unidirectionally to novel regions of ever increasing capillary pressure.

Figure 1 shows an autonomous microfluidic CS and how to operate it. The user needs only to deliver the desired quantity of each solution in the selected sequence to a service port, from where the liquid passes through the reaction chamber into the capillary pump (CP). The CS is schematically represented in Fig 2A and B. The pressure curves for a wetting and dewetting liquid-air interface (solid and dashed line in Fig. 2C) were calculated for deionized water under the assumption that the liquid surface tension ( $\gamma = 70 \text{ mN m}^{-1}$ ) and the wettability of the surfaces of the CS are invariant. The slight difference between these pressures originates from the hysteresis between the advancing and receding contact angles (24). The capillary pressure that generates the motion of the liquid is the difference in the pressure of the wetting meniscus in the CP and that of the dewetting meniscus in the filling port or access channel, Fig 2C. As indicated, the CP in this device produces sufficient capillary pressure to drain both the service port and its appended access channel. The constriction (inlet via) present just before the reaction chamber was designed to be the smallest structure of the CS and has the highest capillary pressure. It plays the role of a valve, which pins the interfacial meniscus of the dewetting liquid and protects the reaction chamber from adventitious

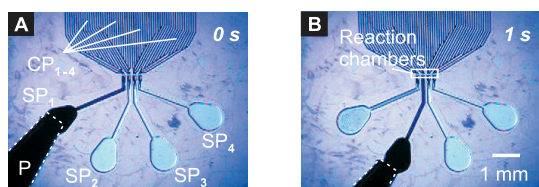


**Fig. 1.** Images (extracted from a video) showing how to use an array of four adjacent autonomous microfluidic CSs microfabricated in Si. **(A)** The CSs are contacted with a PDMS layer (underneath and not visible) and approximately 150 nl of water are dispensed with a pipette (P) into the service port  $SP_1$  of the first CS. The solution flows from there to an access channel, through the Si layer and reaches the reaction chamber which is in contact with the PDMS layer, flows back to the upper face of the CS and enters the arborescent  $CP_1$ . **(B)** The solution dispensed in  $SP_1$  was entirely displaced to the reaction chamber and  $CP_1$  so that  $SP_1$  can be filled with another aliquot of solution. All SPs can be filled repeatedly and independently from each other; the only task of the user (or the pipetting robot) is to dispense the solutions.

drying. We call it therefore a capillary retention valve (CRV). The functionalities defined by the structure of the CS used throughout this report thus include (i) pumping the solution from the service port to the reaction chamber, (ii) draining the service port, (iii) stopping the flow when the service port is empty to keep the reaction chamber wet, and (iv) enabling multiple cycles. This series of actions is effective to transport sequences of liquids, and it is performed autonomously by the CS.

The dynamic description of the liquid motion necessitates an exact value of the resistance to flow of the rectangular channels, which can be calculated with a Fourier series (25). We derived a first-degree approximation, which converges to the exact solution when the height-to-width ratio tends to zero, and deviates by no more than 10% from the exact solution for any other aspect ratio. The mass

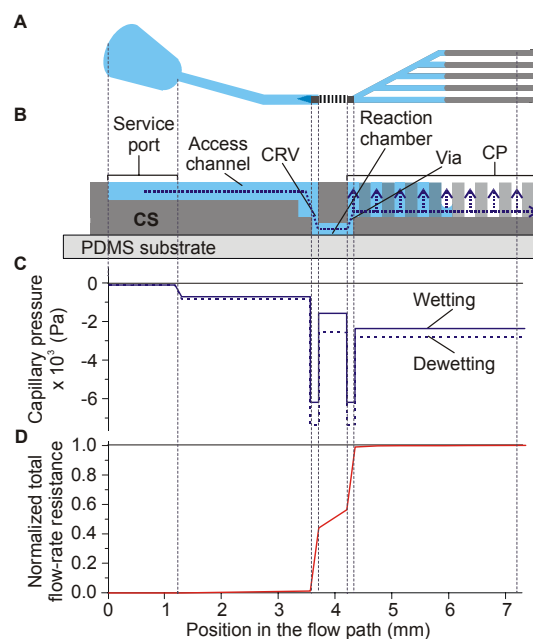


**Fig. 2.** Geometry and hydrodynamic characteristics of the CS shown in Fig. 1. **(A)** Schematic of a CS viewed from above. **(B)** The flow of liquid (arrows) is superposed to the cross section (not to scale) of the CS. **(C)** The capillary pressure at the front of water is calculated in all points of the CS for a filling (solid line) and an emptying (dashed line) liquid front. The liquid flows towards a zone of the CS of lower capillary pressure (more negative value), and, once filled, the reaction chamber is protected from drying by a capillary retention valve. **(D)** The flow rate resistance of the CS is nearly invariant once the liquid has passed the reaction chamber, enabling the transport of multiple samples of different solutions under similar flow conditions.

flow rate  $D$  becomes

$$D = \frac{1}{12\eta} \left(1 + \frac{5a}{6b}\right) \frac{R_h^2 A}{L} \Delta P \equiv \frac{1}{\eta R_{FR}}, \quad (2)$$

where  $a$  and  $b$  are either width or height to satisfy the condition  $b \geq a$ ,  $R_h$  is the hydraulic radius defined as  $R_h = 2A/P$ , with  $A$  and  $P$  being the cross section and perimeter of the conduit, respectively;  $L$  is the filled length of the conduit,  $\Delta P$  the difference of pressure between the two liquid fronts, and  $\eta$  the viscosity of the liquid. For simplification, the geometric features can be written as the flow-rate resistance  $R_{FR}$  of a channel section, which sums up to the total value:  $R_{FR} = 8.5 \times 10^{15} \text{ m}^{-3}$  for the CS represented in Fig. 2. The normalized  $R_{FR}$  is shown in Fig. 2D and reveals that  $R_{FR}$  accumulates mainly in the vias and the reaction chamber of the microfluidic system and, importantly, that the contribution of the CP is negligible because of its arborescent architecture. As the flow resistance is nearly constant in the CP, this pump will draw aliquots successively added to the service port at a constant rate.

One microfluidic capillary system can be readily cloned to form ensembles because each entity contains the entire functionality, rendering parallelization trivial. We fabricated 4-CS-arrays and verified experimentally the flow properties by sequentially flushing the reaction chambers of these arrays with colored liquids, as shown in Fig. 3 and in the video S2 (26). In this example, all liquids supplied after the first aliquot had a flow rate close to the calculated value of  $220 \text{ nl s}^{-1}$  and an average speed of  $v_{\text{avg}} = 55 \text{ mm s}^{-1}$  in the  $500\text{-}\mu\text{m}$ -long and  $50\text{-}\mu\text{m}$ -deep reaction chamber. Importantly, the CRV also prevents the entrapment of air in the

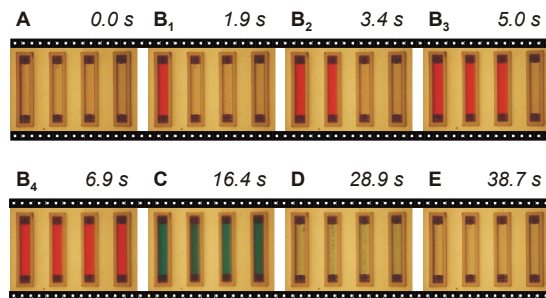


**Fig. 3.** Images (extracted from a video) illustrating the autonomous transport of liquids in four separate reaction chambers. The chambers ( $500 \times 80 \times 50 \mu\text{m}^3$ ) were sealed with a layer of PDMS through which the video was recorded. These chambers are filled sequentially with  $150 \text{ nl}$  aliquots of water (A), of water containing colorants (B, C), and finally flushed and filled with water again within a few seconds (D, E). This result is also available as movie S1 (26).

conduits. The integrated CSs fabricated with different dimensions (see Table S1 in ref. 26) and presented here are three-dimensional but can also be made planar. We prefer to use three-dimensional systems because they are easily filled from the back-side, while a reaction can occur in the chamber on the front (processing) side (15, 27).

Reactants dispensed into the service port of a CS

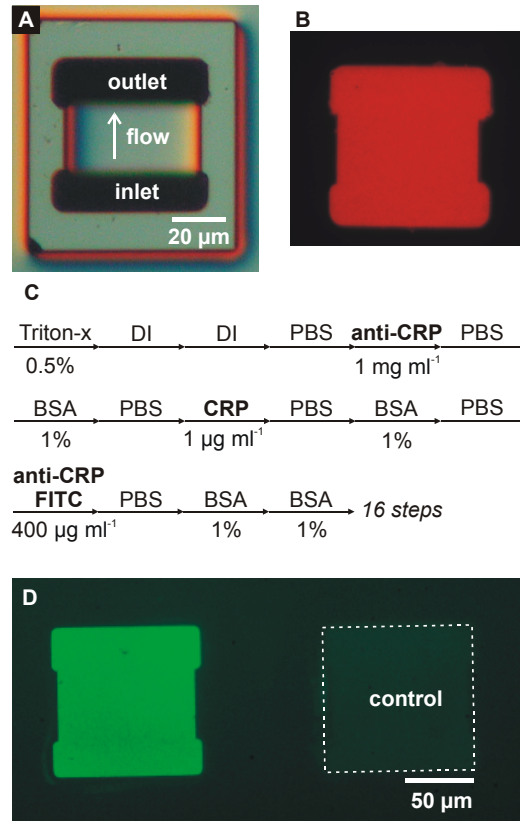


**Fig. 4.** All the steps to perform a miniaturized immunoassay on a surface can be easily done with a microfluidic CS. (A) The  $15\text{-pL}$  reaction chamber visible in the microscope image can localize the deposition of fluorescently tagged antibodies from solution onto an elastomeric substrate. (B) This fluorescence micrograph reveals a highly homogeneous deposited pattern of antibodies that mirrors the outline of the chamber. (C) The sandwich-type immunoassay to detect CRP comprises 16 elementary steps, including depositing anti-CRP antibodies onto the substrate, and filling the chamber with solutions containing the blocking agent (BSA), the analyte (CRP), and the second anti-CRP antibody tagged with fluorescein. Aliquots of  $\sim 200 \text{ nl}$  for each solution were manually dispensed into the service ports. (D) This assay is analyzed using fluorescence microscopy after separation of the CS from the substrate. The left pattern indicates a positive result, whereas the negative control on the right-hand side is negative as expected.

will not flow when the connected CP is entirely filled. To pump more solutions and larger volumes of liquids, the size of the CP has to be increased at the expense of the overall compactness of the CS. A small CP can be sufficient, however, if liquid is actively evaporated out of it using an air stream (28), or a heat source, or if a secondary CP can be reversibly connected to the embedded one when desired. Moreover, either of these methods creates the opportunity to control interactively the flow rate inside a single CS, or even inside many CSs in parallel. For example, it is possible to prefill many service ports, and trigger additional flow from them to their respective reaction chamber in a synchronized manner by contacting all CPs with a single, large secondary CP. The key for controlling the flow of liquids here is the synchronization of the capillary pressure of the secondary pump with the pressures generated by the arrayed CSs.

We were able to deliver between 4 and 20 nl s<sup>-1</sup> (using passive and forced evaporation, respectively) of solution to a 6- $\mu$ m-deep reaction chamber, which, using dispensed aliquots of 300 nl, is sufficient to ensure a continuous supply to the reaction chamber for at least 6 min. The absence of dead volumes becomes crucial here, and slower flow rates can be tuned if necessary, for example to achieve a homogeneous concentration of the reactants by diffusion in the chamber. We found these concepts robust and suited to transport solutions such as water, water with surfactants, buffers, electrolytes, ethanol, and solutions containing biomolecules or beads. We used CSs for patterning small areas on surfaces and for conducting miniaturized solid-phase sandwich immunoassays on PDMS surfaces (29), Fig. 4. PDMS was used because this elastomer induces the deposition of proteins from solution (21, 27) and can seal the reaction chamber of a CS (15). The amount of labeled protein adsorbed directly from solution to the 50  $\times$  50  $\mu$ m<sup>2</sup> area of the PDMS substrate that was covered by the reaction chamber (15 pl in volume) was followed using fluorescence microscopy, Fig. 4B. The measured fluorescence reflects the conditions for the deposition, of course, and has a root mean square intensity-variation of only 2.5% on the central 80% of the surface. The quality of this patterned area of proteins compares favorably with the typical inhomogeneities of protein-microarraying techniques (1) for which drying effects, surface wetting phenomena and the absence of a rinse step impair the quality of the patterns of proteins. In a second type of experiment, monoclonal antibodies against human C-reactive protein (CRP) were adsorbed on PDMS and, after a blocking step using bovine serum albumin (BSA),

they were used to capture CRPs from a sample according to the procedure described in Fig. 4C. CRP is an indicator of general inflammatory response, and of special interest for the prognosis and diagnosis of coronary diseases (30), e.g. myocardial infarction. The CRPs captured on the surface were then detected using fluorescently-tagged anti-CRP antibodies, Fig. 4D. For this experiment, the 4  $\times$  16  $\times$  200-nl-aliquots of samples (4 arrayed CSs  $\times$  16 sequential filling steps, ref. 31) and buffers were distributed manually in the microfluidic CSs, and the entire assay was done in less than 25 min; Figure 4D shows two of the four zones of the substrate where the immunoassay and an adjacent negative control were done.

The microfluidic CS introduced here combines effectiveness and convenience of use because it is autonomous. Such a CS is self-sufficient and arrayable *per se*, and multiple systems can be interconnected to form networks. The liquid transport can, if desired, be tuned using a tailored secondary CP and/or air convection, which is not more difficult to do for multiple CSs than for a single one. Because the CP is at the end of the flow path and also acts as the waste collector, a simple conduit is sufficient to connect the unique service port to a reaction chamber, no adverse mixing of samples occurs before they react, and the system is free of coupling elements. In principle, the capillary pressure of the CP can be increased by making it porous (4) or filling it with a porous material or with a gel, and thus used to propel the liquids through a large number of functional elements such as sampling zones, valves, mixers, and reaction chambers. The concepts presented here may contribute to the building of microfluidic systems useful for portable diagnostics (12), combinatorial assays (32), as well as for applications requiring high throughput (1). The combination of autonomous CSs with selective valving (33), which can distribute liquids according to their composition, could lead to "smart", integrated microfluidic systems. Models found in Nature, such as the perplexing ability of trees to transport a liquid from the roots to the leaves 100 m above ground, reveal that there should still be ample room for perfection of microfluidic systems.

## References and Notes

1. H. Zhu, *et al.*, *Science* **293**, 2101 (2001).
2. M. A. Burns, *et al.*, *Science* **282**, 484 (1998)
3. M. Ramsey, A. van den Berg, *Micro Total Analysis Systems 2001* (Kluwer Academic Publishers, Dordrecht, 2001).

4. J. J. Oertli, Der Saftaufstieg in Bäumen. *Vierteljahresschrift der Naturforschenden Gesellschaft in Zürich* **183/3**, 169 (1993).
5. R. Lösch, *Wasserhaushalt der Pflanzen* (Quelle & Meyer Verlag, Wiebelsheim, 2001).
6. P. J. Kramer, J. S. Boyer, *Water Relations of Plants and Soils* (Academic Press, San Diego, 1995).
7. P. G. de Gennes, *Rev. Mod. Phys.* **57**, 827 (1985).
8. E. Delamarche, *et al.*, *Science* **276**, 779 (1997).
9. E. Kim, Y. Xia, G. M. *Nature* **376**, 581 (1995).
10. M. Gleiche, L. F. Chi, H. Fuchs, *Nature* **403**, 173 (2000).
11. R. Jackman *et al.*, *Anal. Chem.* **70**, 2280 (1998).
12. K. F. Buechler, *et al.*, Microarray Immunoassays in the Microfluidic Triage® Protein Chip. In Ref. 3, pp. 42-44.
13. M. McNeely, *et al.*, *J. Assoc. Lab. Auto.* **4**, 30 (1999).
14. B. Zhao, J. S. Moore, D. J. Beebe, *Science* **291**, 1023 (2001).
15. D. Juncker, *et al.*, *J. Micromech. Microeng.* **11**, 532 (2001).
16. B. S. Gallardo, *et al.*, *Science* **283**, 57 (1999).
17. M. W. J. Prins, M. W. J. Welters, J. W. Weekamp, *Science* **291**, 277 (2001).
18. D. E. Kataoka, S. M. Troian, *Nature* **402**, 794 (1999).
19. S. Daniel, M. K. Chaudhury, J. C. Chen, *Science* **291**, 633 (2001).
20. K. Ichimura, S. K. Oh, M. Nakagawa, *Science* **288**, 1624 (2000).
21. E. Delamarche, *et al.*, *J. Am. Chem. Soc.* **120**, 500 (1998).
22. E. Washburn, The Dynamics of Capillary Flow. *The Physical Review* **XVII**, 273 (1921).
23. G. B. West, J. H. Brown, B. J. Enquist, *Nature* **400**, 664 (1999).
24. D. Öner, T. J. McCarthy. *Langmuir* **16**, 7777 (2000).
25. J. H. Spurk, *Strömungslehre* (Springer, Berlin), 4th Ed., pp. 160-167
26. Data and video are available as supporting material on *Science Online*.
27. D. T. Chiu, *et al.*, *PNAS* **97**, 2408 (2000).
28. N. Goedecke, A. Manz, Towards Evaporation-Driven HPLC on a Chip: An Alternative Transport Process for Micro Analysis Systems. In Ref. 3, 375-376.
29. A. Dodge, *et al.*, *Anal. Chem.* **73**, 3400 (2001).
30. P. Tarkkinen, T. Palenius, T. Lövgren, *Clin. Chem.* **48**, 269 (2002).
31. Such a large number of solutions could be filled into these CSs because forced evaporation and a secondary CP were used to interactively tune the flow and extract liquid from all the embedded CPs in parallel.
32. A. Bernard, B. Michel, E. Delamarche, *Anal. Chem.* **73**, 8 (2001).
33. D. J. Beebe, *et al.*, *Nature* **404**, 588 (2000).
34. We thank M. Despont, A. Bietsch, M. Geissler, S. Amontov, A. Bernard, J.-P. Renault and P. Hunziker for helpful discussions, R. Stutz for technical assistance, and A. M. Young and P. F. Seidler for their financial support.

## Supplementary Material - Materials & Methods

The microfluidic CSs were fabricated in double-side-polished Si wafers (Siltronic, Geneva, Switzerland) using photolithography and a deep reactive ion etcher (STS ICP, Surface Technology Systems plc, Newport, U.K.) in a four-step procedure. Top structures and the upper half of vias were patterned on one side, the reaction chamber and the lower half of vias on the other. The photoresist and oxide masks corresponding to the structures and vias were transferred into the Si sequentially (*SI*). 10 nm of Ti (adhesion layer) and 50 nm of Au were sputtered (LA440S, VonArdenne Anlagetechnik GmbH, Dresden, Germany) on both sides of the structured Si wafer. Networks of CSs were diced and microcontact-printed on both sides with a flat Poly(dimethylsiloxane) (PDMS, Sylgard 184, Dow Corning, Midland, MI) stamp, which was inked with an ethanolic solution of eicosanethiol to render these surfaces non-wettable. The other parts of the CS were derivatized with a thiolated poly(ethylene glycol) (Rapp Polymere, Heidelberg, Germany) to make these surfaces hydrophilic and protein-repellent.

The elastomeric substrates for the deposition of proteins were ~ 1-mm-thick pieces of PDMS cured against the bottom of a petri dish. This PDMS was formulated using Sylgard 184, low-molecular-weight crosslinkers, and a methylhydrosiloxane homopolymer to increase the hardness of this material. The elastomeric substrates were separated from the CS after the patterning processes, and rinsed with deionized water prior to being dried under a stream of N<sub>2</sub>.

Deionized water was produced with a Simplicity 185 system (Millipore). Chemicals were from Fluka and proteins from Sigma unless otherwise indicated. CRP, the monoclonal anti-CRP antibodies used for capture and recognition (labelled with fluorescein isothiocyanate, FITC, green,  $\lambda_{FE} = 520$  nm), were purchased from Hytest (Turku, Finland). Solutions of BSA were dissolved in phosphate buffer saline (PBS, BupH™, Pierce, Rockford, IL) at 1% w/w and passed through 0.22- $\mu$ m filters (Millipore). The solutions of proteins used in adsorption experiments were prepared in PBS, whereas the analyte and recognition proteins were prepared in a 1% solution of BSA in PBS. The rabbit antibodies labelled with tetramethyl rhodamine isothiocyanate (TRITC, red,  $\lambda_{FE} = 570$  nm) were prepared as a 500- $\mu$ g ml<sup>-1</sup> solution.

The secondary Capillary pump was formed by two hydrophilic cover slides held together — but with a 90- $\mu$ m gap — by double-sided Scotch tape (3M). They were contacted by their edges with the embedded capillary pumps to extract liquid as desired. A stream of N<sub>2</sub> was directed through four Cu tubes (~ 0.5 mm diameter each), located a few millimetres above the embedded capillary pumps to force evaporation, and regulated using a pressure valve.

Video sequences were shot with a digital camera (Coolpix 990, Nikon) affixed to an ocular (Fig. 1) and an inverted microscope (Eclipse TE300, Nikon; Fig. 3). The fluorescent images were obtained using a microscope (Labophot-2, Nikon) equipped with optical filters, and captured by a cooled, low-noise CCD camera (ST-8, SBIG, Santa Barbara, CA), and analysed using a homemade software programmed in Labview (National Instruments).

**Table S1:** Hydraulic parameters of the microfluidic capillary system.

section <sup>a</sup>	service port	access channel	inlet via <sup>b</sup>	reaction chamber <sup>c</sup>	outlet via	capillary pump <sup>d</sup>
length	1.5 mm	2 mm	150 $\mu$ m	500 $\mu$ m	150 $\mu$ m	6 mm
width	1.5 mm	140 $\mu$ m	80 $\mu$ m	80 $\mu$ m	80 $\mu$ m	42 $\mu$ m
depth	150 $\mu$ m	150 $\mu$ m	30 $\mu$ m	50 $\mu$ m	30 $\mu$ m	250 $\mu$ m

<sup>a</sup>Advancing and receding contact angles of deionized water on the walls of the channels: 45° and 33°; on the elastomeric substrate: 123° and 100°.

<sup>b</sup>The inlet via functions as capillary retention valve.

<sup>c</sup>These parameters have been varied as follows: *l*, 50–5000  $\mu$ m; *w*, 50–100  $\mu$ m; *d*, 4–50  $\mu$ m.

### Video

The video sequence CS1.avi corresponding to the results of Figure 3 can be found on the Internet: <http://www.zurich.ibm.com/st/microcontact/video/>. The time periods needed for the successive exchanges of one solution in the pipette with the next one were cut out of the video sequence. The total time is reported in Fig. 3. The successive filling of the four reaction chambers with one type of solution, however, is shown in real time. The water dispensed after the blue solution contains 5- $\mu$ m polystyrene beads that reveal the direction and the speed of the flow of liquid in the reaction chamber. All the reaction chambers remain permanently wetted because the CRV protects the liquid from draining them.

## Supplementary material II

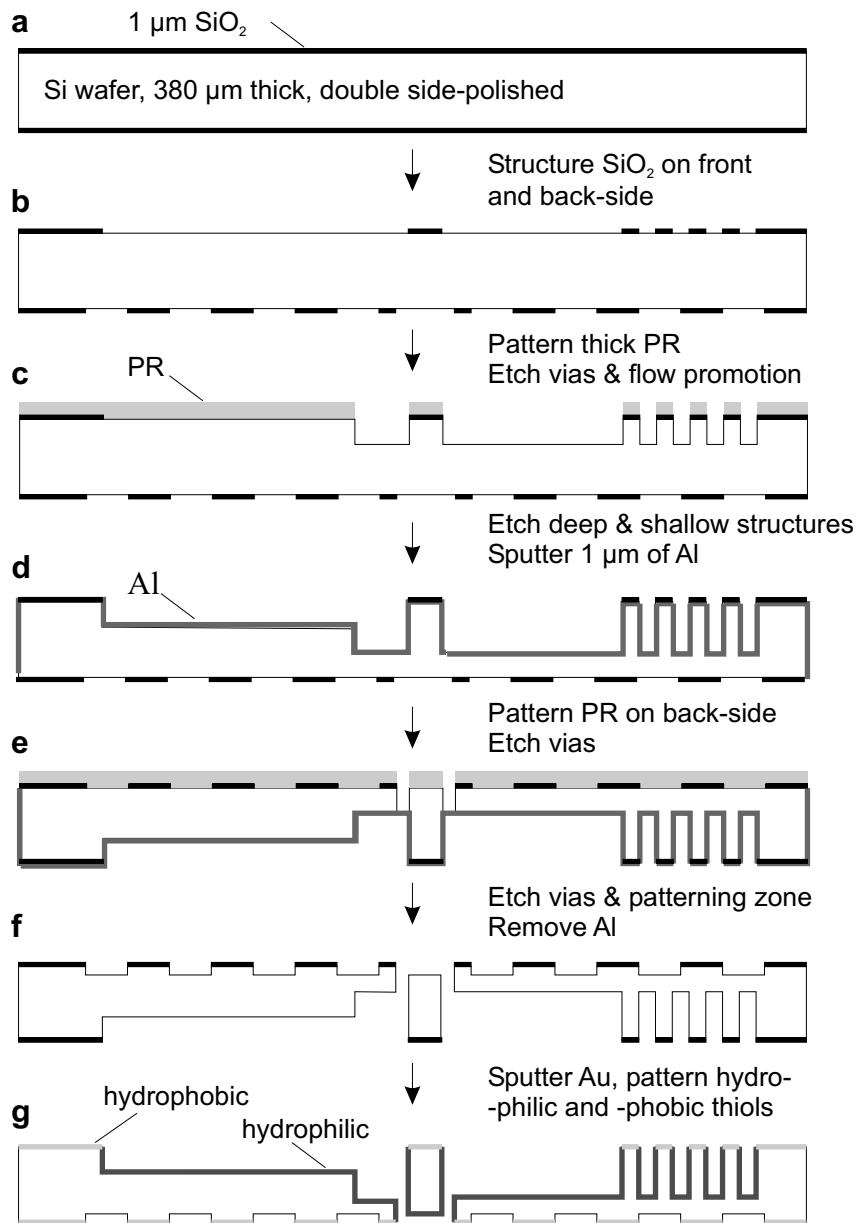


Figure 1. Fabrication procedure for making an autonomous microfluidic CS in Si (PR stands for photoresist).



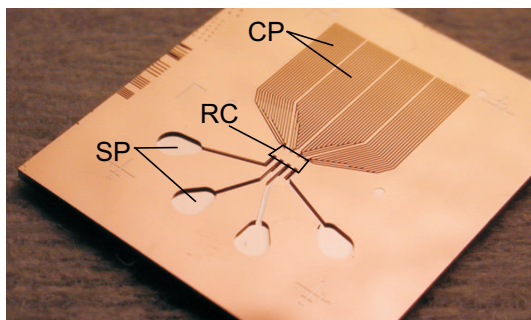


Figure 2: Photograph of a CS diced to size, covered with Au and ready to be used. SP, service port; RC, reaction chamber (underneath, not visible), CP, capillary pump.

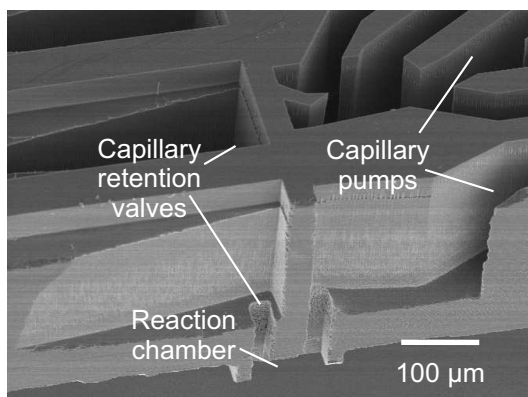


Figure 3: Scanning electron micrograph of the central section of a CS structured in Si that was diced. The flow path goes from the capillary retention valve, through the reaction chamber, and into the capillary pump.



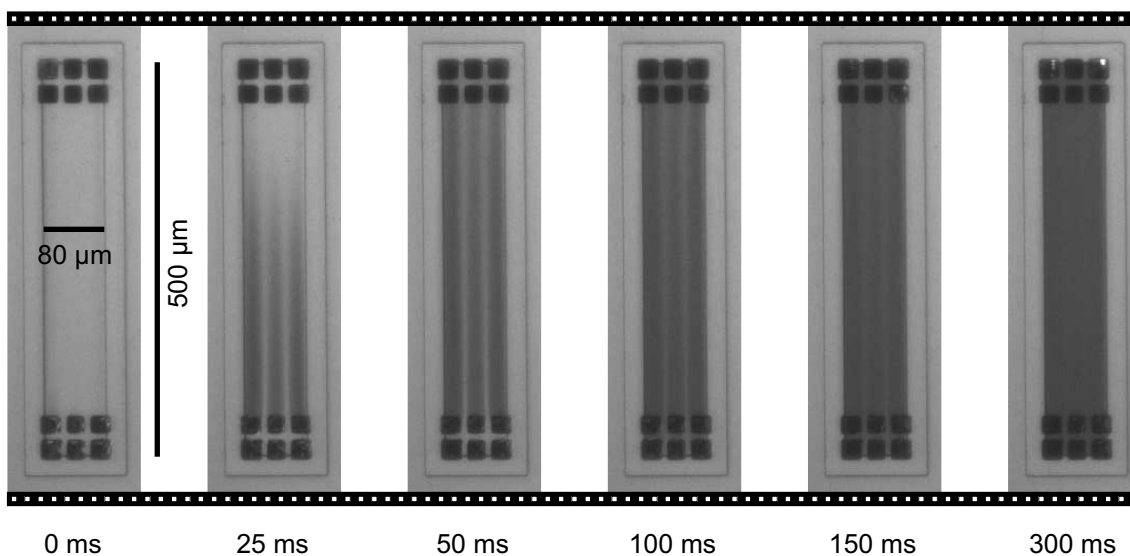


Figure 4. Displacement of water from a 6 μm deep reaction chamber of a CS by a black aqueous solution. The formation of the black stripes separated by water, which reflect the position of the inlet hole and the separation wall, respectively, stand for the highly laminar flow. The speed is approximately  $1.5 \text{ cm s}^{-1}$ , but 300 ms are required to completely flush out the original solution because of the laminar flow field. The pattern gradually vanishes as the water is slowly exchanged by diffusion with the fresh solution and transported out of the reaction chamber.

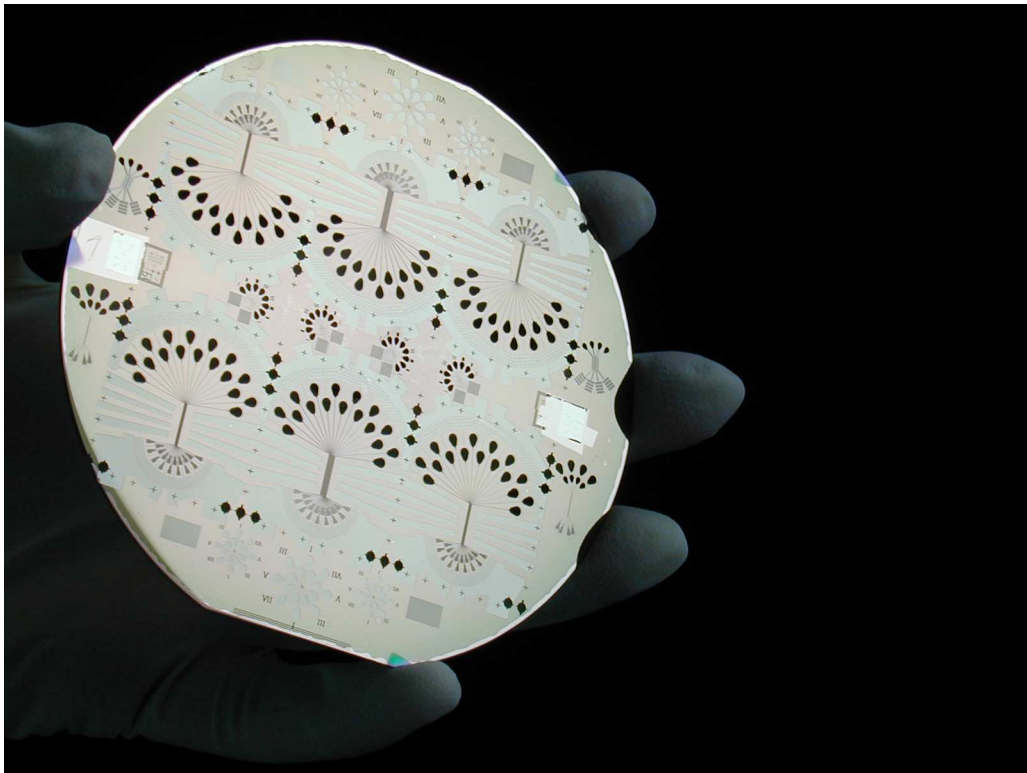


Figure 5. 4"-wafer structured on 2-levels with the latest generation of autonomous microfluidic capillary systems, and recovered with gold.

# Conclusion

The microfluidic CSs developed here require no peripheral equipment but a pipette for supplying the reagents. Hence, they have a considerable advantage over other microfluidic systems that necessitate external actuation, such as pumps, and most often a computer.

In this work, the existing CSs, formerly called microfluidic networks ( $\mu$ FNs), were improved in various respects. The original single-level systems were enhanced into multi-level ones for simplified utilization, because they provide access from the back-side and allow processing an arbitrary zone on a large substrate. The surface chemistry outside and inside of the channels was optimized, and by using self-assembled monolayers with polyethylene oxide groups, the channels could be made non-fouling if required. The flow speed and replenishment were finely tuned for optimal reaction conditions and allowed precise control on, for example, the density of adsorped molecules on the surface as function of the position.

The usage of CSs was extended to the fabrication of “smart” stamps, as described in Chapter 5, which by drawing on biological recognition and self-assembly principles, proved powerful enough for repetitive extracting, purifying and parallel arraying of proteins in just a few simple steps.

In the last part of this thesis, the crucial shortcoming of capillary systems, namely the impossibility to transport more than one solution only, was overcome. The intrinsic advantages of (i) self-containment, (ii) scaling of the filling force along with size reduction, (iii) no need for neither fluidic nor electric connections, and (iv) the absence of moving parts were combined and allowed creating autonomous microfluidic CSs. Here, the different tasks are “programmed” not into the memory of an IC chip, but directly into the structure of the capillary system, and the energy is not supplied by a battery, but is directly stored in the surface chemistry of the capillary conduits. Because of this autonomy, arrays of CSs can be straightforwardly made by cloning of a working system. The use of a small array (four systems) was demonstrated in Chapter 6. Another advantage of CSs is that although autonomous, the liquid transport can simply be controlled, if desired, along two different schemes: firstly, by appending a removable secondary capillary pump, and secondly, by locally increasing the evaporation rate using, for example, a stream of dry air. Moreover, this can be done for an array of systems without increase of complexity. The key to such advanced capillary operation is the synchronization of the meniscus pressure of the liquid in the different sections of the microfluidic CSs in a way that fulfills the desired functionality. As shown, this renders the control on many systems possible and paves the way for making interconnected networks of microfluidic capillary systems.

Further, the different characteristics of CSs indicate that their fabrication should be doable using polymers and mass-replication processes.

Evaporation can compromise the operation of CSs, but can be reduced by minimizing the liquid-air interfaces and by controlling the relative humidity, which becomes primordial as the dimensions and the volume are reduced. Further, the dewetting of the liquid from a section of the CS is critical, because drying of left-over solution can lead to contamination of this area. This issue is a remarkable challenge that needs to be solved before the full potential of CSs can be exploited.

The combination of the above-mentioned characteristics impart CSs with unique and unmatched advantages that in practice should make them the most convenient, and economically the most efficient, “microfluidic solution” for performing certain types of multi-step bio/chemical processes, provided that additional research efforts are directed into overcoming the few, yet critical shortcomings that remain.

# Acknowledgments

I first wish to address my deepest thanks to Emmanuel Delamarche for his profound commitment, his great patience in explaining, correcting, and writing, and his unlimited availability for fascinating discussions about science and the world, all of which were invaluable. He was simply indispensable to the fertile work atmosphere which made my three-year stay in the lab truly enriching and fruitful.

I also wish to specially thank those who took the responsibility for the project. Bruno Michel for his help on mask designing, his enduring support and the indispensable freedom of action which he always granted me, Prof. Nicolaas F. de Rooij (Université de Neuchâtel) for his deep confidence, his forthcoming attitude and his willingness to help whenever possible during this thesis, and P. Seidler for his continuous support our group and myself.

It is a special pleasure to acknowledge all the people who specially committed themselves to help me and who were particularly sympathetic with my work. Heinz Schmid for the solution to complicated problems and questions of all kind that he just “sees” with his crystal mind, his exceptional manual skills that were so helpful, and his wit that was sometimes more than entertaining. Ute Drechsler from the Micromechanics group for her prompt, continuous and wide technical assistance in microfabrication, and the good time in the clean room and outside. Michel Despont from the same group for his many precious advices on microfabrication, and interesting discussions on microsystems, amongst other. Alex Bietsch for his help on flow calculations and the discussions about the physical models of capillary flow, and for his participation in comprehensive experiments in cold environment on the “flow” of powdery crystalized water below waxed boards affixed to one’s feet.

I warmly thank all the past and present members of our group who contributed to the great atmosphere, exciting discussions and who shared a range of non-work-related activities, and who are in alphabetical order: Sergey Amontov, André Bernard, Alain Carvalho, Isabelle Caelen, Christian Donzel, Matthias Geissler, Nils Omland, Jean-Philippe Renault, Patrick Schmidt-Winkel, Richard Stutz, Heiko Wolf, and Marc Wolf. Thank you all for the great memories you bestowed me with.

I further wish to thank Roland Widmer for his enthusiasm and his technical assistance. I am soooo grateful to all the people in the publication department who corrected and lightened up my English in innumerable documents, and who in particular made this thesis more agreeable to read for you, to our nice and quick librarians who get my articles in less time than it takes you (*again*) to read this sentence, and to the skillful staff in the

model shop who would improve the models I had drawn. And I finally wish to thank all the other people working on the premises who contributed to the friendly atmosphere, succulent food and who made these 3 years a pleasant time.

I also address a special thank to my experts, and in particular Prof. Raphael Tabacchi for kindly accepting to read and evaluate my work.

And Most importantly, my family to whom I dedicate this work. I profoundly thank my parents for raising me and giving me so much of themselves, my brother Christophe for all the great adventures we shared, my grand-mother for her gentleness, the rest of my family, and very specially Wen-Chuan for her love, her extraordinary Support to my work and her understanding for my coming home later than acceptable.

At last, but by far not least, I wish to thank all my friends who are here in Zürich, in Neuchâtel, in Switzerland and around the world for all the good time we had together and for enriching my mind.

# List of Publications

Juncker, D., Schmid, H., Drechsler, U., Wolf, H., Wolf, M., Michel, B., de Rooij N., and Delamarche, E. *Autonomous microfluidic capillary system.*, manuscript.

Renault, J.-P., Bernard, A., Juncker, D., Michel, B., Bosshard, H. R. and Delamarche, E. *Fabricating microarrays of functional proteins using affinity contact printing.* **Angew. Chem. Int'l. Ed.** *41*, 2320-2323 (2002).

Juncker, D., Schmid, H., Bernard, A., Caelen, I., Michel, B., de Rooij N., and Delamarche, E. *Soft and rigid two-level microfluidic networks for patterning surfaces* **J. Micromech. and Microeng.** *11*, 532-541 (2001).

Michel, B., Bernard, A., Bietsch, A., Delamarche, E., Geissler, M., Juncker, D., Kind, H., Renault, J.-P., Rothuizen, H., Schmid, H., Schmidt-Winkel, P., Stutz, R., and Wolf, H. *Printing meets lithography: Soft approaches to high-resolution patterning.* **IBM J. Res. & Dev.** *45*, 697-719 (2001) .

Bernard, A., Juncker, D., Larsen, N., Michel, B., and Delamarche, E. *Microfluidic networks made of poly(dimethylsiloxane), Si, and Au coated with polyethylene glycol for patterning proteins onto surfaces.* **Langmuir** *17*, 4090-4095 (2001).

Juncker, D., Bernard, A., Caelen, I., Schmid, H., Papra, A., Michel, B., de Rooij N., and Delamarche, E. *Microfluidic networks for patterning biomolecules and performing bioassays.* Proceedings of the  $\mu$ TAS 2001 Symposium, Monterrey, USA. Ramsey, M. & van den Berg, A. (editors). **Micro total analysis systems 2001** (Kluwer Academic Publishers, Dordrecht, 2001).

Caelen, I., Bernard, A., Juncker, D., Michel, B., Heinzelmann, H., and Delamarche, E. *Formation of gradients of proteins on surfaces with microfluidic networks.* **Langmuir** *16*, 9125-9130 (2000).





# Curriculum Vitae

## David Juncker

1999-2002	Thesis at the IBM Zurich Research Laboratory, Rüschlikon, Switzerland in the Microcontact Processing group under the supervision of Dr. E. Delamarche and Prof. N. de Rooij (Université de Neuchâtel).
1997-1998	Work on micromechanical accelerometers at the National Research Laboratory of Metrology (NRLM), Tsukuba, Japan, on a Research Grant awarded from the Swiss Academy of Engineering Sciences.
1996-1997	Work on a detection platform for bovine spongiform encephalopathy (BSE), at the Centre Suisse d'Électronique et de Microtechnique (CSEM), Neuchâtel.
1996	Diplôme in Microtechnology, Université de Neuchâtel.
1996	Diploma work on the replica molding of diffractive micro-optical structures at the Paul Scherrer Institute in Zürich (now CSEM).
1991-1995	Internships that included programming a user-interface in C-language, network managing and wireless IC design at CSEM and SGI Inc. in Neuchâtel
1991-1995	Studies at the Institut de Microtechnique of the Université de Neuchâtel, Switzerland.
1991	Baccalaureat of type C (scientific) in Neuchâtel, Switzerland.
8 April 1973	Born in Aarau, Switzerland.